Department of Precision and Microsystems Engineering

Thermo-optic modeling for a microlithographic projection system

Wahhe Ajroemjan

Report no	: 2021.082
Coach	: Dr. ir. J. De Boeij
Professor	: Dr. ir. L.A. Cacace
Specialisation	: Micro-optics and Opto-mechatronics
Type of report	: Master thesis
Date	: 13 October 2021

Delft
University of
Technology

Challenge the future

DELFT UNIVERSITY OF TECHNOLOGY

FINAL REPORT

MASTER THESIS

Thermo-optic modeling for a microlithographic projection system

---

Authors:
Wahhe Ajroemjan (4497244)

October 13, 2021

Supervisors:	Dr. ir. L.A. Cacace,	TU Delft
	Dr. ir. J. De Boeij,	Company supervisor
	Dr. M. Loktev,	Company supervisor

MSc program Mechanical Engineering, High-Tech Engineering track

Executive Summary

The packaging of a microchip affects its size, performance and cost. With advanced packaging, more efficient and smaller microchips can be produced. For this, advanced packaging stepper systems are used, which are lithography machines with a highly optimized projection lens system, that use a powerful light source. The projection lens system for lithography machines are highly accurate optical assemblies with stringent optical requirements, such as a small wavefront error. These requirements need to be fulfilled, while also dealing with a high throughput. Due to the high throughput and the powerful light source, some of the light passing the projection lens system gets absorbed by the lenses. This causes local lens heating, which degrades the optical performance.

Local lens heating causes thermal gradients to arise in the lenses, which cause refractive index gradients. Due to thermal expansion, the lenses will also deform, therefore changing the geometry of the optical surfaces. To analyze the lens heating effects, a Structural, Thermal and Optical Performance (STOP) analysis is performed. A multiphysics Finite Element Method (FEM) analysis model is build in COMSOL, which couples the structural, thermal and optical physics in a single model, which can model both steady-state and transient behaviour.

The STOP analysis is performed for a Wynne-Dyson projection lens system, which is a catadioptric lens system. First, the optical performance of the nominal lens system obtained from COMSOL is evaluated and compared to results from Zemax. Spot diagrams, Zernike wavefront aberrations and the Maréchal criterion are used to evaluate the optical performance. COMSOL showed to be capable of producing similar results and of the same order of magnitude as Zemax. The lens system proved to be a diffraction limited system with good image quality.

Next, a thermal analysis is performed for the Wynne-Dyson projection lens system, which shows that radiative heat transfer is an important heat transfer path in transferring heat away from the lenses. To model this properly, the directional dependence of the emissivity of the lenses is experimentally determined. To gain trust in the thermal results from the simulations, an analytical lens heating model of a simplified single lens is made to compare with.

The STOP analysis model evaluated the optical performance after lens heating. This showed that the optical performance degrades significantly. The lens system is not diffraction limited for all wavelengths in the spectrum of the light source after lens heating. After looking at the influences of thermal and structural loads on the lenses separately, it showed that reducing the structural deformations in one of the lenses would improve the optical performance significantly. The lens system would even become diffraction limited again. Some thermal design changes were analyzed to improve the thermal design. Using a different filling medium with a higher conductivity in the enclosures between lenses, reduces the thermal gradients in the lenses and therefore also improves the optical performance.

Contents

Chapter 1

Introduction

Chip packaging started as simply providing protection and a way for in- and output connections for chips. With the semiconductor industry aiming for smaller, thinner, cheaper and faster microchips, advanced packaging starts to play an important role in pushing these boundaries. With advanced packaging more efficient interconnections between multiple types of chips are possible within a single packaging, which is called System in Package (SiP). Advanced packaging also allows for packaging sizes nearly the same as the die when using Wafer-Level Packaging (WLP), which is a technique to package integrated circuits (IC's) while they are still part of the wafer.[1]

Advanced packaging stepper systems play a crucial role in the manufacturing of IC's. These systems are lithography machines with a highly optimized projection lens system, which use a powerful light source. The main focus in this report will be on the Structural, Thermal and Optical Performance (STOP) analysis for a high throughput lithographic projection lens system of an advance packaging stepper.

1.1 Lithography

For the fabrication of microchips, a series of chemical and physical processes on a semiconductor substrate need to be performed. Lithography is an essential step in this fabrication process where light is used to pattern a mask on a photoresist to create 3D relief images on the substrate. With these patterns, millions of transistors can be fit and wired on a single microchip.

The general steps for a lithography process are shown in figure 1.1. First the substrate wafer needs to be prepared, by cleaning, baking and adding an adhesion promoter, as shown in step (a). This is to remove contamination and water, and preventing water from coming back. Next, a thin coating of photoresist is applied by using a technique called spin coating, as shown in step in (b). By spinning the photoresist when it is in liquid form, a uniform and controlled layer thickness can be achieved. After the spin coating process, the photoresist is dried by prebaking, which removes excess solvents from the liquid, as shown in step in (c). Next, the image of a mask is projected on the wafer using a projection lens system, as shown in step in (d). This is done by step-and-repeat systems (steppers). Steppers project the mask on a small section of the wafer, called a die, one at the time in a grid structure until the mask is exposed in all grid sections on the wafer. The mask comprises only the features of a single die. After exposing the photoresist, it is developed and post-baked to remove the exposed parts from the photoresist and transfer the pattern on the photoresist, as shown in step in (e). Now there are three basic options to continue. Either material is removed, called etching, material is added, called selective deposition or contaminants are doped to change the conductive properties, called ion implantation, as shown in step in (f) for etching. The final step is to strip the photoresist from the substrate, as shown in step in (g).[2]

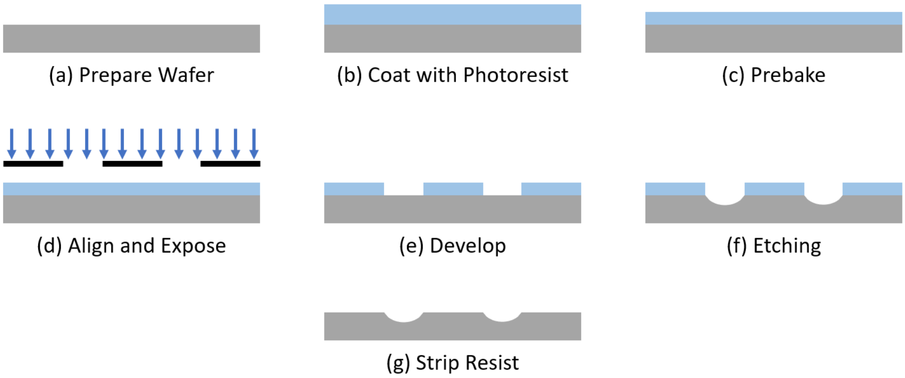

Figure 1.1: General sequence of steps for optical lithography.[2]

1.2 Lens system

For lithography machines which use projection printing in the exposing and patterning step, a complex and highly accurate projection lens system with stringent requirements is used. The projection lens system is an essential part that determines the minimum feature size. Therefore, it is important to have a lens system that is highly optimized to reduce wavefront errors and distortion. On the other hand, there is a need for high speed production which uses high power light passing through the lens system. When even a small amount of the light gets absorbed by the lenses, due to the high throughput, it can induce local lens heating and cause degradation in the optical performance. Therefore, the projection lens design should be analyzed for the structural and thermal effects on the optical performance.

A design of a Wynne-Dyson projection lens system is analyzed, which is a catadioptric design consisting of several lenses and mirrors. Figure 1.2 shows an example of a Wynne-Dyson projection lens design, with all the lenses highlighted in blue and the mirror surfaces in red. Light is entering the system from the top and reflects into the lenses system. After passing through the lenses, the light reflects from the main mirror and travels back through the lenses again until it gets reflected and focused onto the wafer. Typical for a Wynne-Dyson design is that it has unity magnification and the object and image are located on the same side. The lens heating effects need to be investigated to ensure high optical performance even when dealing with a high throughput.

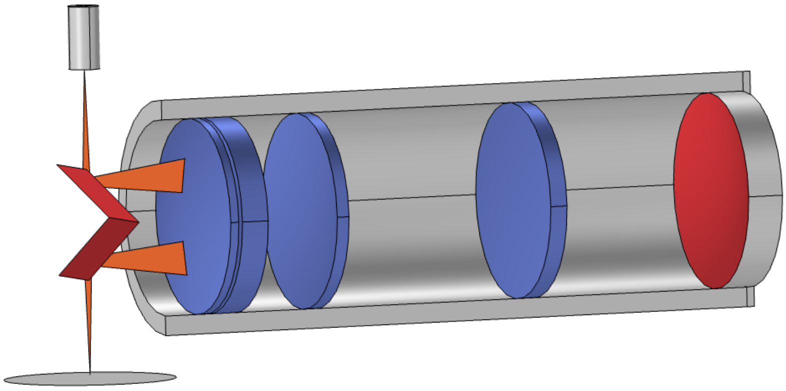

Figure 1.2: Example of a Wynne-Dyson projection lens system. Lenses are highlighted blue and mirrors red. Light is coming in from a light source and is focused on a wafer.

1.3 Problem and goal

To analyze the lens heating effects on the projection lens system, a Structural, Thermal and Optical Performance (STOP) analysis needs to be performed. For this a multiphysics finite element method (FEM) simulation model is needed, which couples the structural, thermal and optical physics in a STOP analysis model.

1.3.1 Problem

When thermal and structural effects on the optical performance need to be analysed, first an initial optical analysis is performed to obtain the initial conditions of the heat loads from absorbed rays. These results are then used to perform a separate thermal and structural analysis, often in different software packages then used for the optical analysis. The results form the thermal and structural analysis are then used in yet another optical analysis to evaluate the optical performance after the lens heating effects. In each step, the results need to be exported and prepared to be able to properly import the results in a different software package. This typically introduces numerical errors. In a typical STOP analysis several iterations between the optical analysis and the thermal and structural analysis need to be done. This is because the optical analysis and the thermal and structural analysis are influencing each other. The iterations are done until a self-consistent solution is found. Besides that this is not very efficient and prone for mistakes along each step, transient behaviour is difficult to study.

1.3.2 Goals

The goal is to perform a STOP analysis in COMSOL on a Wynne-Dyson projection lens design, where optical, structural and thermal physics are coupled into a single multiphysics FEM model. This is then used to evaluate the optical performance of the lens design for both steady-state and transient case. The model is extended to also consider directional dependent surface-to-surface radiation for the radiative heat transfer.

1.3.3 Sub goals

- Investigate the capabilities/performance limits of COMSOL in performing a multiphysics lens heating analysis. This was part of the literature study together with learning how to build FEM models in COMSOL.

- Model a lens system in a single ray-tracing model considering only optical physics and evaluating the optical performance.
- Identify thermal paths and their importance to the total heat transfer inside a lens system undergoing lens heating.
- Create an analytic lens heating model for a single lens at steady state.
- Finding the directional dependence of the emissivity coefficients experimentally for the lens elements.
- Model a lens system in a single steady-state model considering only thermal and structural physics.
- Model a lens system in a single steady-state STOP analysis model.
- Model a lens system in a single transient STOP analysis model.
- Design change suggestions to improve the optical performance from knowledge obtained from simulations and results.

Chapter 2

Optical system

The projection lens system involves optics as the basis for its design. Therefore, to understand the system the optics are considered first in this chapter.

2.1 Lens system overview

The projection lens system in question is based on a Wynne-Dyson catadioptric lens system design. Wynne-Dyson projection lens systems typically consists of multiple lenses and a mirror, making it a catadioptric system. The lens system is used in photolithography steppers at ultraviolet (UV) wavelengths. The lenses are selected from optical glass types which have a low absorption for electromagnetic UV radiation. This is needed because the portion of UV light that gets absorbed will locally heat up the lens elements, which will cause changes in the refractive index and structural deformations to the lenses and hence degrade the optical performance. Nevertheless, a Wynne-Dyson design provides sufficient degree of freedom to correct for abberations.

Typically, a Wynne-Dyson projection lens system consists of a concave mirror, a positive lens group and two mirror surfaces. The two mirror surfaces and the concave mirror are on opposite sides of the lens group on the optical axis. Light coming from the object gets reflected from the first mirror surface into the lens column. Traveling through the lenses and reaching the end of the column, the light gets reflected by the concave mirror. The reflected light travels back through the lenses and reflects from the second mirror surface in the image plane. The two mirror surfaces are typically established with 2 separate mirrors, but some designs use prisms, like in [3]. The two mirror surfaces have respective surfaces adjacent to the object and image planes. The reticle resides at the object plane and the wafer resides at the image plane. A Wynne-Dyson lens design has typically a numerical aperture between 0.1 and 0.2, a unity magnification, is double telecentric and has a Strehl ratio of $>$0.95 for a spectral bandwidth including 436 nm, 405 nm and 365 nm wavelengths (g-,h- and i-line radiation respectively, or simply ghi radiation). Wynne-Dyson lens designs are typically used for a broadband spectrum.[3]

To go into more detail about a typical Wynne-Dyson projection lens system, an example system is given in figure 2.1 from [3], which consists of 2 prisms (PA and PB), 4 lens elements (L_i), a mirror (M), a reticle plane (RP) and a wafer plane (WP). Also, all the surfaces are labelled (S_i) as well as lens groups (G_i) and the aperture stop (AS). Generally, Wynne-Dyson projection lens designs for lithography systems follow the same optical principles, therefore this example is shown here.

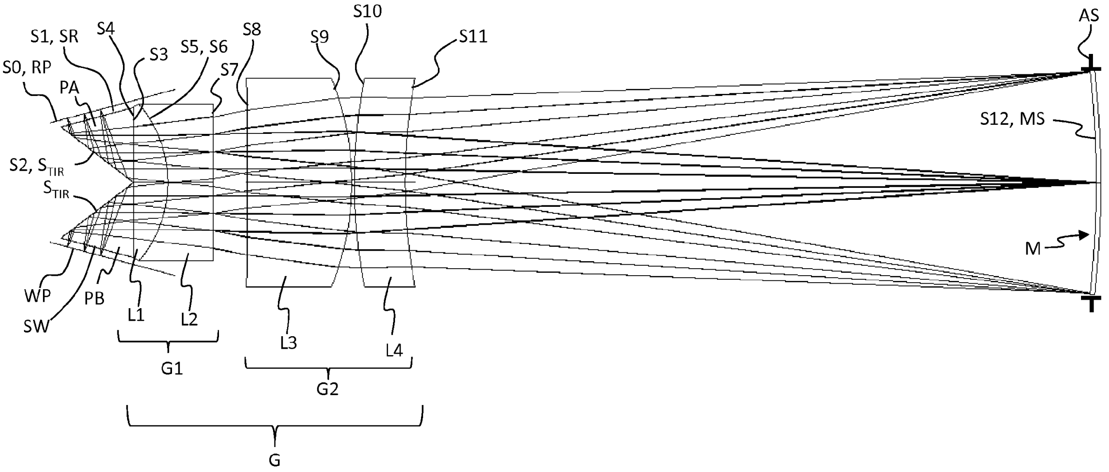

Figure 2.1: Optical diagram of an example Wynne-Dyson projection lens system. The drawing is not to scale.[3]

This example of a Wynne-Dyson projection lens system is well-corrected for ghi radiation. Prims PA and PB in this example are isosceles prisms. The prisms have both a total internal reflective surface (S_{TIR}). PA also has surface SR adjacent to RP, which resides with the object plane (OP). PB has surface SW adjacent to WP, which resides with the image plane (IP). The positive lens group (G) can be subdivided into the first lens group (G1) and second lens group (G2). G1 consists of a doublet made up of a plano-convex lens element (L1) and a plano-concave lens element (L2). G2 consists of two lens elements (L3 and L4) that resides between G1 and M.

Abberations

Because of symmetry about mirror M, the system is self-corrected for distorion, coma and lateral chromatic abberations, but M does introduce astigmatism and field curvature abberations. The lens groups are designed to compensate these abberations, as well as spherical abberations.[3] In this example, L4 which has a meniscus shape has relatively little optical power. However, L4 is dominant in compensating the astigmatism and field curvature abberations, because of its aspherical surface. L2 and M dominate the optical power.

The lens elements are another degree of freedom in the projection lens design to deal with aberrations like astigmatism and field curvature generated by the mirror. However, the lens elements also introduce aberrations in the form of spherical aberrations and coma.

Usually, L1 and L2 are a doublet and the other lens elements can be used to compensate the abberations introduced by the mirror. The amount of lens elements varies in different designs. Therefore, a Wynne-Dyson lens design has enough degrees of freedom to compensate abberations introduced by the mirror or one of the lenses by other lenses.

2.2 Lens system properties

Typical Wynne-Dyson projection lens systems have some common optical properties, which are also useful when modelling the system to obtain insight in the optical performance.

These lens system properties are given in table 2.1 accompanied with their common specifications.

Table 2.1: Lens system properties for a typical Wynne-Dyson projection lens systems design

Property	**Specification**	**Remark**
NA	0.1 - 0.2	
Partial coherence factor σ	0.5 - 0.75	
Spectral range	350 - 450 nm	
Magnification	1×	
Resolution	2 µm L/S	L/S = Line space; 4 µm pitch
Strehl ratio	> 0.95	
Source UV intensity	25 - 100 W	
Illumination intensity	500 - 2500 $\mathrm{mW/cm^2}$	
Temperature	21 °C	
Pressure	1 atm	

Spectral range

Wynne-Dyson designs are typically used for a broadband spectrum. For the projection lens design of interest, a spectral range from 350 nm to 450 nm is used. This fits partly in the near ultra violet (NUV) and visible light range. For the FEM modelling only three wavelengths are evaluated. The wavelengths are 365 nm (i-line), 405 nm (h-line) and 436 nm (g-line), also called ghi radiation, which correspond to the spectral lines of a mercury light source.

Field points and NA

Characteristic of a Wynne-Dyson design is that incoming light from the reticle is decentered in Y-direction. For the FEM modelling a total of 9 field points are used which are arranged like in figure 2.2 for the reticle. The NA will be different for the optical analysis and the thermal analysis. For the thermal analysis the NA will be reduced by the partial coherence factor σ. Lower σ improves the modulation contrast for low spatial frequencies. Setting it close to 0 would give almost perfect modulation contrast but the power would then be concentrated in a smaller area on the lens elements.[4] Therefore, σ is chosen such that there is a balance between the modulation contrast and spread of the power.

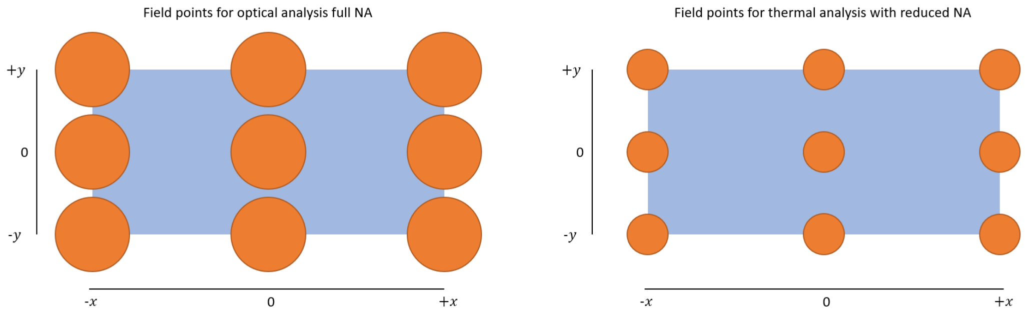

Figure 2.2: Field points (orange) used from reticle (blue) with full NA for optical analysis (left) and σ·NA for heat transfer analysis (right).

Field variation and telecentricity

The light on both the object and image has a telecentricity pattern and hits/leaves S4 from L1 with a specific angle w.r.t. the optical axis. The telecentric pattern is to reduce the magnification error. The double telecentricity pattern consists of a certain tilt w.r.t. the optical axis combined with a field variation for magnification correction. Figure 2.3 shows how the chief rays enter/leave S4 and also how the patterns for telecentricity and field variation respectively look like.

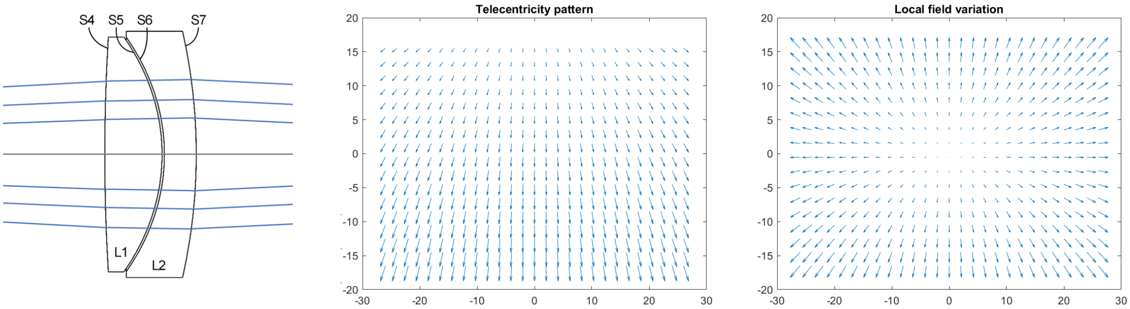

Figure 2.3: Left: Chief rays entering/leaving S4 with an angle w.r.t. the optical axis. Middle: telecentricity pattern. Right: Local field variation pattern to correct for magnification.

2.3 Material properties

2.3.1 Refractive index

The lens elements in the system are of different glass types and thus have different refractive indices. When light passes through the lens elements, lens heating will play a role in changing the refractive index caused by temperature changes. The refractive index consists of a real and imaginary part. Therefore, the refractive index is given by equation 2.1, which is a function of wavelength and temperature.[5]

$$\tilde{n}(\lambda, T) = n(\lambda, T) + i\kappa(\lambda) \tag{2.1}$$

Here, the real part of the refractive index n indicates the phase velocity and the imaginary part κ is the attenuation coefficient. The imaginary part governs the absorption of light causing lenses to heat up in the first place.

Thermo-optic coefficient dn/dT

The real part of the refractive index governs the change of the refractive index over changes in temperature of a medium. The refractive index is given by equation 2.2.

$$n(\lambda, T) = n_r(\lambda) + \frac{dn(\lambda)}{dT}(T - T_r) \tag{2.2}$$

Here, T is the actual temperature of the medium, T_r is the reference temperature, n_r the refractive index at the reference temperature and $\frac{dn}{dT}$ is known as the thermo-optic coefficient. The thermo-optic coefficient can be derived from the Sellmeier equations.[6]

Absolute vs relative

The refractive index from equation 2.2 is called the absolute refractive index, which means the index of refraction relative to vacuum. However, the surrounding medium of the lenses is not necessarily vacuum. To account for this, the so called relative index of refraction can be calculated with equation 2.3.

$$n_{\mathrm{rel}}(\lambda, T) = \frac{n_{\mathrm{abs}}(\lambda, T)}{n_{\mathrm{med}}(\lambda, T, P)} \tag{2.3}$$

Empirical relations are used to determine $n_{\mathrm{med}}(\lambda, T, P)$. Typically, the surrounding medium is air, but in projection lens systems also nitrogen gas is used in the enclosures between lenses. The refractive index of these gasses not only changes with temperature but also with pressure P.

Attenuation

When light travels through a medium, a small part of the intensity gets attenuated. The attenuation is governed by the imaginary part of the refractive index denoted as κ, which is given in equation 2.4.

$$\kappa = \frac{-\lambda \ln\left(\frac{I}{I_0}\right)}{4\pi z} \tag{2.4}$$

Here, λ is the wavelength, I/I_0 is the ratio of intensity of light passing through the medium and z is the path length through the medium. Usually, glass suppliers specify the transmission for a certain thickness of the glass over a range of wavelengths, or they provide a spectral transmission plot. This data can be used in equation 2.4 to calculate the imaginary part of the refractive index. The transmission corresponds to I/I_0 and z is the thickness for which the transmittance is specified by the supplier.

2.3.2 Abbe number

The projection lens system in question is designed to operate over a wavelength range between 350 nm to 450 nm. Because of dispersion of the light chromatic aberration will arise. Chromatic aberration can be of two types. There is axial and lateral chromatic aberration. With axial aberrations, different wavelengths of light will focus at different focus spots, which causes a shift in focus. With lateral aberrations, different wavelengths of light will focus at different positions within the focus plane. Because of the symmetry about the mirror lateral aberrations are generally well corrected in Wynne-Dyson projection lens designs. However, axial aberration still can occur.[3][7] By choosing glass types with different Abbe numbers the axial aberration can also be dealt with. Typically, different materials are used for different lens elements with Abbe numbers ranging between 40 and 90. This gives sufficient degree of freedom in correcting chromatic aberrations.

2.3.3 Coefficient of thermal expansion

Materials tend to change in size when their temperature changes. The coefficient of thermal expansion (CTE) governs the fractional change in size over a change in temperature of a material and is given by equation 2.5 as α.[8]

$$\frac{\Delta L}{L} = \alpha \Delta T \tag{2.5}$$

The CTE is usually assumed to be constant, which means a linear thermal expansion, however it is temperature dependent. The dependency of temperature is mainly considered in applications where large changes in temperature occur. The lens elements in the projection lens system will mostly change a few Kelvin around room temperature, so a constant CTE can be assumed.

When choosing different materials, the CTE's should match as close as possible. This is to reduce stresses to build up between components because of different rates of expansion at temperature changes. This can happen for example between a lens element made out of fused silica and its aluminium mount. Fused silica has a much lower CTE compared to aluminium. When the temperature changes, the mount will expand more than the lens element and it will start exerting pressure, which will cause stresses to build up in the lens elements. Matching CTE's can minimize stresses to build up.

2.4 Optical performance indicators

To analyse the optical performance of a system, several different optical performance indicators can be used. Below are three indicators introduced that will be used to analyze the optical performance of the Wynne-Dyson projection lens design.

2.4.1 Spot Diagrams

A spot diagram is a plot where the intersection of rays with a certain plane is visualized. The plane can be arbitrarily chosen, but to analyse the optical performance of the projection lens system, the plane is chosen such that it coincides with the image plane from a point source in the object plane. From the spot diagram several characteristics of the ray bundle can be obtained, like the radial RMS spot size value, the shape of the spot and some aberrations like coma or astigmatism can be observed. In figure 2.4 an example of a spot diagram is shown for a conical beam that is refocused after passing 2 lens elements.

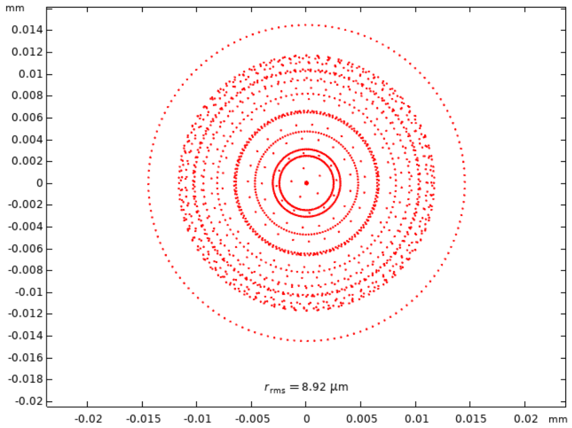

Figure 2.4: Example of a spot diagram

In figure 2.4 also the r_{RMS} value is shown. This is the radial root-mean-square spot size calculated from all the rays of the spot and it is calculated by equation 2.6.

$$r_{RMS} = \sqrt{\frac{\sum_i^n ((q_{x_i} - \overline{q_x})^2 + (q_{y_i} - \overline{q_y})^2)}{n}} \tag{2.6}$$

Here, $q_{x,y}$ are the x- and y-positions of the rays and n is the total number of rays. Often also a geometrical radius r_{GEO} is given which is calculated as given in equation 2.7

$$r_{GEO} = \max\left(\sqrt{\left(q_x - q_{x_0}\right)^2 + \left(q_y - q_{y_0}\right)^2}\right) \tag{2.7}$$

Here, q_{x_0,y_0} are the x- and y-positions of the center of the spot.

2.4.2 Zernike Wavefront Decomposition

Zernike polynomials are an infinite continuous and orthogonal sequence of polynomials over a unit circle, which give a mathematical description of a surface. It is used to identify the contribution of individual types of aberrations in a wavefront. An advantage of using Zernike polynomials is that because of the orthogonality, each polynomial can be calculated independent without affecting other polynomials. The magnitude of the polynomials indicate how much a certain aberration contributes to the total wavefront error. A disadvantage of using Zernike polynomials is that it can give a poor depiction of the wavefront in the mid- and high-spatial frequency errors. Even expanding to a large number of polynomials often still does not suffice. This becomes important because the discretization of the wavefront in a FEM analysis makes the Zernike wavefront decomposition less accurate, since Zernike polynomials are based on a continuous surface function. Also, local deformations typically need a lot of polynomials to represent them. In theory, by using an infinite amount of polynomials, every surface should be representable, but this makes it quickly impractical. Another disadvantage of using Zernike polynomials is that it is only orthogonal over a unit circle. So, for non-circular optics there is a loss in orthogonality. However, here 9 field points will be used which are all circular as described in section 2.2.

2.4.3 Maréchal criterion

The image quality of highly optimized optical systems that are well corrected can be evaluated by the Maréchal criterion. The Maréchal criterion states that the Strehl ratio should be higher than 0.8, which corresponds to a quarter-wave peak-to-valley optical path difference of the wavefront, in order to have a good image quality and the system to be considered diffraction-limited. To evaluate a wavefront for the Maréchal criterion, equation 2.8 is used. Here, S is the Strehl ratio and σ_W is the RMS wavefront error.

$$S \approx 1 - \frac{4\pi^2}{\lambda^2}\sigma_W^2 > 0,8 \Leftrightarrow \sigma_W < \frac{\lambda}{14} \tag{2.8}$$

Equation 2.8 shows that the Maréchal criterion is met when either the Strehl ratio is larger than 0.8, or equivalently, when the RMS wavefront error is smaller than a fourteenth of the wavelength.

Chapter 3

STOP Analysis

By performing a combined Structural, Thermal and Optical Performance (STOP) analysis, the optical performance and thermal and structural behaviour of the Wynne-Dyson projection lens system can be studied. STOP analysis is used to predict thermal effects on optical performance and is often used for applications with extreme environmental changes, for example in space travel purposes. There, the changes in temperature and mechanical loads on the systems have a significant impact on the optical performance. These environmental changes are much greater compared to the changes in a lithography system. However, in lithographic projection lens systems, even seemingly small thermal changes are significant enough to degrade optical performance. STOP analysis is therefore also suitable here to take into account the combined structural, thermal and optical behaviour.

3.1 Coupling of physics

STOP analysis helps to analyze the opto-mechanical performance by means of a multi-physics coupling between structural mechanics, heat transfer and geometrical optics. This coupling between the different types of physics is shown in the flow chart in figure 3.1

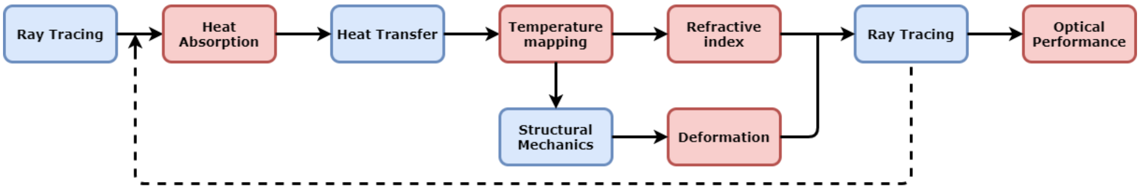

Figure 3.1: STOP Analysis implementation for lithography projection lens system

Initially, the temperature of the entire system is at room temperature and only intended stresses apply, for example when mounting the lenses. First, ray tracing is performed to calculate the absorbed power of the light by the lenses traveling in the intended optical ray paths. Because the lens elements are not ideally transparent, a small portion of the ray bundle will be attenuated in the form of local heat absorption. This causes local temperature changes in the lenses. With the obtained heat load, a heat transfer study is performed, which consists of conductive, convective and radiative heat transfer, to obtain a temperature mapping for the entire system (lenses, mirror, mountings, housing and insulating gas). Due to the temperature dependence of the refractive index, the temperature mapping is used to calculate a new refractive index mapping in the lenses. The temperature changes are also used in a structural mechanics study to calculate deformations of the lenses, mirror, mounts and housing. The deformations are caused by thermal expansion and thermal stresses which build up due to CTE mismatches. With the new refractive indices and the deformed structure, a ray tracing study is performed, from which the optical performance can be assessed.

In a typical STOP analysis, the optical path changes significantly after the system is deformed, causing the local heat absorption to also change in location. Therefore, the analysis is repeated with the new locally absorbed heat in the deformed system. This is iterated until a self-consistent solution is found for the degraded system. Notice that the feedback loop in figure 3.1 is a dashed line. This is because in the case of performing a STOP analysis for a lithographic projection lens system, the optical path of the rays does not change significantly to create a different heat absorption profile. Therefore, in the case of a lithographic projection lens system, no feedback iterations are needed and it can be considered as only a feedforward STOP analysis.

STOP analysis can be extended to also account for stress-induced birefringence, however, including this would extend the scope to wave optics along with geometrical optics. Also, the Wynne-Dyson projection lens system is highly optimized and no polarization effects are expected because of the low NA. It is also common in a STOP analysis to also include external mechanical loads, e.g. gravity or other external forces. However, these external loads are not relevant in a lithographic projection lens system. Therefore, only thermally induced mechanical loads are considered.

Optics

The optics in the STOP analysis serve two purposes. First, it is part of the multiphysics coupling from which the locally absorbed heat loads in the lenses are calculated by means of ray tracing. Second, it is to actually evaluate the optical performance in the thermally and structurally deformed lens system. Again, a ray tracing is performed, but the ray bundles are evaluated for optical performance indicators like spot diagrams, Zernike wavefront aberrations and the Maréchal criterion. Note that for a lithographic projection lens system, the ray tracing is not fed back to iterate the STOP analysis and therefore ray tracing is only performed twice in total.

Heat Transfer

The heat transfer in the STOP analysis requires a heat source from which to calculate a temperature change in the system. Based on the multiphysics coupling between the optics and heat transfer, a heat source is defined in the lenses from the locally absorbed ray power. By taking into account conductive, convective and radiative heat transfer, a temperature change in the system is obtained. The temperature change is then used in two multiphysics couplings. First with structural mechanics to calculate structural deformation. Second with optics to calculate changed refractive indices in the lenses.

Structural Mechanics

The structural mechanics in the STOP analysis requires a multiphysics coupling with the heat transfer to calculate the thermal expansion and thermal stresses from the temperature changes in the system. The structural deformations are also coupled to the optics, as this will directly degrade the optical performance due to the changes in geometry. Typically, external mechanical loads, e.g. gravitational or other external forces, are included. However, in a lithographic projection lens system these are not relevant. Therefore, only thermally induced mechanical loads are considered.

3.2 Lens heating

To reduce the cost per wafer, throughput is increased, which generally means a longer exposure time. This causes a local accumulation of light absorption in the lenses, which degrades the optical performance over time. This effect is referred to as lens heating.

Lens heating causes a temperature gradient in the lenses, due to local light absorption. The temperature typically becomes hotter in the center compared to the edge of the lenses. This inhomogeneous heating of the lenses causes a gradient in the refractive index, which is quantified by the thermo-optic coefficient dn/dT. The temperature gradient also causes mechanical stresses, which lead to deformations such as bulging of the optical surfaces. The mechanical stresses can also cause changes in refractive indices by means of the photoelastic effect. However, in the Wynne-Dyson projection lens system this can be neglected. These lensing effects form the basis of the lens heating effect. Typically, the change in refractive index and bulging of the optical surfaces are the most important effects.

Due to the change in geometry and refractive index of the lens elements, an optical path difference will occur, causing wavefront aberrations and reduced imaging performance. In addition to the deformation of the lens elements, the housing and lens mounts can also deform. This will result in positional shifts of the optical elements. Both the optical path difference and drift play a role in degrading the optical performance. These effects are shown in figure 3.2 of an exaggerated case of lens heating, which shows that the changed optical path due to lens heating in red. However, in a lithographic projection lens system, the change in the optical path is not significant enough to feed the ray tracing back in the STOP analysis and recalculate the local heat absorption of the light.

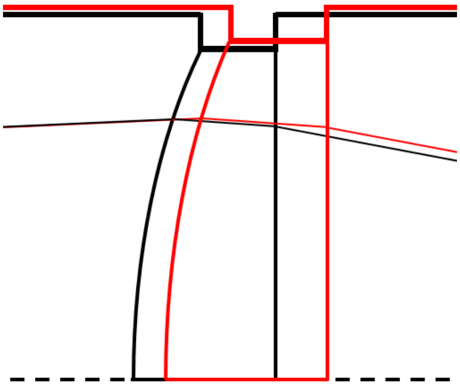

Figure 3.2: Exaggerated view of the change in optical path of a ray through a lens element which is deformed and shifted due to lens heating.

3.3 Previous lens heating analysis process

The current method of performing a lens heating analysis uses different software packages with many work-arounds to obtain reasonable results.

First, a ray tracing model is built in an optical design software package, such as Zemax or Code V. This is to obtain the distribution of absorbed power for each optical element, assuming certain illumination conditions (such as source power and spectrum, partial coherence factor, field geometry and reticle transmission). The absorbed power distribution is then imported into a finite element method (FEM) analysis software package, such as ANSYS, to analyze the thermal and structural behaviour of the optical elements. From this analysis, a temperature profile and the structural deformations are obtained, which are then imported into the optical design software to evaluate changes in the imaging performance. However, because of the structural deformations, the optical elements need to be modified to include the geometry changes. This is typically done by changing the optical surfaces by adding a thickness and using a Zernike polynomial model for the deformed surfaces. To describe changes in the refractive index according to temperature changes, a gradient index model is typically used. The ray tracing can then be performed again to analyze the optical performance.

The use of different software packages is not efficient, because different data points are used when exporting and importing data between software packages. The data needs to be interpolated, introducing additional numerical errors, which accumulates each time data is transferred. This method also makes it very difficult to analyze transient behaviour, as it needs to be iterated for multiple time instances where data from previous time instances is needed. Chapter 5 describes a modeling approach to perform a STOP analysis in a single software package, with which even the transient behaviour of a lithographic projection lens system can be modeled.

Chapter 4

Heat transfer

Once light passes through the lens system and is partially absorbed, local temperature changes occur in the lens elements. The temperature differences drive heat to be transferred through out the system in the form of conduction, convection and radiation. This chapter discusses the different heat transfer modes, as well as their significance and how they fit inside a lens heating model of a lithographic projection lens system.

4.1 Heat source

In lithographic projection lens systems, the main heat source is the absorption of light by the lenses. The heat source induces a local change in temperature, which eventually causes a temperature gradient to arise in the system. When considering two adjacent lenses inside a lens barrel, 3 heat paths can be identified as heat sources, which are described in table 4.1 and shown in figure 4.1. The absorption of the incoming light with the initial power by the first lens is the first heat source (A). The transmitted light from A is then partially absorbed in the second lens, which is the second heat source (B). The absorption of its transmitted light is then the heat source for the next lens (C). This is repeated for all subsequent lenses until the light passes through the entire system. Note that the power of the transmitted light decreases each time it passes through a lens. Therefore, with a Wynne-Dyson lens design, when the light passes through the lenses the second time after reflecting off the mirror, less power is absorbed. This causes an asymmetric heat source in each lens.

Heat path	Description
A	Absoption of light with initial power
B	Absorption of transmitted light from A
C	Transmitted light from B

Table 4.1: Description of the heat sources shown in figure 4.1.

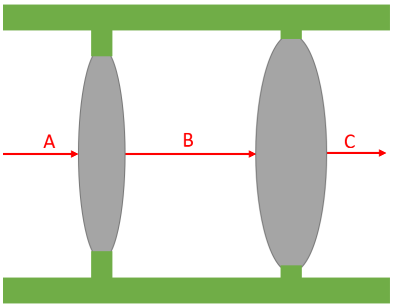

Figure 4.1: Overview of heat sources

4.2 Conduction

Once heat from the light is absorbed into the lenses, conduction is one of the heat transfer mechanisms to spread the heat throughout the system. Table 4.2 and figure 4.2 provide an overview of the conductive heat transfer paths in a lens system.

Heat path	**Description**
D	Conduction inside lens
E	Conduction from lens to housing
F	Conduction inside housing
G	Conduction form lens to stagnant gas
H	Conduction inside gas
I	Conduction from gas to housing

Table 4.2: Description of the conductive heat transfer paths shown in figure 4.2.

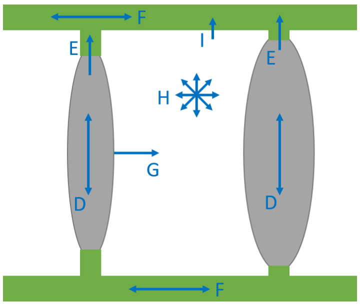

Figure 4.2: Overview of conductive heat transfer paths.

The heat transfer starts by spreading the heat inside the lenses by means of thermal conduction (D). At the edge of the lenses, heat is conducted into the housing (E). However, the lenses are mounted on lens mounts. Because the lenses are typically glued to the mount, they only make contact at certain points. The reduced contact area between a lens and the lens mount adds thermal resistance. The lens mounts also contain cutouts to create flexures, which also introduce thermal resistance, because the cross-sectional area for the conduction reduces. Both thermal resistances can be modeled as a thermal contact conductance (TCC) boundary layer. This is further elaborated in section 4.2.1. Once the heat has entered the mounts and housing, it will spread and conduct towards the colder outer rim of the housing (F). The optical surface area of the lens, which is not in contact with the mounts, is in contact with an insulating gas. When the gas is stagnant, there will be heat conducting from the lens into the gas (G). At the interfaces between gases and solids there is no thermal contact resistance. Typically, the conductivity of gases is very low, making it less effective at transferring heat from a lens into the gas compared to conduction to the housing. Once the gas starts flowing due to buoyancy forces, this heat transfer is considered as convection instead of conduction. Within the gas volume, heat also spreads by conduction (H). Since the gas is also in contact with the housing, heat is also transferred by means of conduction between the gas and the housing (I).

4.2.1 Thermal Contact Conductance

To more accurately predict the conductive heat transfer for a lithographic projection lens system, it is important to include thermal contact conductance (TCC) boundary conditions in the model. This is used to include the thermal resistances added by the interface between the lens and the lens mounts and the nest of flexures in the lens mounts.

To help understand what a TCC boundary condition is, this is first discussed in more detail. Looking at two objects in contact with each other, as shown in the left image of figure 4.3, it is assumed that the temperature at the interface of two objects is equal. This is only true if both surfaces are perfectly smooth and in full contact with each other. In reality, this is never the case, as both surfaces will have some degree of surface roughness. Therefore, the contact area will be smaller. In the gaps convection and radiation are the main forms of heat transfer. If the objects are in vacuum, only radiative heat transfer applies. The heat transfer in the gap and the smaller contact area adds an additional resistance between two objects in contact, called the contact resistance. The thermal contact conductance and resistance are the inverse of each other. The temperature of the two objects at the interface is different due to the added thermal resistance, as shown in the right image of figure 4.3.

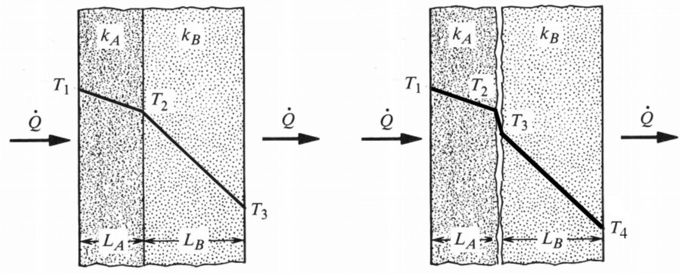

Figure 4.3: Left: Ideal contact between surfaces. Right: Surface roughness reducing contacting points between surfaces.

If a liquid or a gas is in contact with a solid, they can fill in the gaps and conduction can occur throughout the entire interface. Therefore, when gluing a lens to a mount, there is negligible thermal contact resistance in the contact area. However, when looking at an example of a lens mount as shown in figure 4.4, it becomes clear that only a fraction of the edge of the lens is in contact with the adhesive, therefore reducing the conduction area. Also, in the flexure structure, the cross-sectional area becomes thinner, which adds additional conduction resistance.

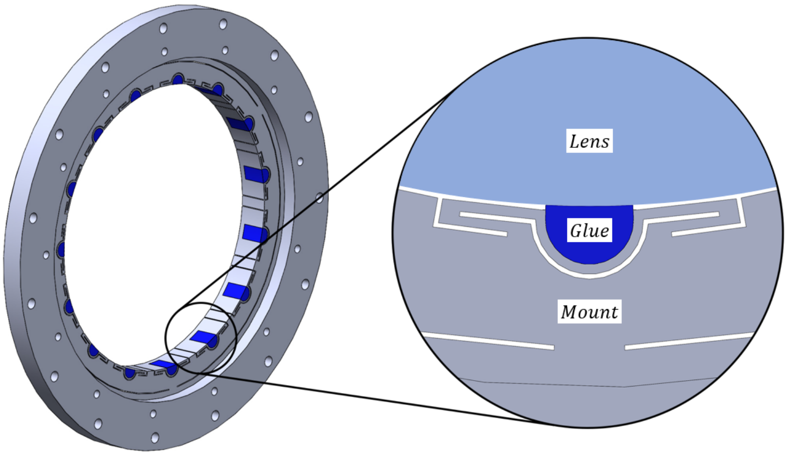

Figure 4.4: Example of a lens mount with a nest of flexures and the adhesive marked in blue.

Modeling the flexures in a FEM simulation would make the model computationally expensive and inefficient. Instead, the mount and adhesive can be modeled as a single solid ring with a thermal contact conductance boundary condition layer at the interface of the lens and the solid ring.

To calculate the equivalent TCC of the solid ring as that of the lens mount, a single flexure is modeled as shown in figure 4.5. From the top-side a power source of 1 W is applied, while the bottom-side is fixed at T_0. This creates a temperature gradient in the flexure. Dividing the temperature difference by the 1 W of power, gives the value for the thermal contact resistance of the single flexure. This is then divided by the number of flexures since the flexures are in parallel with each other. Now taking the inverse and also dividing by the area of the interface between the lenses and the mount gives the equivalent TCC value. This comes down to equation 4.1. There, n is the number of flexures, $\dot{Q}$ is the input power, ΔT is the temperature difference and A is the total area of the interface between the lenses and the mount.

$$TCC = \frac{n\dot{Q}}{A\Delta T} \tag{4.1}$$

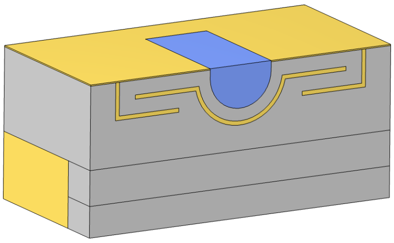

Figure 4.5: Single flexure from the flexure nest of a lens mount. adhesive is marked blue, gas in yellow.

Note that in the mount from figure 4.4 there are two flexure groups. The first one contains 15 flexures, where the adhesive can be applied. The second group contains only 3 flexures. In the flexure model from figure 4.5 only the first group is included in the geometry. The second flexure group can be included by adding a TCC boundary condition. The value of this TCC can be calculated with the following equation.

$$TCC = \frac{k_{\text{gas}}A_{\text{gas}} + k_{\text{metal}}A_{\text{metal}}}{t_{\text{gap}}A_{\text{tot}}} \tag{4.2}$$

Here, k_i is the thermal conductivity of the respective medium, A_i is the cross-sectional area and t_{gap} is the thickness of the gap.

4.3 Convection

After the heat is conducted throughout the system and reaches interfaces with air or the insulating gas, convective heat transfer can take place at these interfaces. Table 4.3 and figure 4.6 show an overview of the convective heat transfer paths in a lens system.

Heat path	**Description**
J	Convection from lens to gas
K	Convection from gas to housing
L	Convection from housing to ambient

Table 4.3: Description of the convective heat transfer paths shown in figure 4.6.

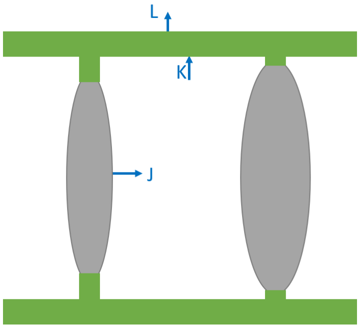

Figure 4.6: Overview of convective heat transfer paths.

Looking at the convective heat transfer from the lens to the gas, a natural convective boundary layer can form on the lens surface. As the gas heats up, it will rise due to the buoyancy forces, creating a flow that transfers heat from the lens to the gas (J). The gas rises until it reaches the housing, where the relatively hot gas will transfer its heat to the housing (K) and the cooled air descends down. The flow describes 2 vortices, which meet somewhere in the middle, because convection takes place on both opposing lens surfaces. On the external surfaces of the lens system, heat is transferred by means of convection (L). This can be forced or natural convection, depending on the environmental conditions. However, for convective heat transfer to be significant, the convective heat transfer coefficient h_c must be evaluated.

4.3.1 Heat transfer coefficient inside an enclosed cylinder

For most simple geometries, there are general empirical relations available that can be used to derive the convective heat transfer coefficient h_c. However, an enclosed horizontal cylinder that is heated on two sides and cooled on the cylindrical surface is actually a complex problem. Especially since the heated surfaces are lens surfaces, which are curved. To simplify the geometry, the curvature of the lenses is neglected. This gives the geometry of figure 4.7a. However, even for this geometry no empirical relations are found. To get a feeling for the order of h_c, an enclosed box can be considered where 1 side is hot, the opposite side is cold and the other surfaces are thermally insulated, as shown in figure 4.7b. In this case, the cold side is assumed to be the center of the actual enclosed cylindrical cell and therefore the width of the box is taken only half the length of the cylinder.

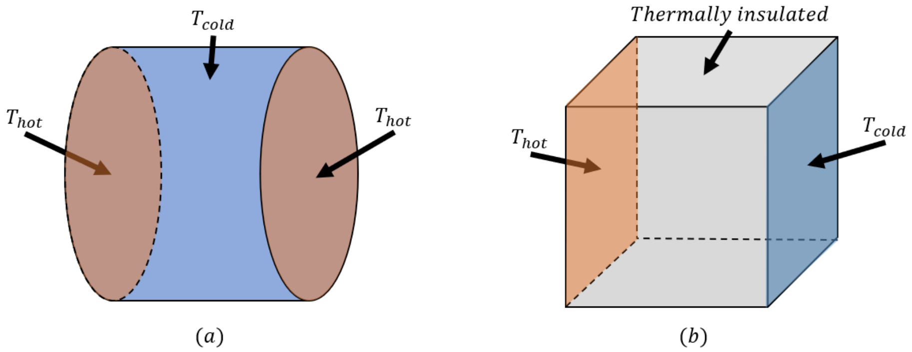

(a)

(b)

Figure 4.7: Geometry simplifications to determine h_c inside an enclosed cell.

To estimate the heat transfer coefficient, empirical relations for the Nusselt number are used. The Nusselt number is a dimensionless number that gives the ratio of convective to conductive heat transfer at a boundary, as given in the equation below.

$$\mathrm{Nu}_H = \frac{h_c}{k/H} \tag{4.3}$$

Here, h_c is the convective heat transfer coefficient, k is the thermal conductivity of the fluid and H is the characteristic length. Because k and H are generally constant, the Nusselt number can be seen as a dimensionless heat transfer coefficient. For the geometry from figure 4.7b, equations 4.4[9] and 4.5[10] can be used to estimate the average Nusselt number, from which h_c can be derived.

$$\overline{\mathrm{Nu}}_H = 0.22\left(\frac{\mathrm{Pr}}{0.2+\mathrm{Pr}}\mathrm{Ra}_H\right)^{0.28}\left(\frac{L}{H}\right)^{0.09} \tag{4.4}$$

$$\overline{\mathrm{Nu}}_H = 0.256\left(\mathrm{Gr}_H\right)^{0.24} \tag{4.5}$$

Here, $\overline{\mathrm{Nu}}_H$ is the average Nusselt number with the height of the box as the characteristic length, Pr is the dimensionless Prandtl number defined as the ratio of momentum diffusivity to thermal diffusivity and Ra_H is the dimensionless Rayleigh number associated with buoyancy-driven flow, and L is the length of the box.

Filling in appropriate numbers corresponding to an enclosure as found in a typical projection lens system, a value for h_c is found between 0.75-0.87 W/(m^{2}K), depending on the geometry of the cell. However, the volume in the cylindrical enclosure is smaller compared to the enclosed box when using the same height and length. Also, the curvature of the lenses and the cylindrical barrel, restrain the development of a convective boundary layer. In the projection lens system, the lenses are locally heated, which means that most of the convective heat transfer happens locally, but equations 4.4 and 4.5 assume an average heat transfer coefficient over the entire hot surface. For these reasons, the calculated h_c for an enclosed box gives an overestimation for the convection in a lens system. The convective heat transfer in the enclosure of a lens system is thus even smaller to a point that it can be modelled as a stagnant gas, especially when the temperature difference between the lens and the gas is expected to be small. Therefore, instead of convection, only conduction from the lens to the gas will be considered.

4.3.2 Heat transfer coefficient on a horizontal cylinder

The convection on the outside of the housing can be either natural or forced convection, depending on design choices. For natural convection, equation 4.6 can be used, which gives a value of $h_c = 1$ W/(m^{2}K) assuming a difference of 0.2 K between the housing and the ambient temperature.

$$\overline{\mathrm{Nu}}_D = 0.36 + \frac{0.518\mathrm{Ra}_D^{1/4}}{[1+(0.559/\mathrm{Pr})^{9/16}]^{4/9}} \quad \text{for} \quad 10^{-6} < \mathrm{Ra}_D \lesssim 10^9 \tag{4.6}$$

Here, $\overline{\mathrm{Nu}}_D$ and Ra_D are the average Nusselt number and Rayleigh number respectively, with the diameter of the cylinder D as the characteristic length and Pr is the Prandtl number.

By applying an airflow over the cylinder, forced convection can be induced. Flow across a cylinder is strongly dependent on the dimensionless Reynolds number Re, because it determines what kind of flow regime is present by taking the undisturbed flow velocity into account. Equation 4.7 gives empirical relations for the average Nusselt number for different Reynolds numbers, which are valid for Pr > 0.5. A flow velocity of 0.65 m/s, which is a typical value for fan-filter modules used in lithography machines, gives $h_c = 6.2$ W/(m^{2}K), assuming that the temperature difference is 0.2 K between the housing and the ambient temperature.

$$
\begin{gathered}
\overline{\mathrm{Nu}}_D = 0.3 + \frac{0.62\,\mathrm{Re}_D^{1/2}\,\mathrm{Pr}^{1/3}}{\left[1+(0.4/\,\mathrm{Pr})^{2/3}\right]^{1/4}}; \quad \mathrm{Re}_D < 10^4 \\
\overline{\mathrm{Nu}}_D = 0.3 + \frac{0.62\,\mathrm{Re}_D^{1/2}\,\mathrm{Pr}^{1/3}}{\left[1+(0.4/\,\mathrm{Pr})^{2/3}\right]^{1/4}} \left[1+\left(\frac{\mathrm{Re}_D}{282{,}000}\right)^{1/2}\right]; \quad 2\times10^4 < \mathrm{Re}_D < 4\times10^5 \qquad (4.7) \\
\overline{\mathrm{Nu}}_D = 0.3 + \frac{0.62\,\mathrm{Re}_D^{1/2}\,\mathrm{Pr}^{1/3}}{\left[1+(0.4/\,\mathrm{Pr})^{2/3}\right]^{1/4}} \left[1+\left(\frac{\mathrm{Re}_D}{282{,}000}\right)^{5/8}\right]^{4/5}; \quad 4\times10^5 < \mathrm{Re}_D < 5\times10^6
\end{gathered}
$$

4.4 Radiation

When dealing with radiative heat transfer, surfaces emit, absorb, transmit and reflect radiation. The fraction of the irradiation that is absorbed is called the absorptance α. Surfaces where α is constant and does not depend on the incident angle of the irradiation is called a gray body. The fraction of reflected radiation is called the reflectance ρ. If the body is not (completely) opaque, there is also some transmittance τ going through the material. This can often be neglected for thermal radiation, but will be verified experimentally for lenses in section 4.6.1. Since all incoming radiation has to be either absorbed, reflected or transmitted, equation 4.8 below is obtained.

$$\alpha + \rho + \tau = 1 \tag{4.8}$$

A surface also emits radiation. The ratio of energy emitted by a surface to the energy emitted by an equivalent ideal black surface at the same temperature is called the emissivity ϵ. For gray bodies $\epsilon = \alpha$. A surface with a value of $\epsilon = 1$ is an ideal black surface. A value of $\epsilon = 0$ corresponds to an ideal thermal mirror. Real surfaces have an emissivity between 0 and 1.

In a projection lens system, besides conduction and convection, there will also be radiative heat transfer, which plays an important role in the total heat transfer in lithographic projection lens systems. Table 4.4 and figure 4.8 provide an overview of the radiative heat transfer paths in a lens system.

Heat path	Description
M	Radiation between lenses
N	Radiation between housing and lens
O	Radiation between housing
P	Radiation between housing and ambient

Table 4.4: Description of the radiative heat transfer paths shown in figure 4.8.

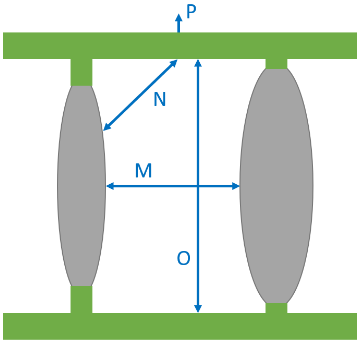

Figure 4.8: Overview of radiative heat transfer paths.

Inside the enclosed cell constructed by two lenses and the housing, radiative heat transfer takes place between surfaces that are in view of each other. The amount of heat transfer is a function of the emissivity, view factor and temperature. Because the emissivity is an important parameter for heat transfer, it will be elaborated further in section 4.4.1. The temperature is proportional to the fourth power, making it more significant at small temperature differences compared to convection and conduction when the enclosure is filled with a stagnant insulating gas.

Inside the enclosure, radiative heat transfer takes place between lens surfaces facing each other (M), from the lens surfaces to the housing (N), and between the housing surfaces facing each other (O). The heat exchange between a lens surface and the housing (M) will be the most dominant of the radiative heat transfer paths in the enclosure. This is because the temperature difference between the lens surfaces and the housing is the largest in the enclosure.

On the external surface of the housing, there is also radiative heat exchange with the surroundings (P). The significance of this strongly depends on the emissivity and the surrounding radiation. Metals such as aluminium typically have a low emissivity (∼0.05) making the radiative heat transfer inefficient and convection will dominate in this case. However, the surface can be treated to have a high emissivity (∼0.95). This makes the amount of radiative heat transfer comparable to the convective heat transfer (assuming $h_c = 5$ W/(m^{2}K)). The disadvantage is that heat from the surroundings also get absorbed. So, if there are other hot objects in the vicinity, the housing will absorb the heat radiating from them. The view factor of distant objects, however, reduces the radiative heat transfer. Nevertheless, this will be an external heat source that is difficult to evaluate and control. Therefore, the metal surface is not treated and maintains its low emissivity, and thus the radiative heat exchange with the surroundings (P) can be neglected.

4.4.1 Emissivity

The emissivity is a material property defined as the ratio between the emitted power of a surface to the emitted power of the black body equivalent of that surface under the same conditions. The emissivity can depend on wavelength, direction and temperature. Because the temperature dependence is negligible for small temperature changes, only the spectral and directional dependence of the emissivity are taken into account. When the emissivity is constant for all wavelengths, the surface is considered a gray surface. If it is also direction independent, it is called a diffuse gray surface. When talking about emissivity, it is important to know the difference between hemispherical, directional, total and spectral emissivity. Hemispherical and directional govern the directional dependence of emissivity, while total and spectral govern the spectral dependency. In table 4.5 below, 4 definitions are given for the emissivity.[11]

Table 4.5: Definitions of combinations of hemispherical or directional, and total or spectral emissivity.

	Hemispherical	**Directional**
Total	$\epsilon = \frac{I}{I_b}$	$\epsilon'(\theta, \phi) = \frac{I^+(\theta,\phi)}{I_b}$
Spectral	$\epsilon_\lambda(\lambda) = \frac{I_\lambda(\lambda)}{I_{b\lambda}(\lambda)}$	$\epsilon'_\lambda(\theta, \phi, \lambda) = \frac{I^+_\lambda(\theta,\phi,\lambda)}{I_{b\lambda}(\lambda)}$

The emissivity can have a value between 0 and 1, where 1 corresponds to the surface being an ideal black surface and 0 to an ideal thermal mirror. Real surfaces never reach these ideal values, however there are materials that get pretty close. Polished glass for example can reach a total hemispherical emissivity of 0.92[12], while the surface of polished aluminium can be as low as 0.05[13].

Hemispherical vs directional

The emissivity is typically given as the hemispherical emissivity, which is an averaged emissivity over a hemisphere. Diffuse gray surfaces obey Lambert's law, which states that the intensity of the emitted radiation is independent of the direction. Therefore, the emittance and reflectance of a diffuse gray surface are independent of the zenith angle. In that case, even looking at a surface from grazing angles would give similar intensities as looking from the normal of the surface. This is not the case for real surfaces. There, the emissivity decreases for larger zenith angles. Figure 4.9 shows the directional dependency of the emissivity for some materials. For glasses, the emissivity typically starts decreasing for zenith angles larger than 60°.

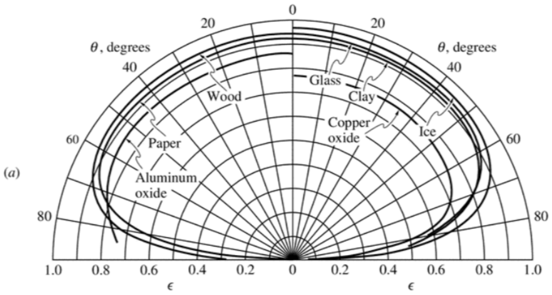

Figure 4.9: Directional emissivity for several materials.[12]

In the enclosure, only a small part of the radiation from the lenses reaches the housing within a zenith angle smaller than 60°, as can be seen in figure 4.10. A large portion of the radiation goes towards the opposite lens surface, which is also a relatively hot surface compared to the housing. Due to the relatively small temperature difference between the lens surfaces, no effective heat transfer is radiated away from the lenses. The portion of the radiation directed towards the housing that is within 60° zenith angle can also become less effective if the surface of the housing also has a strong directional dependent emissivity. Therefore, by assuming a diffuse hemispherical emissivity, the radiative heat transfer is overestimated. It is therefore important to take into account the directional dependency of emissivity for all surfaces. To determine the directional dependency, the results of the experiment described in section 4.6.2 will be used.

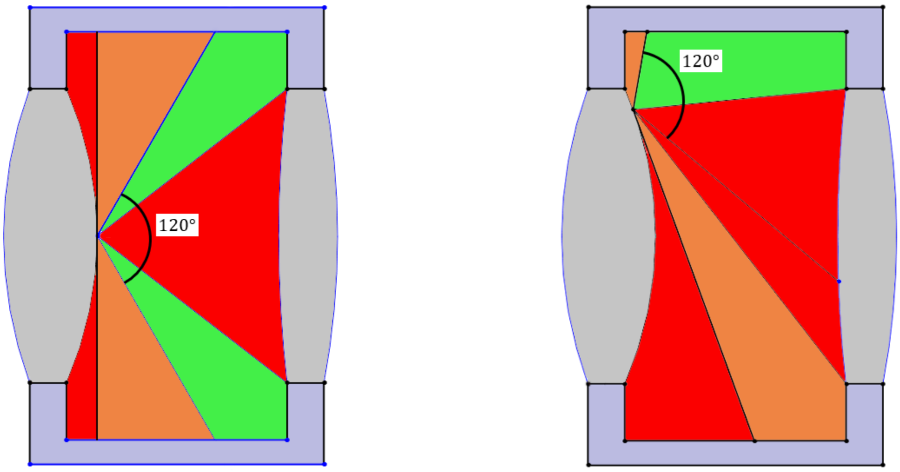

Figure 4.10: Radiative heat transfer when directional emissivity is added. Green: high effective heat transfer. Orange: low effective heat transfer. Red: no effective heat transfer.

Spectral vs total

Real surfaces are never truly black or gray, but the wavelength dependence can often be considered constant for the wavelength range where thermal radiation is applicable. Therefore, the spectral dependence of the emissivity can be neglected.

4.5 Analytic heat transfer balance for single lens

Having an analytical model is a tool to gain confidence in FEM simulation results. The FEM results should be in line with the analytical model. However, it is unfeasible to create an analytical model for the complete Wynne-Dyson projection lens system and include all heat transfer paths. Therefore, an analytical model of a single lens is considered. The main purpose of the analytical model is to give an impression of how the heat transfer is distributed between conduction, convection and radiation and to give an indication of the temperature profile for a single lens.

4.5.1 Analytical model

The single lens is modeled as two annular fins of radius r_1 and r_2, with the inner fin containing internal heat generation, which represents the absorbed heat from the light. On the optical surfaces of the lens convective $\dot{Q}_{\text{conv}}$ and radiative $\dot{Q}_{\text{rad}}$ heat transfer is included. Inside the lens conductive heat transfer $\dot{Q}_{\text{cond}}$ is included. The absorption of light is applied only to the inner annular fin, where it generates internal volumetric heat $\dot{Q}'''_{\text{gen}}$. Figure 4.11 shows the lens with the heat transfer paths and the heat generation in the orange section.

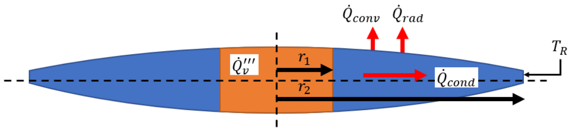

Figure 4.11: Schematic drawing of the analytical model of heat transfer in a single lens.

Heat balance

The heat transfer balance for the analytical model from figure 4.11 is given in equation 4.9 when the lens is in steady-state. Note that for the outer fin $\dot{Q}'''_{\text{gen}} = 0$ and this term drops out of the heat balance.

$$\begin{aligned}
\dot{Q}_{\text{cond}}\Big|_{r} - \dot{Q}_{\text{cond}}\Big|_{r+\Delta r} - 2\dot{Q}_{\text{conv}} - 2\dot{Q}_{\text{rad}} + \dot{Q}'''_{\text{gen}} 2\pi r \Delta r t(r) = 0 \\
\dot{Q}_{\text{cond}} = -2\pi r t(r) k \frac{dT}{dr} \\
\dot{Q}_{\text{conv}} = 2\pi r \Delta r h_c \left(T - T_e\right) \\
\dot{Q}_{\text{rad}} = 2\pi r \Delta r \epsilon \sigma 4 T_M^3 \left(T - T_e\right) \\
\dot{Q}'''_{\text{gen}} = \alpha t(r) I(r)
\end{aligned} \tag{4.9}$$

The convective and radiative heat transfer terms $\dot{Q}_{\text{conv}}$ and $\dot{Q}_{\text{rad}}$ are multiplied by 2 because convection and radiation happens on both sides of the lens. To make the analytical model more simple to solve, the lens is assumed to have a constant thickness, making it a flat disk. Also, the intensity of the light is assumed to be constant for $r \leq r_1$. For $r > r_1$ the intensity is zero. After the simplifications, the differential equations from equation 4.10 are obtained.

$$\begin{cases} r \leq r_1 & r^2 \frac{d^2T}{dr^2} + r\frac{dT}{dr} - \left(\frac{2h_c + 2\epsilon\sigma 4 T_M^3}{kt}\right)\left(T - T_e\right) r^2 + \frac{\alpha}{k} I(r) r^2 = 0 \\ r_1 < r \leq r_2 & r^2 \frac{d^2T}{dr^2} + r\frac{dT}{dr} - \left(\frac{2h_c + 2\epsilon\sigma 4 T_M^3}{kt}\right)\left(T - T_e\right) r^2 = 0 \end{cases} \tag{4.10}$$

Solving differential equations

To solve the differential equations, the equations are rewritten in the following form:

$$z^2 \frac{d^2\theta_{1,2}}{dz^2} + z\frac{d\theta_{1,2}}{dz} - z^2 \theta_{1,2} = 0 \tag{4.11}$$

This is a modified Bessel's differential equation of zero order and has the following solutions:

$$\begin{aligned} \theta_1 = C_1 I_0(z) + C_2 K_0(z) \\ \theta_2 = C_3 I_0(z) + C_4 K_0(z) \end{aligned} \tag{4.12}$$

Here, θ_1 and θ_2 are solutions for the inner and outer annular disks respectively, I_0 and K_0 are zero-order modified Bessel functions of the first and second kind respectively. To calculate the constants C_1 to C_4, 4 boundary conditions are needed. The boundary conditions are given in equation 4.13.

$$\begin{aligned} r = 0 \rightarrow \frac{dT_1}{dr} = 0 \\ r = r_1 \rightarrow T_1 = T_2 \\ r = r_1 \rightarrow \frac{dT_1}{dr} = \frac{dT_2}{dr} \\ r = r_2 \rightarrow T_2 = T_R \end{aligned} \tag{4.13}$$

The first boundary condition provides a symmetry in the temperature around the center of the lens. The second and third boundary conditions cause the two temperature functions obtained from the two differential equations to have the same value and slope at $r = r_1$. The fourth boundary condition sets the temperature at the edge of the lens at T_R. Rewriting the boundary conditions in the same form as equation 4.12 and solving for the constants

C_1 to C_4, two functions for the temperature are obtained, $T_1(r)$ and $T_2(r)$. $T_1(r)$ and $T_2(r)$ are only valid for $r \leq r_1$ and $r_1 \leq r \leq r_2$ respectively.

4.5.2 Analytic results

With the temperature functions $T_1(r)$ and $T_2(r)$, typical values for lens are tested to obtain a temperature profile inside the lens. The heat source is applied on the center of the lens for $r < r_{\text{lens}}/2$. For comparison, the same model is build in COMSOL Multiphysics, to check how much the analytical model and COMSOL model correspond with each other. The left plot in figure 4.12 shows the average radial temperature profile obtained from the analytical model and the COMSOL model. The right plot shows the difference between the analytical model and the COMSOL model.

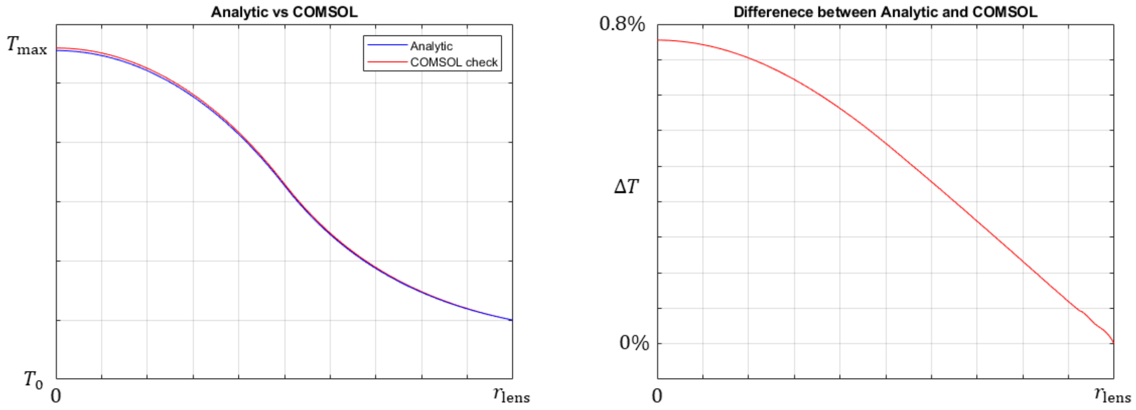

Figure 4.12: Average radial temperature plot from the analytic and COMSOL model for a single lens as shown in figure 4.11.

The shape of the curves in the left image show that the center has the highest temperature and gradually lowers as it reaches the edge of the lens. This is as expected because the center is also where the heat source is located. From the turning point where the curves become decreasingly decaying, no heat source is applied. The maximum temperature difference between the analytical model and the COMSOL model accounts for $\sim 0.8\%$ of the total temperature difference in the lens, from which can be concluded that the analytical model and COMSOL model correspond well with each other.

To compare the heat transfer distribution between conductive, radiative and convective heat transfer in a lens, table 4.6 shows the percentage of heat transfer per heat transfer mode as a percentage of the total heat generated. Since the heat transfer in the lens is solved at steady state, the balance adds up to zero.

Table 4.6: Heat transfer distribution by conduction, radiation and convection according to the analytical and COMSOL model of a single lens as shown in figure 4.11.

	Analytic	**COMSOL**
Heat generation	100%	100%
Conductive HT	-19%	-20%
Radiative HT	-69%	-68%
Convective HT	-12%	-12%
Balance	0%	0%

Table 4.6 shows that radiation plays a dominant role in the heat transfer. This indicates that in the actual model of the Wynne-Dyson projection lens system, radiation must be accurately modeled in order to obtain accurate results of the total heat transfer. The contribution of conduction and convection in the total heat transfer is smaller, but not negligible. Especially when including directional emissivity, the radiative heat transfer contribution will drop and this will mainly result in more conductive heat transfer. Convection will not change much because of the stagnant and insulating gas.

4.6 Radiative heat transfer experiments

4.6.1 Lens heat transmission

To justify that the lenses in the FEM model can be assumed to be completely opaque to thermal radiation, the transmittance τ of a typical lens from a lithography system is measured.

Method

To measure the transmittance, a thermal camera, a lens and a hot object are needed. With the thermal camera a thermal image of the lens is taken where a hot object is located partially behind the lens. Figure 4.13 shows the setup where a hot plate is placed behind a lens. Here, the setup is placed inside an incubator to block external irradiation and to control the ambient temperature. Only one hole is left open to perform measurements. The ambient temperature is controlled around 25 °C, the hot plate has a temperature of approximately 38.7 °C and the lens surface is at approximately 19.4 °C. The normal image shows that part of the hot plate is visible through the lens. If there would be any significant transmission of thermal radiation through the lens, it would be visible in the thermal image as well. The black tape on the lens is for the directional emissivity experiment from section 4.6.2.

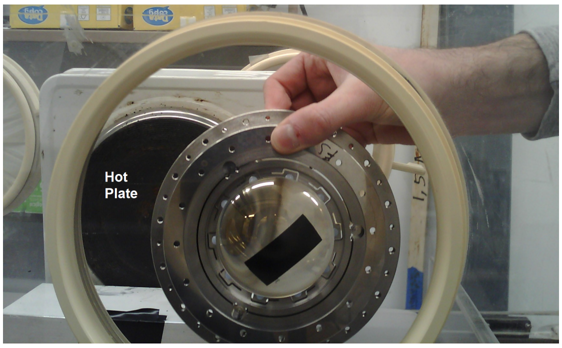

Figure 4.13: Experimental setup to measure transmission of thermal radiation through a lens.

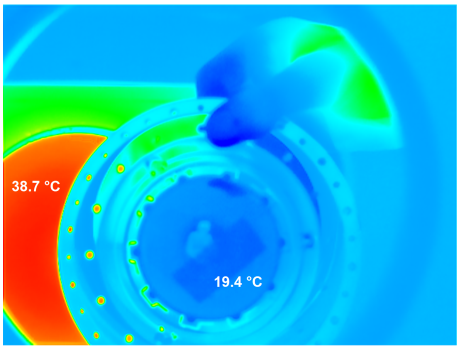

Figure 4.14: Thermal image of a lens in front of a hot plate to measure transmission of thermal radiation.

Results and conclusion

Looking at the thermal image in figure 4.14, it can be seen that no traces of the hot plate are visible through the lens, as the lens surface is evenly colored where the hot plate is expected. However, the thermal reflection from the person behind the thermal camera and some reflection from the finger holding the lens are visible, which indicates that the reflectivity ρ is more significant than the transmission τ. Also, the tape which has a different emissivity than the lens surface is visible in the thermal image, even though it has the same temperature as the lens surface. This is the reason not to include a temperature scale in the image, because the scale would be set for a specific emissivity. But since not every surface in the image has the same emissivity, the scale would indicate a wrong temperature. From this experiment it can be concluded that a typical lithography lens can be assumed to have zero transmittance ($\tau = 0$).

4.6.2 Directional emissivity

Radiative heat transfer inside the projection lens system will be effectively between the lens surfaces and the housing, which is a dominant heat transfer path. Because the direction of the radiation from the lens surfaces to the housing has large zenith angles w.r.t. the lens surfaces, the emissivity decreases with increasing zenith angle. To include the directional dependency of the emissivity in the FEM model, it must first be determined experimentally for typical lithography lenses.

Method

To determine the directional dependency of the emissivity, the following equipment is needed:

- Lens
- Lens mount
- Thermal camera
- Black electrical tape
- Protractor
- Thermocouple
- Incubator
- Bucket with hot water

On the lens surface, first some 3M Scotch Super 33+ black electrical tape is stuck, which has a hemispherical emissivity of 0.95 for a spectral range of 8-14 µm[13], which corresponds to the spectral detection range of the thermal camera. The tape will have the same surface temperature as the lens surface. Since the emissivity of the tape is known, it will be a reference to calibrate the emissivity of the lens to match the surface temperature of the lens to the temperature of the tape.

The lens is then uniformly heated in a bucket of hot water to a temperature of about 40 °C. Once heated up, the lens is attached to a mount and placed in the incubator. The incubator is again used to block external irradiation and to regulate the ambient temperature. With the thermocouple, the ambient temperature in the incubator is measured. One hole of the incubator is left open to allow the thermal camera to look inside the incubator and perform measurements. An additional sheet of foam is placed inside the incubator to block the reflections from the internal surfaces of the incubator. A schematic drawing of the setup is shown in figure 4.15. The real setup is shown in figure 4.16.

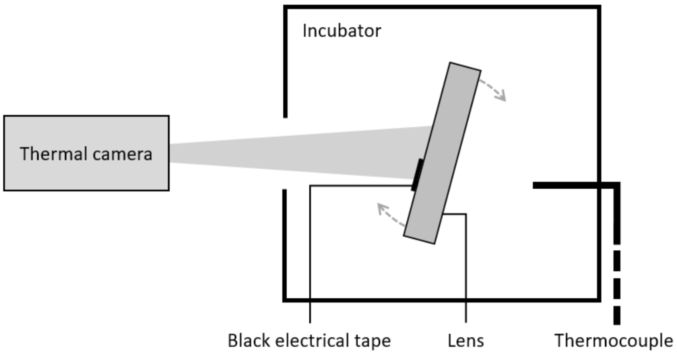

Figure 4.15: Schematic drawing of the setup to determine the directional dependency of the emissivity of a lithography lens.

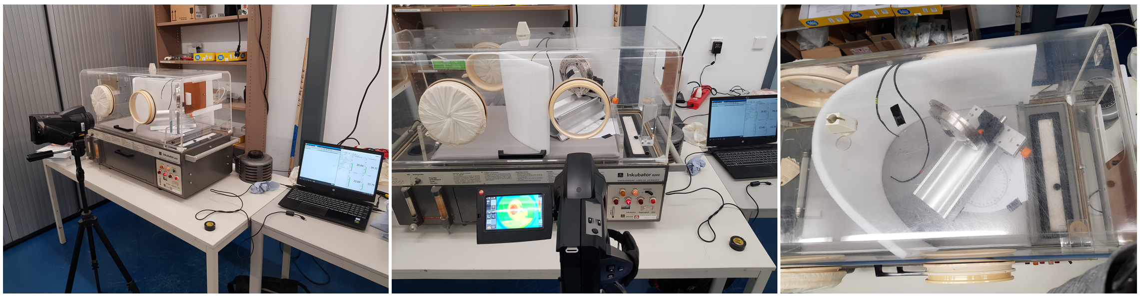

Figure 4.16: Experimental setup to determine the directional dependency of the emissivity of a lithography lens.

Once the setup is made, measurements can be performed. Thermal images are taken of the lens from different angles by rotating the lens. During the post-processing of the thermal images, the temperature of the lens is matched to the temperature of the tape by adjusting the emissivity. The measurements are done for angles between 0° and 80° in steps of 10°.

To use the tape as a reference for the temperature, its directional dependence of the emissivity needs to be known as well, especially for large zenith angles. To determine this, the same setup is used, except that the tape is applied on a block of aluminium which has a thermocouple inside it to measure the temperature. Also, the aluminium block is continuously heated on a hot plate. Since aluminium has a high thermal conductivity, the temperature is assumed to be homogeneous. The temperature measurement from the thermocouple is then used as a reference to determine the directional emissivity of the tape. A schematic drawing of the slightly changed setup is shown in figure 4.17.

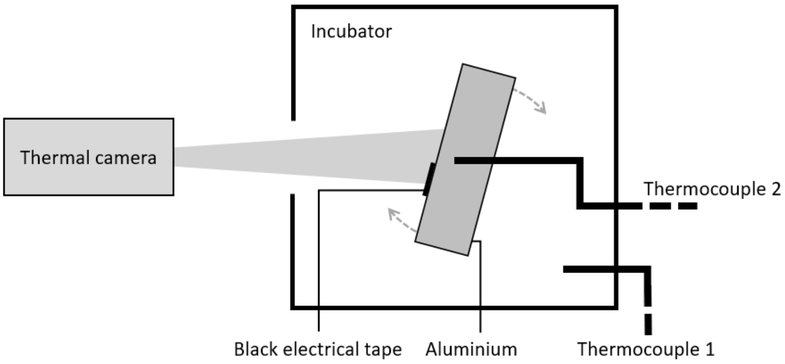

Figure 4.17: Schematic drawing of the setup to determine the directional dependency of the emissivity of the reference tape.

Results and conclusion

First, the directional dependency of the emissivity of the tape is measured. Figure 4.18 shows the experimental setup of a measurement of the tape on the aluminium block. The aluminium block is covered with other high emissivity tapes, but here only the black tape on the left surface is of interest. Figure 4.19 shows the corresponding thermal image.

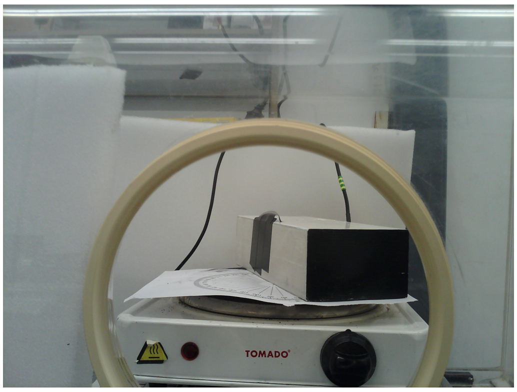

Figure 4.18: Experimental setup to measure the directional dependency of the emissivity.

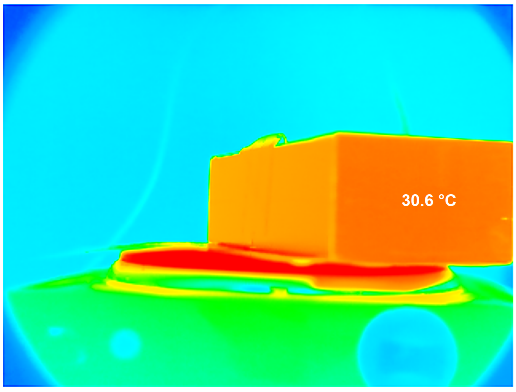

Figure 4.19: Thermal image to measure the directional dependency of the emissivity of the reference tape.

By repeating the measurements for different angles, the emissivity can be determined, from which the plot from figure 4.20 is created. The plot also contains the fitted function from equation 4.14, which will be used in the FEM model. The plot shows a strong decrease in emissivity for large zenith angles. This means that the emissivity of the reference tape, which is considered to have a high hemispherical emissivity, also has a significant directional dependency.

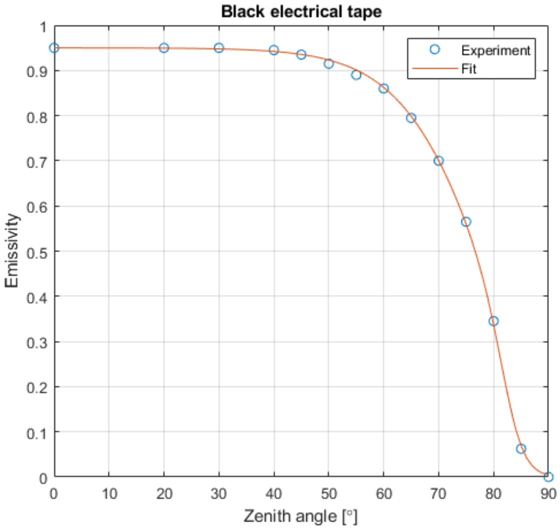

Figure 4.20: Emissivity against zenith angle plots for the black reference tape.

$$f_{\text{tape}}(\theta) = 0.95\left(1 - \frac{1}{1 + exp(\frac{78.3° - |\theta|}{8}))}\right)\left(1 - \frac{1}{1 + exp(\frac{82.7° - |\theta|}{2}))}\right) \tag{4.14}$$

With the directional emissivity obtained for the reference tape, measurements are performed for a fused silica lens and an I-line glass lens. Figure 4.21 shows an image of the setup for one of the measurement samples on the fused silica lens. Figure 4.22 shows the corresponding thermal image.

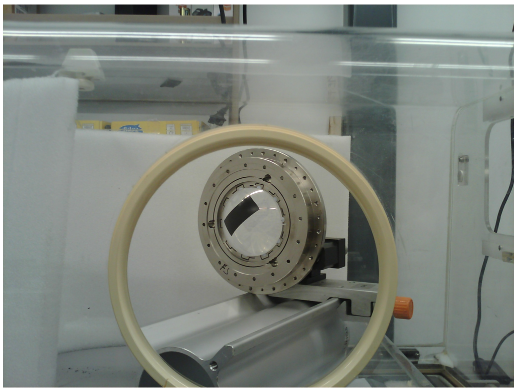

Figure 4.21: Experimental setup to measure the directional dependency of the emissivity.

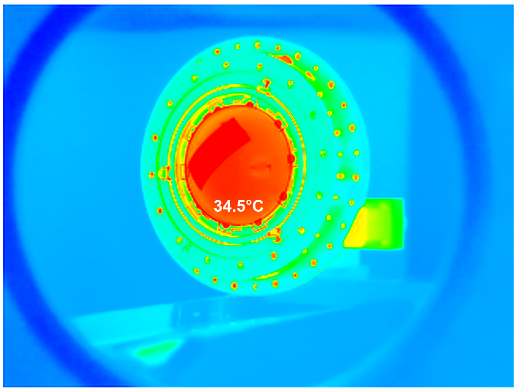

Figure 4.22: Thermal image of a heated lens to measure the directional dependency of the emissivity.

The thermal image from figure 4.22 clearly shows the reference tape which has a darker color, meaning it has a higher emissivity than the lens surface, since their surface temperatures are the same. Also, a gradient towards the edge is visible on the lens surface, which is because the lens has a spherical surface, and thus multiple zenith angles are visible in a single measurement. The gradient becomes more apparent when looking at different angles, as shown in figure 4.23 for the fused silica lens and in figure 4.24 for the I-line glass lens. There the color mapping indicates the emissivity. The figures show that the emissivity decreases with increasing zenith angles.

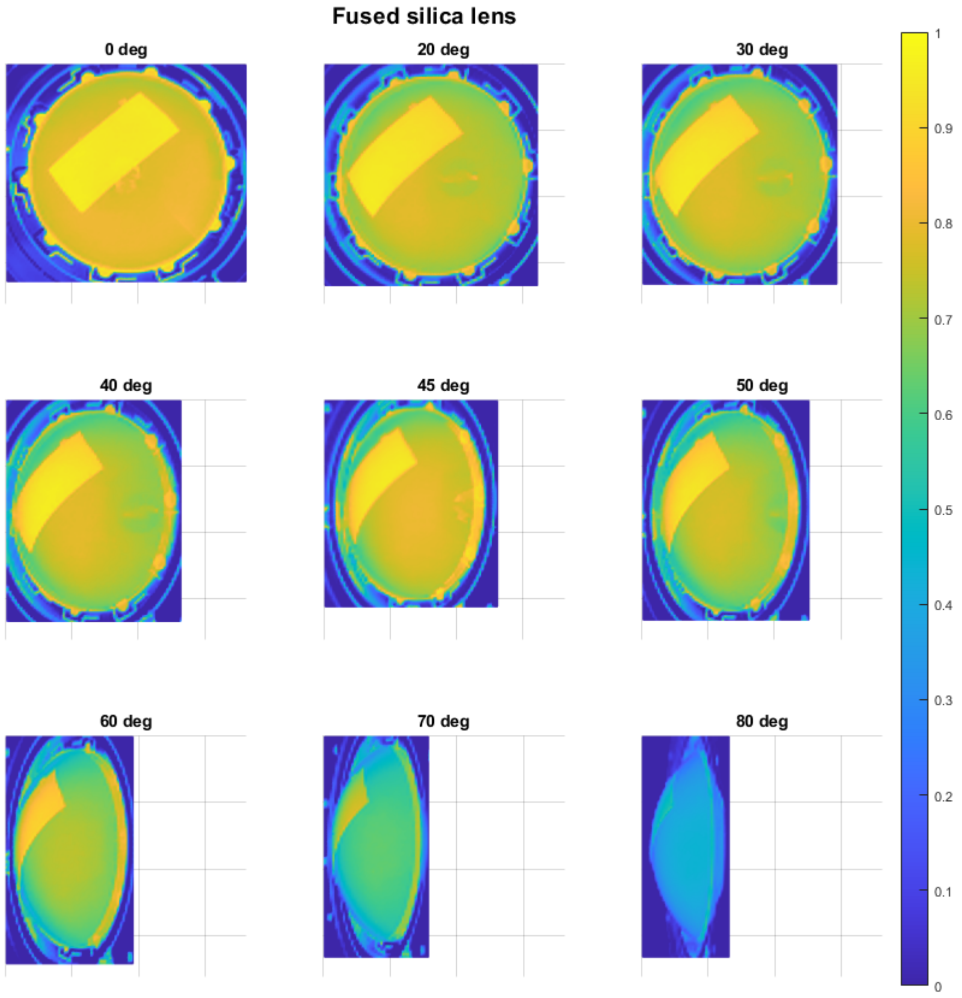

Figure 4.23: Emissivity mapping for a fused silica lens at different angles.

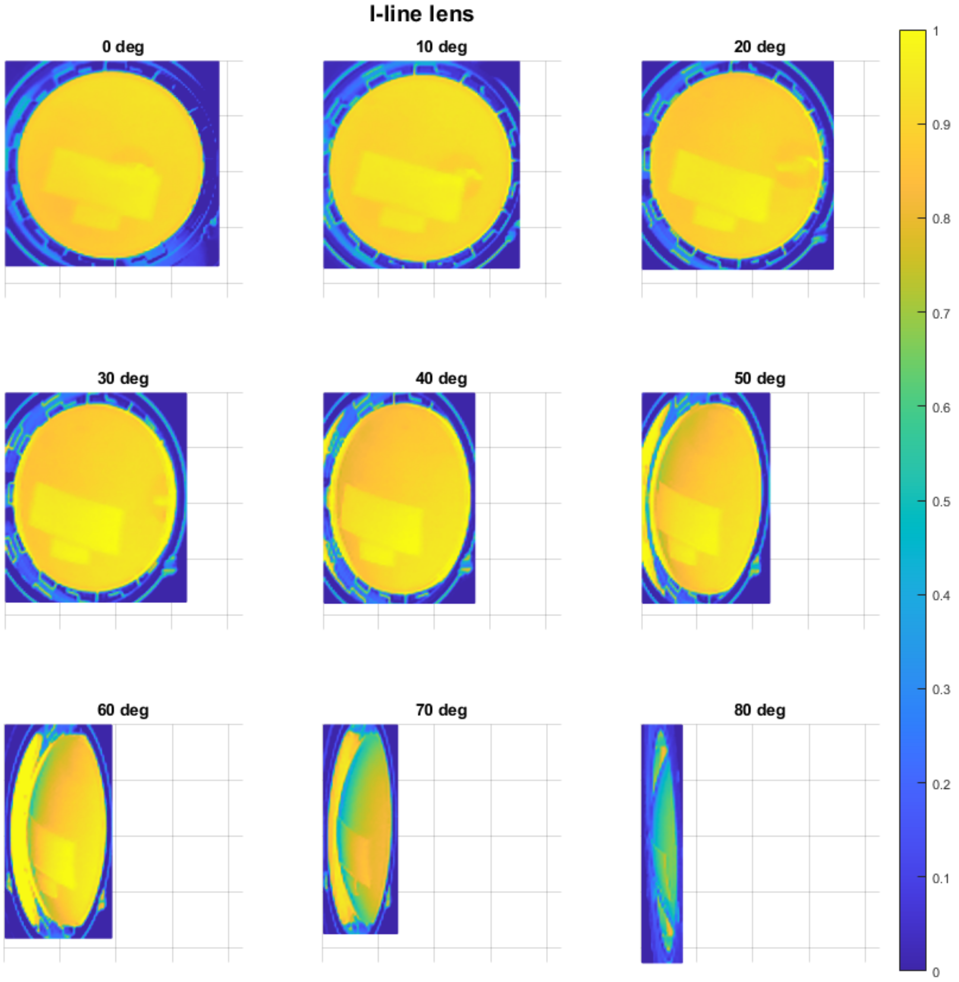

Figure 4.24: Emissivity mapping for a I-line glass lens at different angles.

From these results, the plots from figure 4.25 are created. The plots also contain the fitted functions given in equations 4.15 and 4.16, which will be used in the FEM model.

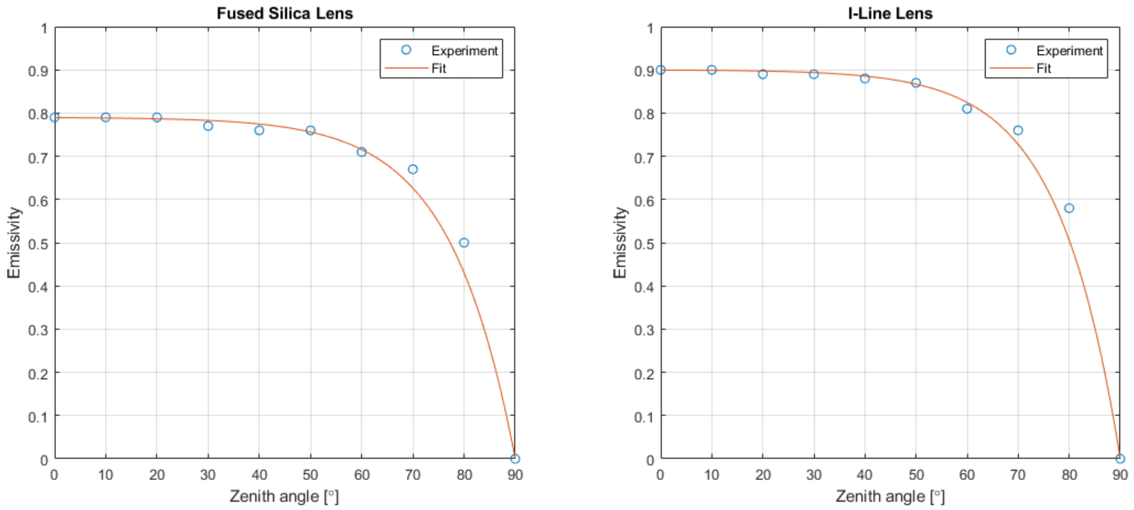

Figure 4.25: Emissivity against zenith angle plots for a fused silica and a I-line glass lens.

$$f_{\text{FS}}(\theta) = 0.79\left(1 - exp\left(\frac{\theta - 90^\circ}{12.7}\right)\right) \tag{4.15}$$

$$f_{\text{I-Line}}(\theta) = 0.9\left(1 - exp\left(\frac{\theta - 90^\circ}{12.1}\right)\right) \tag{4.16}$$

Here, again a strong dependency of the emissivity is seen for increasing zenith angles for both glass types. Up to approximately 50° the emissivity can be assumed to be constant. For comparison, the three fitted functions for the two glass types and the tape are plotted on a polar plot, shown in figure 4.26. The polar plot shows that the emissivity of the tape starts to decrease at a smaller zenith angle compared to the two glass types.

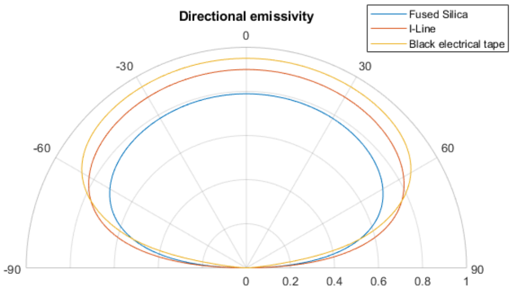

Figure 4.26: Emissivity against zenith angle plots for a fused silica lens, I-line glass lens and black electrical tape.

Chapter 5

Multiphysics modeling

In order to perform a STOP analysis, a multiphysics finite element method (FEM) model is build. To build the model, different modeling approaches are needed for each of the physics involved in the STOP analysis. In this chapter the optical modeling and the heat transfer and structural mechanics modeling are covered. How the physics are coupled and solved for are also discussed at the end of this chapter.

5.1 Optical modeling approach

Typically, in designing opto-mechanical systems, the optics are leading in the design choices. In the designing of the Wynne-Dyson projection lens system this also holds true. The STOP analysis is essentially performed to determine the optical performance under thermal and mechanical loads. Therefore, first the modeling of the optics are considered.

5.1.1 Ray tracing

To model the optics, the light passing through the lens system needs to be modeled. This is done by solving a geometrical optics model with a ray tracing algorithm in COMSOL Multiphysics.

Ray release properties

Essential to a ray tracing algorithm is how the rays are released. The initial position and direction are prescribed in a grid-based release feature in COMSOL. To represent the light coming from the reticle, 9 field points are defined in a 3-by-3 grid as discussed in section 2.2. The field points are point sources from which a conical bundle of rays is released, with the cone angle defined as the inverse sine of the numerical aperture (NA). The numerical aperture is reduced by the partial coherence factor when calculating the absorbed heat from the light in the lenses. For the optical performance evaluation, the ray tracing is done with the full NA. Only primary rays are released, while all the secondary rays are omitted. Because the projection lens system is a Wynne-Dyson design, all the field points are decentered in the y-direction w.r.t. the optical axis of the lenses. In the ray release feature also the telecentricity pattern from section 2.2 is specified in the release direction of the rays. A total of 1000 rays are released per field point per wavelength, which are uniformly distributed in the volume of the cone. For the heat load calculations with the reduced NA, 300 rays are released per field point per wavelength.

Wavelength and power distribution

Because the spectral range is between 350 nm to 450, a polychromatic wavelength distribution is used. This means that rays with multiple different frequencies are traced. Only ghi-radiation is modeled, which is light with a wavelength of 365 nm, 405 nm and 436 nm. With the three wavelengths and nine field points, a total of 27000 rays are traced. The total power of the light is uniformly distributed between the 27000 rays. It is important to add an anti-reflective coating boundary layer on the lens surfaces, otherwise the power of unreleased secondary rays are still absorbed by the lenses in COMSOL.

Optical surface normals

How rays refract or reflect from boundaries depends strongly on how the surface normal is computed. COMSOL offers a feature where geometry normals are calculated, which means that the surface normals are computed from an analytic representation of the geometry surfaces if applicable. This reduces mesh discretization errors. However, this feature does not have an effect if the mesh is subject to thermal stresses or structural loads. In case of these deformations, the mesh normals are used to calculate the surface normals.

For the Wynne-Dyson projection lens model, when only an optical performance of the unpertrubed system is calculated, the geometry normals feature can be used to get accurate results. When a STOP analysis is performed, using the geometry normals feature will not have an effect and the mesh normals are used.

Numerical aperture

For the calculation of the absorbed heat from the light in the lenses, the numerical aperture is reduced by the partial coherence factor, as also described in section 2.2. For the second ray tracing to evaluate the optical performance, the full NA will be used. Since this is not coupled as a heat source, the power of the light in the second ray tracing does not interfere with the heat transfer calculated in previous steps.

5.1.2 Meshing

When building a model in a FEM software package, the model first needs to be discretized by building a mesh model. The quality of the mesh is often the key factor in determining the accuracy of the simulation. The output of a model should converge towards a single solution. When the solution produces a negligible change in the solution after further refinement of the mesh, the solution is considered to be converged. There are 3 aspects that need to be considered when building a mesh, which are the mesh size, mesh order and mesh type. Each of these aspects can add more degrees of freedom to the model, making the solution more accurate, but also more computationally costly.

Mesh size

Refinement in mesh size is often denoted as h-refinement. Smaller mesh elements are used of the same type and order of when h-refinement is performed. It is called h-refinement because the characteristic length h of the mesh elements are refined. An example of h-refinement is shown in figure 5.1, where the size of a mesh element is decreasing.[14]

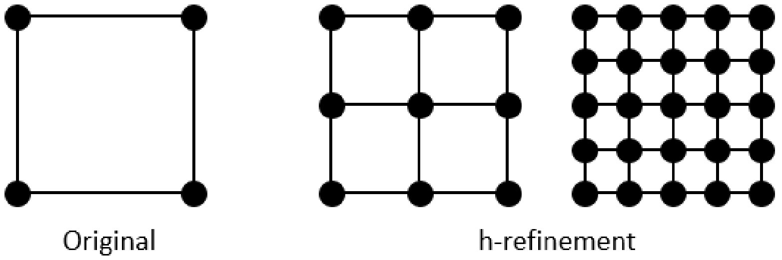

Figure 5.1: Mesh element refinement using h-refinement.

Mesh order

Refinement in mesh order is often denoted as p-refinement. The order of the shape functions is increased for the same size and type of mesh elements. Shape functions are functions in the form of polynomials that are used to interpolate between mesh nodes. Therefore, this method is called p-refinement. An example of p-refinement is shown in figure 5.2, where more mesh nodes are added which means that a higher order polynomial is needed to describe the mesh element.[14]

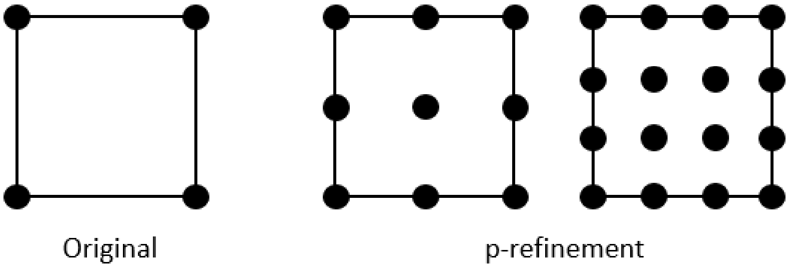

Figure 5.2: Mesh element refinement using p-refinement.

Mesh types

Mesh types are the general shape of the mesh elements. In 2D there are 2 commonly used mesh types, which are the triangle and the quadrilateral. In 3D there are 4 common mesh types, but the tetrahedron is most commonly used, since it can mesh any 3D volume regardless of shape or topology. Figure 5.3 shows the most common 2D and 3D mesh types.

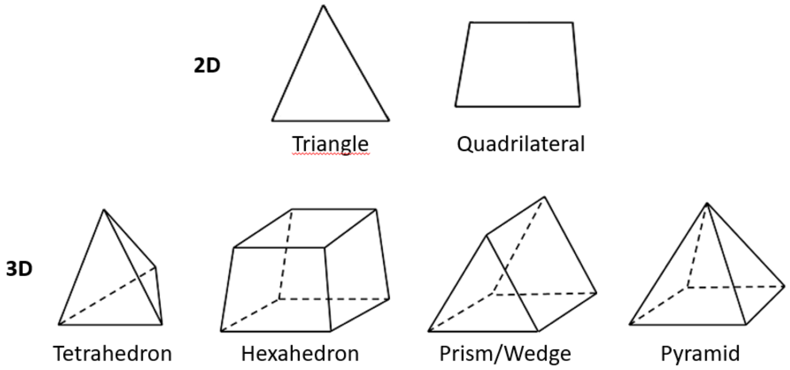

Figure 5.3: Most common mesh types in 2D and 3D meshing.[15]

Choosing a mesh type depends on the application and the importance of accuracy. The mesh generation process start with building a default tetrahedron mesh. Then, the quality of the boundary mesh needs to be examined and refined. Once the boundary mesh is sufficiently refined, the volume mesh can be generated. A final inspection and refinement of the total mesh can be performed to finish the mesh. There are 3 common measures of mesh quality expressed as skewness, smoothness and aspect ratio.[16]

Skewness

Skewness is a measure of how close the shape of a mesh element resembles an ideal equilateral triangle or equiangular quadrilateral element. A skewness value of 0 means a perfect mesh element shape and a value of 1 indicates a completely degenerate cell. Skewness values up to 0.5 are considered still good, however for excellent quality the skewness value should be smaller than 0.25. Figure 5.4 shows the skewness based on the equilateral volume.[16]

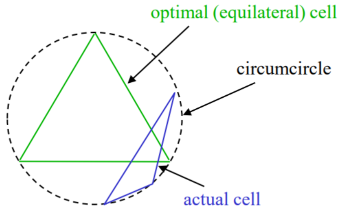

Figure 5.4: Skewness measure based on equilateral volume

Smoothness

Smoothness is the difference in element size between neighbouring elements. A smooth mesh gradually changes in size between elements. Figure 5.5 shown a smooth and a non-smooth transition of some mesh element.[16]

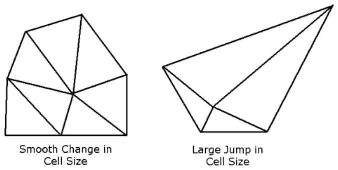

Figure 5.5: Smooth and non-smooth transition of element size.

Aspect ratio

The aspect ratio of an element is the ratio between the largest to the smallest side length. An aspect ratio close to 1 is often desired. A large aspect ratio typically means less accurate results in the direction of the large side. Figure 5.6 shows elements of different aspect ratios.[16]

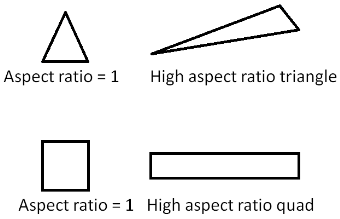

Figure 5.6: Mesh elements of different aspect ratios

Mesh refinement for projection lens system

A mesh is refined enough when the solutions are converged and further refinement does not improve the accuracy of the solutions. However, this strongly depends on what solutions need to converge. Since the model includes multiple different and coupled physics, the mesh needs to be refined for the solution that needs the highest accuracy. This means that some solutions are solved for a mesh that is too finely refined and thus use more computational power than needed to converge that solution. Using different meshes for different solutions would computationally be more efficient, but this also introduces additional mesh discretization errors when a particular solution is used as an input to compute another solution. The mesh refinement to perform ray tracing needs to be much finer and of higher order compared to the mesh needed to calculate heat transfer and structural deformations. The optical surfaces need at least a quartic element order to converge the ray tracing results. For heat transfer and structural deformations, quadratic element order is enough. Also, the mesh size needs to be more refined for the ray tracing to converge compared to the heat transfer and structural deformations.

Geometry

Building the geometry of the system can be done directly in COMSOL with the geometry builder or a CAD file can be imported. For the Wynne-Dyson projection lens system, the geometry is build with the COMSOL geometry builder. COMSOL offers a part library from which fully parameterized optical components are selected to build the optical system. These use Bézier surfaces to define the curvature of the optical surfaces, which excludes internal boundaries that get created when the optical components are created by rotating the crossection of the component by its axis. Also, extra radial and azimuthal points can be added, which fixate the mesh to be generated around these points. Especially when the optical surfaces are in direct contact with another object, the mesh tends to be less accurate at the interface. This is for example where the mesh is in contact to the housing and to the gas. Adding radial and azimuthal points makes the representation of the geometry by the mesh more accurate.

5.1.3 Post-processing results

Most of the post-processing of the results will be done in COMSOL directly, like creating temperature and deformation mappings or calculating the amount of heat transferred through a certain heat transfer path. However, for the optical performance analysis, importing the data into Matlab will be more practical, especially when results from Zemax are to be compared with.

Spot diagrams

To analyze spot diagrams, COMSOL has a build in feature to plot them. However, to create the spot diagrams, an intersection plane needs to be defined. This plane is typically defined at the focus plane. For an unfolded ray path, COMSOL has a feature to find the focus plane defined as the minimal radial RMS value. But since the Wynne-Dyson lens system is a catadioptric system and the image and object are located in the same plane, the feature fails to find the focus plane. Therefore, the ray trajectories are imported into Matlab. In Matlab the best focus plane can be found by creating a plot of the radial RMS value against the z-axis. From this plot the focus shift and the minimal radial RMS value can be obtained and used to create spot diagrams for a plane at the corresponding z-coordinate. Also, Zemax data for the spot diagrams can be imported and compared to the COMSOL results in the same plots.

Zernike aberrations

The wavefront error is analyzed by evaluation of Zernike wavefront aberrations. COMSOL has a feature to compute Zernike coefficients and plot the optical wavefront aberrations. But to compare the wavefront composition from the Zernike coefficients obtained from COMSOL and Zemax, a Matlab script is used. The Matlab script uses the obtained Zernike coefficients to calculate the Zernike polynomials. The sum of the polynomials composes the wavefront error.

5.2 Heat transfer and structural deformations modeling approach

Once the optical modeling is finished, the heat transfer and structural mechanics modeling are done. In COMSOL radiative heat transfer between surfaces is calculated by a different physics module than the heat transfer physics module. Therefore, the radiative boundary conditions will be discussed in a separate section from convection and conduction.

5.2.1 Heat transfer boundary conditions

Convection

In section 4.3.2 a convective heat transfer coefficient of $h_c = 6.2$ W/m^{2}K was calculated for forced convection with a flow velocity of 0.65 m/s on a horizontal cylinder. In the STOP analysis model, a forced convective heat flux of $h_c = 6.2$ W/m^{2}K at a reference temperature T_0 is applied on all external surfaces. The air flow of 0.65 m/s, is a typical air flow velocity of fan-filter modules used in lithography machines. In previous FEM models of the same Wynne-Dyson lens model that only simulated the heat transfer and structural deformations in ANSYS, $h_c = 5$ W/m^{2}K was assumed. So to compare the previously obtained ANSYS values with the COMSOL results, the reference model in COMSOL is also solved for the $h_c = 5$ W/m^{2}K.

The lenses and the housing enclose a volume which is filled with nitrogen gas. As explained in section 4.3.1, convective heat transfer with the gas is negligible and it can be assumed to be stagnant. The gas is therefore modeled as a solid volume with the properties of nitrogen gas. This allows for heat to conduct from the lenses into the gas and from the gas into the housing in a computationally cheaper way. The nitrogen gas volume could be modeled as a gas, but this requires the introduction of a fluid flow physics module, which is coupled with the heat transfer module, making the model computationally more expensive for a relatively small heat path. Convection could also be introduced by assigning a thermal contact conductance boundary condition on the interfaces with the lenses and the housing, forcing heat to transfer a certain direction. But again, this is not done because the gas is assume to be stagnant.

Thermal Contact Conductance

In section 4.2.1 it was already mentioned that the flexure design of the mount and the reduced contact area with the glue are adding a thermal resistance. Therefore, the mount is being modeled as a solid ring with a thermal contact conductance layer. COMSOL has a feature to add thermal contact layers between interfaces of solids. This is used at the interface between the lenses and the mounts. The value for the conductance layer is calculated for each lens separately.

5.2.2 Radiation boundary conditions

To include radiative heat transfer, the surface-to-surface radiation physics module is used in COMSOL. This allows heat transfer between surfaces by means of radiation. Radiative heat transfer is accounted for on the red boundaries from figure 5.7, where there is radiative heat transfer between the internal surfaces and from the outside facing surface of lens 1 to the external environment.

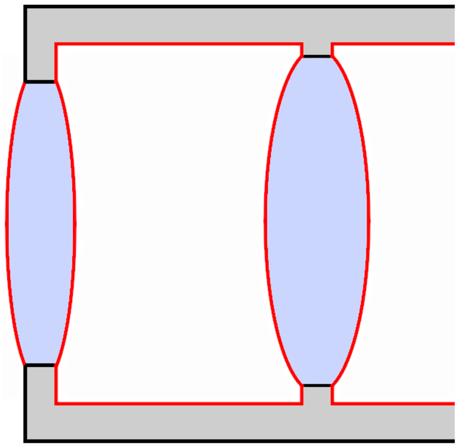

Figure 5.7: Boundaries where radiative heat transfer is applied in the COMSOL model marked in red.

The emissivity of the surfaces can be modeled to be diffuse or directional dependent. For both cases a model is build to evaluate the dependence of the directional emissivity to the total heat transfer.

Diffuse emissivity

Modeling the surfaces to have a constant emissivity in all directions is done by adding a diffuse surface boundary condition. For diffuse radiation, the hemicube method is used for radiative heat transfer interfaces. This method takes shadowing effects into account but does not take directional properties into account. For diffuse surfaces, this method is fast and accurate.

The interior non-optical surfaces can be made black and are assumed to have a hemispherical emissivity of 1. Note that this is an overestimation, as this would imply an ideal black body, which is not possible in practice. Also a significant part of the radiation is from shallow angles which reduces the emissivity strongly. However, using baffles, the emissivity can be assumed to be 1, as will be explained in chapter 7.1. The lenses are assumed to have a reduced hemispherical emissivity according to the results from the experiment from chapter 4.6.2. The mirror is diffuse and is assumed to have a hemispherical emissivity of 0, implying an ideal thermal mirror. Modeling the radiative heat transfer with diffuse emissivity of the surfaces is computationally cheaper compared to directional emissivity, because the direction of the radiation does not have to be calculated and taken into account.

Directional dependent emissivity

To include directional dependent emissivity, the ray shooting algorithm is used. This algorithm computes the trajectories of the rays as they get absorbed or reflected. The accuracy increases by increasing the number of rays. However, this does increase the computational cost significantly.

For the lens surfaces, the opaque surface feature is used in COMSOL. This allows to assign an analytical function for the directional emissivity. The analytical expressions found from the experiments of section 4.6.2, equations 4.15 and 4.16, will be used for the lens surfaces.

For the non-optical internal surfaces again a diffuse surface is used with an emissivity of 1. The mirror will be modeled again to have an emissivity of 0 but it will be specular reflective surface.

5.2.3 Mechanical boundary conditions

Because of the heat transfer in the system, the temperature in the system changes and this will lead to structural deformations. To take these into account, the solid mechanics physics module is used in COMSOL. This allows to add mechanical boundary conditions to constrain the model in a fixed location and compute mechanical stresses and deformations.

Constraints

To calculate mechanical deformations, the model needs to be fixed in space to have a reference for the displacements. In the Wynne-Dyson model, the constraints are placed on the housing as shown in figure 5.8, where the colors indicate the direction of the constraint. The constraints are assigned with the prescribed displacements feature in COMSOL.

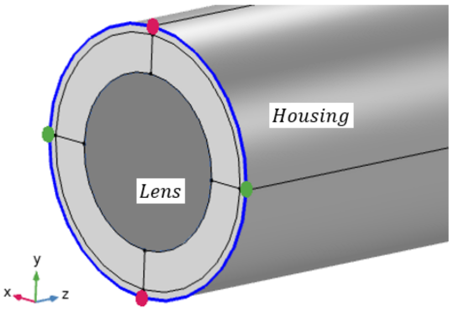

Figure 5.8: Fixed constraint on the Wynne-Dyson model. Red: constrained in x-direction. Green: constrained in y-direction. Blue: constrained in z-direction.

The blue ring is constrained in z-direction, which allows the rest of the system to expand in z-direction. The red dots are constrained in x-direction and the green dots in y-direction, which allows for radial expansion. By constraining the system with these constraints, no additional internal stresses are introduced by the constraints, while allowing for radial expansion and expansion in z-direction.

Equivalent Young's Modulus

As mentioned before, the flexures in the lens mount are not modeled and instead the mount is modeled as a solid ring. However, without the flexures, the mount would have a much higher stiffness in the radial direction, if it is made out of the same material as the lens mount. This would build up structural stresses in the lenses when radially expanding. To account for the flexures, an equivalent Young's Modulus is computed for each lens mount, making the lens mount, which is modeled as a solid ring, less stiff.

The equivalent Young's Modulus is calculated by applying a radial boundary load of 1 N/m^2 on the interface between the glue and the lens, as shown in the left image from figure 5.9. The outer surface of the mount is constrained in all directions.

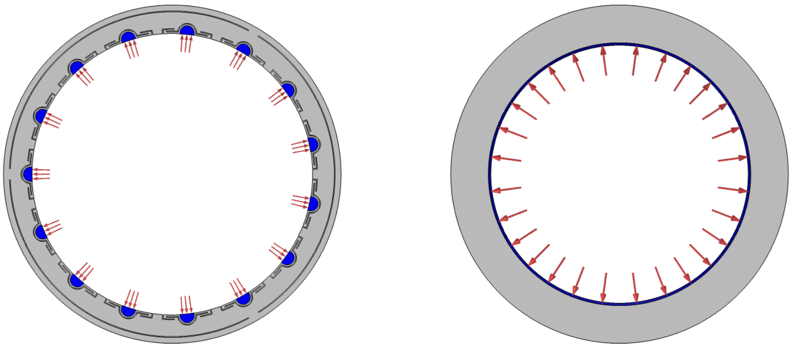

Figure 5.9: Applied boundary loads to derive radial displacement. Left: loads applied on the lens mount with flexures. Right: loads applied on solid ring representing the lens mount in FEM model.

After applying the boundary load, the average radial displacement of the interfaces between the glue and the lens is calculated. The same boundary load is applied on the solid ring, but multiplied by the ratio of the area where the loads are applied in both cases. The applied loads are shown in the right image from figure 5.9. By calculating the average radial displacement again for the solid ring and then dividing it by the average radial displacement of the lens mount with flexures, a reduction factor for the Young's Modulus is obtained. Multiplying this reduction factor with the Young's Modulus allows to have the same radial displacement in the solid ring as for the lens mount with flexures for the same load. For every lens mount in the Wynne-Dyson projection lens model, a reduction factor is calculated and multiplied by the Young's Modulus of the respective solid ring.

5.3 STOP analysis modeling approach

Implementing STOP analysis in COMSOL is done according to the 4 step work flow from figure 5.10. COMSOL also offers a study feature called the Bidirectionally Coupled Ray Tracing, which computes ray trajectories that are affected by external fields, like thermal or structural deformations, which is needed to perform a STOP analysis. However, this method is useful when the ray trajectories change significantly that a feedback loop is needed to calculate new thermal and structural loads for the perturbed rays until a self-consistent solution is obtained. Since this is not the case when modeling the Wynne-Dyson projection lens system, the feedforward work flow from figure 5.10 is used. The reason to split up the modeling approach into 4 separate study steps is to make the model computationally less demanding on the memory. This holds especially in steps 2 and 3 where the heat transfer and structural mechanics are split in different study steps.

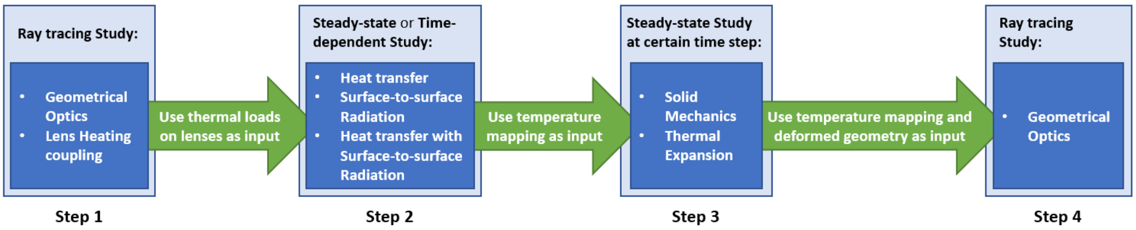

Figure 5.10: Modeling approach to implement STOP analysis in a 4 step work flow.

In the first step, a ray tracing study is solved, which includes the geometrical optics physics module and the lens heating multiphysics coupling. The optics module is to include the physics that allow to solve the ray tracing. The ray tracing in this step is solved for the unperturbed system. The lens heating coupling is used to calculate the absorbed power of the rays by the lenses.

In the second step, either a steady-state or a time-dependent study is solved, which includes the heat transfer physics module and the surface-to-surface radiation physics module as well as a multiphysics coupling between them called the heat transfer with surface-to-surface radiation coupling. The thermal loads calculated from the previous step are use as the heat source in this step to initiate heat transfer in the system. From this step a temperature mapping is obtained. When a time-dependent study is solved, a temperature mapping is obtained for every time instance solved for.

In the third step, a steady-state study is solved, which includes the solid mechanics and the thermal expansion multiphysics coupling. The temperature mapping calculated in step 2 is used as the input to calculate the structural deformations. When a time-dependent study is solved in step 2, a desired time instance is chosen for the temperature mapping.

In the fourth step, a ray tracing study is solved, which only includes the geometrical optics physics module. However, it uses the temperature mapping from step 2 and the structural deformations from step 3 as an input to perform the ray tracing through the perturbed model. The optical performance are evaluated from the ray tracing of this step. To evaluate the transient behaviour of the optical performance, steps 3 and 4 are repeated for desired time instances for which the temperature mapping is solved for in step 2.

Chapter 6

Results

To analyze the performance of the Wynne-Dyson projection lens design, results from the FEM models are compared before and after the lens heating effect. First, the results of the nominal optical model are presented where no lens heating effects are included. Then, the results of a previously calculated ANSYS model are compared with COMSOL results where only heat transfer and structural deformations are solved for. Finally, the results of the STOP analysis models are presented for both the steady state and transient case.

6.1 Optical model

The optical performance of the nominal model, that does not include lens heating effects, is evaluated on the radial RMS focus spot size, the Zernike wavefront aberrations and the Maréchal criterion.

6.1.1 Spot diagrams

To evaluate spot diagrams obtained from COMSOL, a comparison with the results from Zemax are made. Figure 6.1 shows the spot diagrams of the 9 field points individually. The color indicates the wavelength, where the 365 nm wavelength is marked blue, 405 nm is green and 436 nm is red.

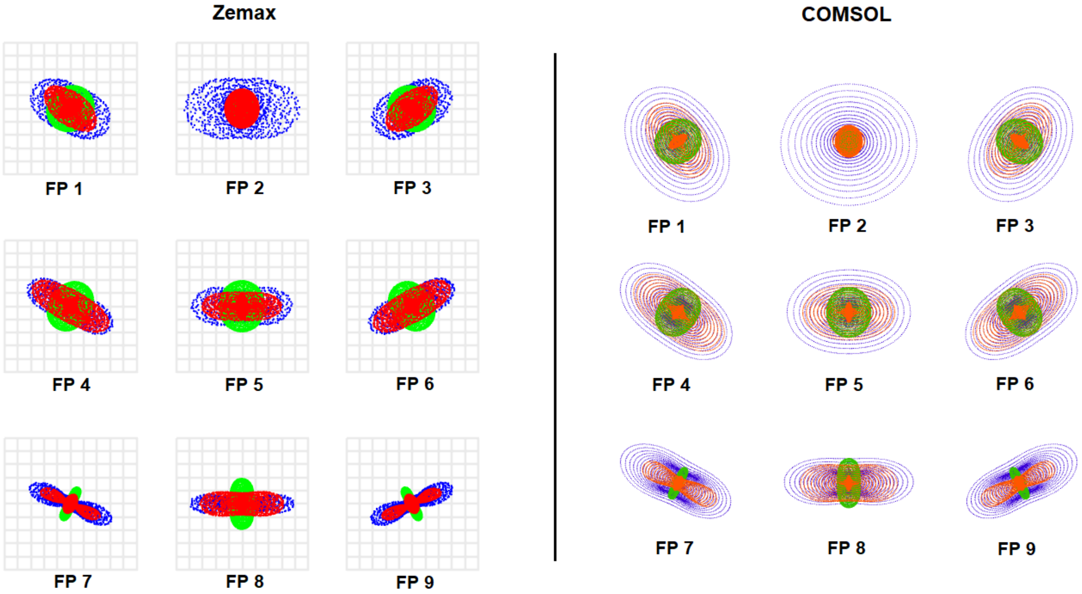

Figure 6.1: Spot diagram of the nominal Wynne-Dyson projection lens system for the 9 field points obtained from Zemax in the left image and from COMSOL in the right image. Colors indicate the wavelength (blue = 365 nm, green = 405 nm and red = 436 nm).

Comparing the spot diagrams, the same general shapes of the spot diagrams from Zemax can be recognized in the COMSOL spot diagrams. The COMSOL spot diagrams show more defocus errors for the 365 nm and some for the 436 nm wavelength compared to the Zemax results. This is also verified when looking at the Zernike coefficients in the next section.

Table 6.1 shows the spot sizes for each field point as a percentage of the diffraction limit of the optical system. The spot sizes for all field points are only a few percent of the diffraction limit. This leaves room for the system to degrade its optical performance when lens heating effects apply and to still have spot sizes below the diffraction limit according to the ray tracing. The diffraction limit is therefore the limiting factor for the resolution in this system. For both Zemax and COMSOL the same order of magnitude is found for the radial RMS spot size. The Zemax spot sizes are between 1.5% and 2.0% smaller for every field point. This is as expected since in COMSOL discretization errors are included due to the meshing of the model and Zemax uses an analytical expression to evaluate the optical interfaces. Even though in COMSOL it is possible to use analytical expressions to evaluate optical interfaces in an undeformed model, this is still based on the mesh grid. Because the spot sizes are in a much smaller order of magnitude compared to the mesh elements, discretization errors are introduced.

Table 6.1: Percentage of the radial RMS spot sizes w.r.t. the diffraction limit for each field point for the nominal model.

Field Point	**Zemax**	**COMSOL**
1	5.1%	7.1%
2	5.0%	6.7%
3	5.1%	7.1%
4	5.6%	7.4%
5	5.6%	7.3%
6	5.6%	7.4%
7	4.1%	5.8%
8	5.3%	6.8%
9	4.1%	5.8%

6.1.2 Zernike wavefront aberrations

To evaluate the wavefront aberrations, a Zernike wavefront composition is made from the Zernike coefficients. The composed wavefronts are shown in figure 6.2 for field point 5. The piston ($Z(0,0)$), tip ($Z(1,1)$) and tilt ($Z(1,-1)$) terms are excluded from the wavefront composition, since they do not contribute in the degradation of the wavefront. The Zernike coefficients are shown in the barplot from figure 6.3. Both the Zernike wavefront composition and the Zernike coefficient barplots are normalized w.r.t. the largest RMS wavefront error σ_W between the computed wavefronts in Zemax and COMSOL.

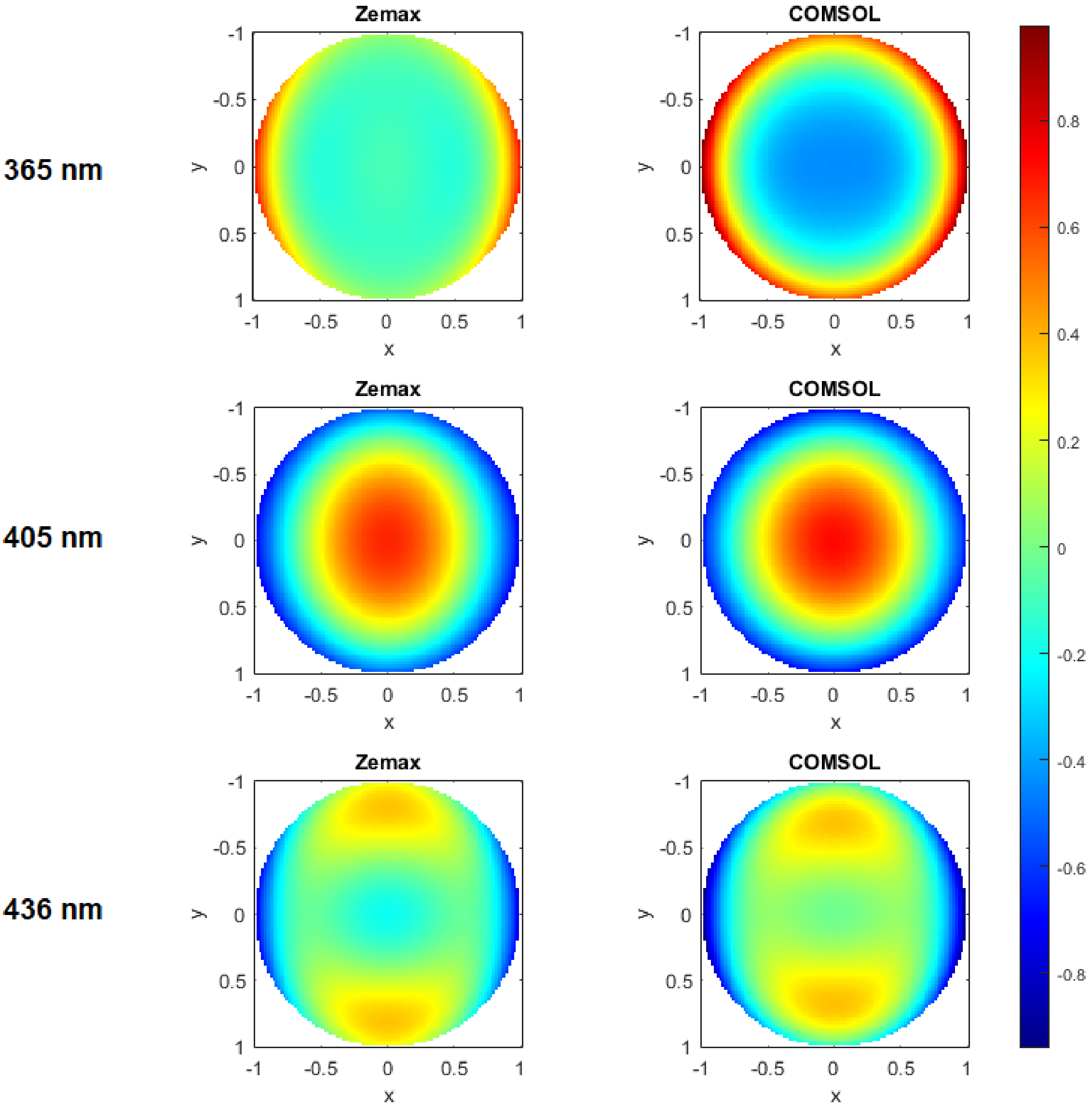

Figure 6.2: Zernike wavefront aberrations composition for field point 5 of the nominal model, normalized w.r.t. largest σ_W between the Zemax and COMSOL computed wavefronts. The piston ($Z(0,0)$), tip ($Z(1,1)$) and tilt ($Z(1,-1)$) terms are not included.

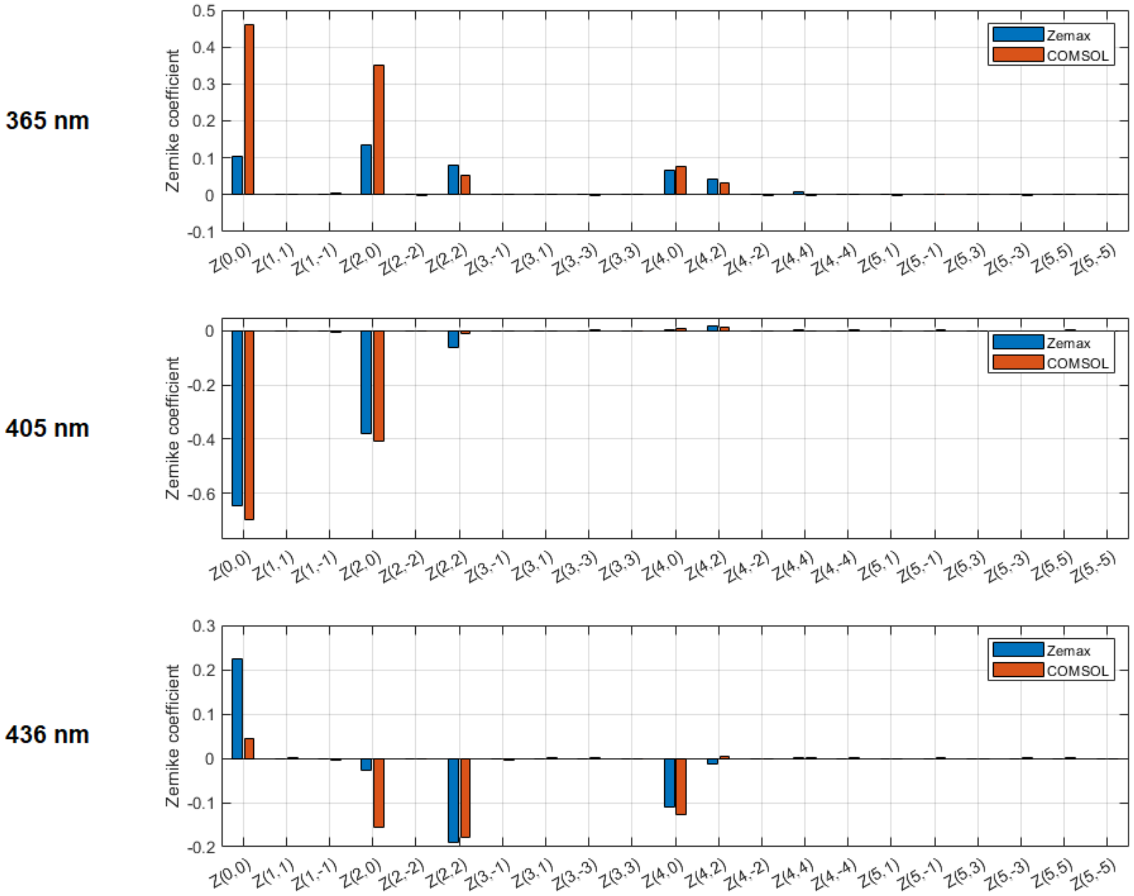

Figure 6.3: Zernike coefficients for field point 5 of the nominal model, normalized w.r.t. largest σ_W between the Zemax and COMSOL computed wavefronts.

The wavefronts for the 365 nm wavelength are mainly constructed by the same dominating aberration terms in Zemax and COMSOL. However, the Zernike coefficients computed in COMSOL show significantly more defocus ($Z(2,0)$), which can also be noticed in the spot diagrams. The vertical astigmatism ($Z(2,2)$), spherical aberrations ($Z(4,0)$) and vertical secondary astigmatism ($Z(4,2)$) are also dominant aberration terms for the 365 nm wavelength. These contribute in similar magnitude to the wavefront error in both Zemax and COMSOL.

The wavefronts for the 405 nm wavelength are very similar between Zemax and COMSOL. The main difference is that Zemax shows more vertical astigmatism ($Z(2,2)$), which is also visible by carefully looking at the wavefront compositions from figure 6.2. Noticeable is that for the 405 nm wavelength the wavefront aberration is mainly constructed by defocus ($Z(2,0)$).

The wavefronts for the 436 nm wavelength are again constructed by the same dominating aberration terms in Zemax and COMSOL, but COMSOL shows a larger defocus ($Z(2,0)$) error compared to Zemax. Noticeable is that for the 436 nm wavelength more vertical astigmatism ($Z(2,2)$) and spherical aberrations ($Z(4,0)$) are introduced compared to the other wavelengths.

6.1.3 Maréchal criterion

To evaluate the image quality, the Maréchal criterion is used, which is met for a Strehl ratio larger than 0.8 or equivalently if the RMS wavefront error is smaller than the wavelength divided by 14. The Strehl ratio is calculated for the composed wavefronts from Zemax and COMSOL for field point 5, for which the results are shown in table 6.2. The Strehl ratio is for all three wavelengths in both Zemax and COMSOL above 0.8 and thus the Maréchal criterion is met. This means that the optical system has a good image quality and is considered to be diffraction limited.

Table 6.2: Strehl ratio for field point 5 of the nominal model.

Wavelength [nm]	**Zemax**	**COMSOL**
365	0.9997	0.9985
405	0.9987	0.9985
436	0.9996	0.9994

6.2 Heat transfer and structural deformations model

To evaluate the heat transfer and structural deformations calculated by COMSOL, first a reference model of the Wynne-Dyson projection lens system is made in COMSOL to compare the results to a previously calculated heat transfer and structural deformations model from ANSYS. This allows to compare results obtained from 2 different and independent people working with different FEM software packages to model the same lens system. The ANSYS model was created without the mirror element and does not consider any radiative heat transfer. Because of the absence of the mirror in the ANSYS model, a convective boundary layer is also applied on the open end where the mirror would be located. On all external boundaries, a 5 W/(m^2K) convective boundary layer is applied. Inside the system, the stagnant gas is modeled as a solid. At the interface between the lenses and the lens mounts, a thermal contact conductance layer is applied. The values for the TCC as used in ANSYS are also used in the COMSOL model to perform the simulations at similar conditions.

For the heat load in the lenses, the absorbed light from the lenses is calculated in Zemax and converted to a heat source which can be imported in ANSYS and COMSOL. Table 6.3 shows the distribution of the total heat generated in the system and divided over the lenses. Because lenses of different materials and thicknesses are used, the total heat generated in each lens is not spread equally. Also, after the rays pass through a lens, the total power of the transmitted rays is lowered. Therefore, after the rays are reflected by the mirror and pass through the lenses for the second time, less power is absorbed. As a result, there is no vertical symmetry in the heat load in the lenses. This effect is visible in figure 6.4 at lenses 1, 2 and 3 where the temperature is higher on the bottom part where the incoming rays pass through the lenses compared to the top part where the reflected rays pass through.

Table 6.3: Heat source distribution between lenses.

Lens	**Heat IN**
1	26%
2	24%
3	28%
4	1%
5	22%
Total heat IN	100%

To be in steady state, the same amount of heat entering the system also should leave the system. Table 6.4 shows a heat balance of the lens system with heat paths that transfer the heat out of the lens system. Most of the heat leaves the system by means of convection from the housing. Between the ANSYS and COMSOL models there is a 1% difference which leaves as convection from the open end where the mirror would be located. However, the results are in the same order of magnitude and this difference can be considered insignificant.

Table 6.5 shows the heat transfer balance for a single lens. In this model, heat from the lenses can only be transferred by means of conduction into the housing or by conducting from the optical surfaces to the gas, since the gas is modeled as a solid. In the COMSOL model, more heat is transferred by conducting to the housing compared to the ANSYS results. The reason for this difference could be a difference in the TCC values between the lenses and the housing. Reducing the TCC values gives a similar temperature distribution as found by the ANSYS model.

Table 6.4: Heat transfer balance with different paths out of the system.

Heat path	**ANSYS**	**COMSOL**
Total heat IN	100%	100%
Convection housing	-88%	-89%
Convection N2	-2%	-1%
Convection L1	-10%	-10%
Heat balance	0%	0%

Table 6.5: Heat balance for one of the lenses of the system.

Heat path	**ANSYS**	**COMSOL**
Heat IN	100%	100%
Contact gas	-36%	-23%
Contact housing	-64%	-77%
Heat balance	0%	0%

Figure 6.4 shows how the temperature is mapped in the system. Here, the locally increased temperature can be seen where the power of rays is absorbed. Compared to the ANSYS model, the COMSOL model gives a difference of 1% in the temperature difference ΔT in the lens system and the maximum temperature T_{max} also differs by 1% in COMSOL. When looking at the same lens as treated in table 6.5, the ΔT differs again 1% between the COMSOL and ANSYS models, and T_{max} differs by 1.9%. So, even though more heat is transferred through conduction into the housing according to the COMSOL results, the change in temperature calculated in ANSYS and COMSOL give similar results.

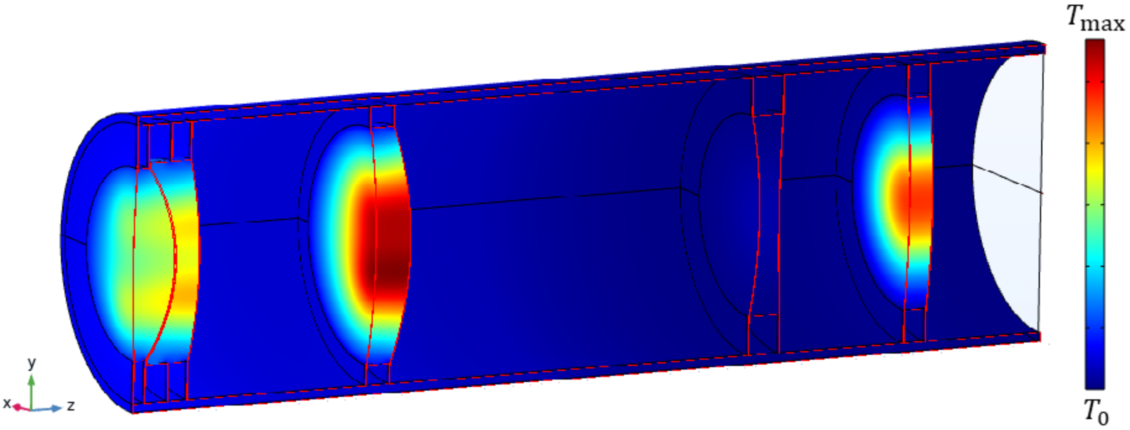

Figure 6.4: Temperature mapping of the system with Zemax provided heat source.

The temperature inside lens 5 is compared to the analytic model for which the radial temperature plot is shown in figure 6.5. Lens 5 is chosen since it has the most radially symmetrical temperature distribution compared to the other lenses. The plot shows a resemblance between the temperature distribution obtained from COMSOL and the analytic model, which gives more confidence in the results obtained from the FEM simulations. The results are not identical because the analytic model is a more simplified model of a lens undergoing the lens heating effect.

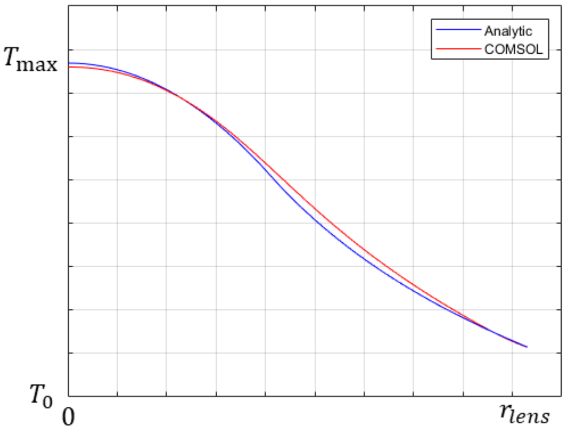

Figure 6.5: Temperature plot against radial distance of the analytic model compared to the COMSOL result for lens 5.

Because of the temperature change in the system, the lenses, mirror, lens mounts and housing will deform. Figure 6.6 shows the radial displacement mapping. Local radial displacements are visible especially close to the edge of the lenses. In lens 3 substantial radial displacements occur, which indicate that this lens might be contributing significantly to the total optical performance degradation after lens heating. Compared to the ANSYS results, a difference of 2% in the maximum radial displacement are found in the COMSOL results.

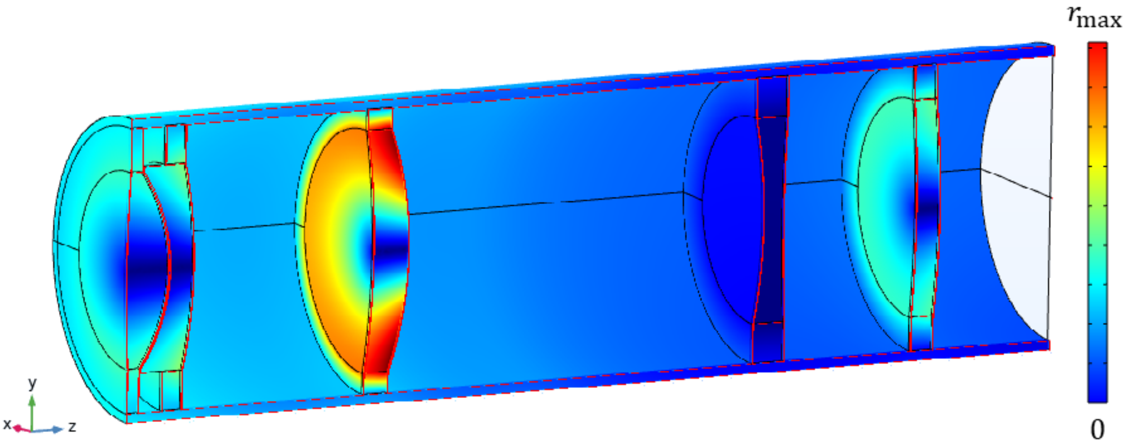

Figure 6.6: Radial displacement mapping of the system with Zemax provided heat source.

Besides a radial displacement, there is also a displacement in z-direction. Figure 6.7 shows the z-displacement mapping in the lens system. In the third and fifth lenses substantial local z-displacements are noticeable and this indicate that these lenses might be contributing significantly to the total optical performance degradation after lens heating. Compared to the ANSYS results, the maximum z-displacement differs by 1% in the COMSOL results.

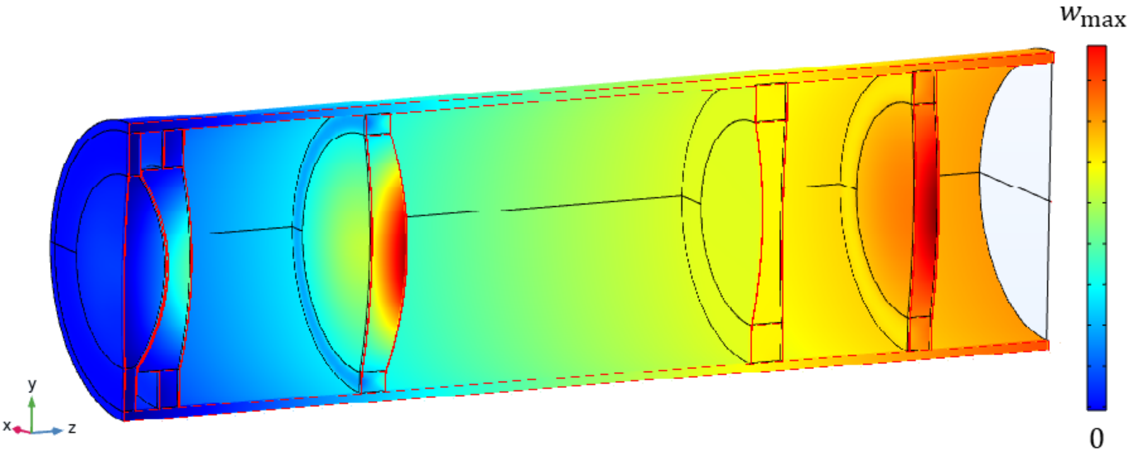

Figure 6.7: Z displacement mapping of the system with Zemax provided heat source.

The differences in the radial and z deformations are in line with the differences in temperature when comparing the ANSYS results with the COMSOL results. The comparison between ANSYS and COMSOL shows that the results are of the same order of magnitude in COMSOL as in ANSYS and therefore more confidence is build in the FEM models and the capabilities of COMSOL.

6.3 STOP analysis model

In COMSOL, a STOP analysis model is build to evaluate the optical performance after the lens system has changed in temperature and structural deformations occur due to lens heating effects. The model is based on the workflow presented in figure 5.10 from chapter 5.3.

6.3.1 Heat transfer and mechanical deformations

First, ray tracing is performed to calculate the amount of light absoption, which is used as the thermal loads on the lenses. Table 6.6 shows that 3.3% of the total ray power is absorbed in the lenses for the COMSOL model. Comparing it to the 4.5% power absobtion according to the analytic calculation, the COMSOL value is in the same order of magnitude as the analytic calculation. The difference is because in the analytic calculation a constant thickness of the lenses is assumed for all rays while in the actual model rays take different paths and thus travel through different thicknesses through the lenses. Comparing with Zemax, in the COMSOL model 0.2% more ray power is absorbed. With more light absorption comes that higher temperatures in the lenses can be expected in similar modeling conditions in COMSOL. However, the difference between the light absorption between COMSOL and Zemax is negligible.

Table 6.6: Heat balance for one of the lenses of the system.

Heat balance	**Analytic**	**COMSOL**	**Zemax**
Total ray power IN	100%	100%	100%
Total ray power OUT	95.5%	96.7%	96.9%
Power loss IN system	4.5%	3.3%	3.1%

In the the second step of the workflow, the lost power from the rays is converted to a heat source in the lenses. A difference of 0.68% occurs in the conversion of the 3.3% power loss from the rays to the heat source in the lenses. This is due to discretization errors in the model. This difference is negligible, especially since it is spread between multiple lenses and is more than 2 orders of magnitude smaller than the total heat source.

Next, a heat balance is presented in table 6.7 for the total heat transfer leaving the system. The results of the COMSOL reference model from section 6.2 are also included for comparison. In the COMSOL STOP analysis model, some changes are made to make the model more realistic compared to the reference model from section 6.2. The STOP analysis model has a 6.2 W/(m^{2}K) convective boundary layer on the outer surfaces of the housing in stead of 5 W/(m^{2}K). Also radiative heat transfer on the lens surface of lens 1 facing the outside is applied, as well as in the interior surfaces, like the optical lens surfaces and the non-optical housing surfaces. Hemispherical emissivities are used according to the results obtained from the emissivity experiments described in chapter 4.6.2. Finally, new values for the thermal contact conductance between the lenses and the lens mounts are calculated according to the method described in 4.2.1. These changes cause the differences in the heat transfer distribution between the results of the reference model and the STOP analysis model. From the table it is clear that still the convective heat transfer from the housing is the most dominant heat transfer path to remove heat out of the system.

Table 6.7: Heat transfer distribution comparison between the reference model and STOP analysis model for different paths out of the system.

Heat Balance	**Reference model**	**STOP analysis model**
Heat IN	100%	100%
Convection housing	-90.2%	-86.0%
Convection lens 1	-9.8%	-7.3%
Radiation lens 1	0.0%	-6.7%
Total	0%	0%

A second heat transfer balance for all the lenses combined is presented in table 6.8. The model is solved for 3 different cases for the emissivities of the fused silica and I-line glass lenses (ϵ_{FS}, $\epsilon_{\text{I-line}}$) and internal non-optical surfaces ϵ_H. The first and second case consider an ideal black surface for the internal non-optical surfaces. The first case is for an ideal hemispherical emissivity of the lenses, which is an overestimation because of the directional dependency of the emissivity. For this reason in the second case the hemispherical emissivity of the lenses are reduced. In the third case the internal non-optical surfaces are considered as ideal thermal mirrors. In this case, only radiative heat transfer happens between lens surfaces, except for the outward facing surface of lens 1, which can still radiate heat out of the system. The table shows that the decreased emissivity evidently decreases the amount of heat transfer through radiation and that is mainly compensated by conduction to the housing. Especially when the internal non-optical surfaces are considered as ideal thermal mirrors ($\epsilon_H = 0$). Having more heat transfer by radiation from the lens surfaces is beneficial, since this would decrease the radial thermal gradient and add an third heat path out of the lenses. The heat transfer out of the lens is then more spread over all surfaces of the lenses instead of mainly going through the edge.

Table 6.8: Heat balance for all the lenses combined for three different cases of the emissivities of the lenses and internal non-optical surfaces.

Heat Balance	ϵ_{FS}=**0.79**, $\epsilon_{\text{I-line}}$=**0.90**, ϵ_H=**1**	ϵ_{FS}=**0.55**, $\epsilon_{\text{I-line}}$=**0.60**, ϵ_H=**1**	ϵ_{FS}=**0.55**, $\epsilon_{\text{I-line}}$=**0.60**, ϵ_H=**0**
Heat IN lenses	100%	100%	100%
Conduction to Gas	-14%	-15%	-22%
Conduction to Housing	-40%	-43%	-64%
Convection Lens 1	-7%	-7%	-8%
Radiation	-38%	-34%	-7%
Total	0%	0%	-0%

For the upcoming results, the reduced hemispherical emissivity on the lenses is used (ϵ_{FS}=0.55, $\epsilon_{\text{I-line}}$=0.6 and ϵ_H=1), because this compensates the reduced emissivity in the radiative heat transfer from the lenses towards the housing, while ϵ_H=1 allows for heat to radiate from the lenses to the housing in the first place. Figure 6.8 shows the temperature mapping in the system. Compared to the temperature mapping from figure 6.4, the temperature difference ΔT in the system is decreased by 38%, and the maximum temperature T_{max} in the system is decreased by 37%. The decrease in ΔT and T_{max} are because of the inclusion of radiative heat transfer in this model allowing for heat to transfer not only through the edge but also from the optical surfaces of the lenses.

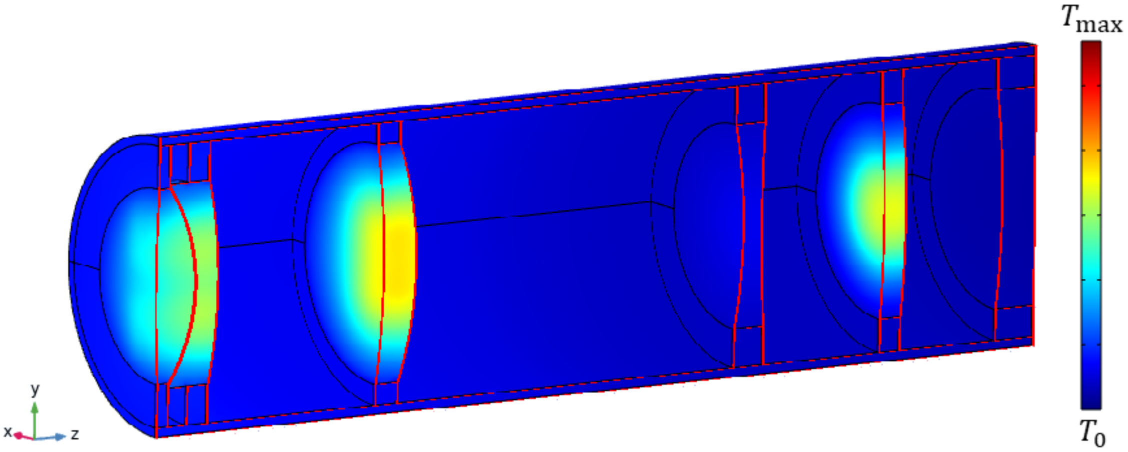

Figure 6.8: Temperature mapping of the lens system for the STOP analysis model which includes radiative heat transfer.

Comparing the temperature profile in lens 5 with the analytic model, the plot in figure 6.9 is obtained. Here, also the plot from the reference model is included, which shows that overall the temperature is lower when including radiative heat transfer in the STOP analysis. The temperature profiles obtained from the reference model and the STOP analysis model show a lot of similarities with their equivalent analytical model, which gives more confidence in the temperature results.

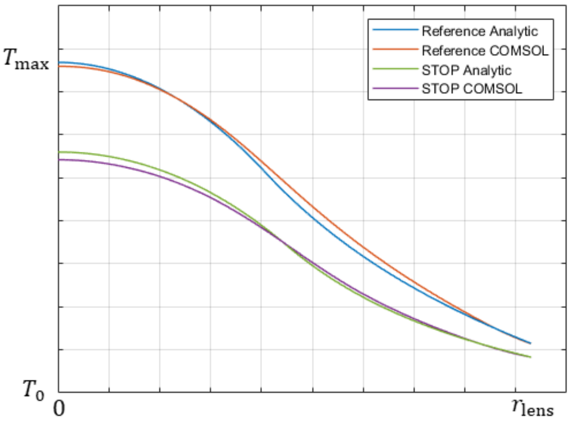

Figure 6.9: Temperature plot against radial distance of the analytic model compared to the COMSOL result for lens 5 for both the reference model and the STOP analysis model which includes radiative heat transfer.

Besides the overall increase in temperature, the temperature gradients in the lenses degrade the optical performance by inducing local deformations. Figure 6.10 shows the radial temperature gradient in the lenses of the STOP analysis model. In the second and fifth lenses strong thermal gradients are visible. Especially in the fifth lens the local structural deformations induced by the temperature gradient will significantly contribute to the total optical degradation. This is shown in the following sections.

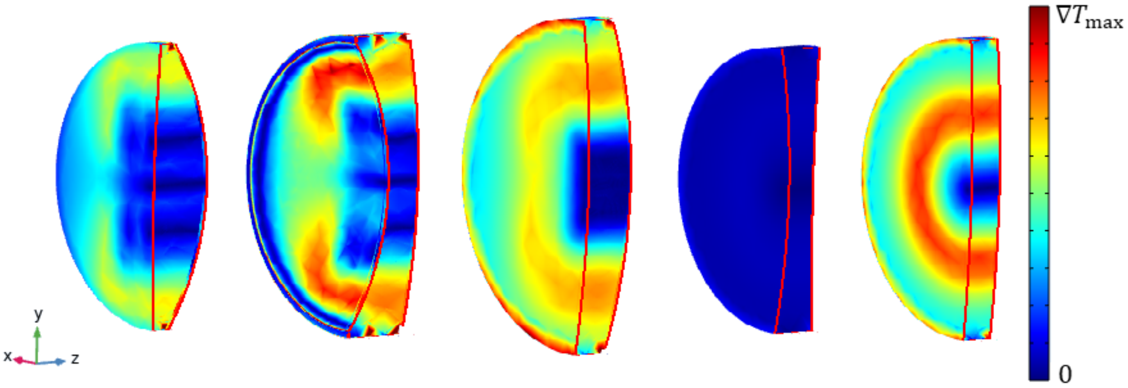

Figure 6.10: Radial temperature gradient mapping of the lenses at steady state for the STOP analysis model.

In the third step of the work flow of the STOP analysis, the temperature mapping is used to calculate displacements in the model. The radial and z-displacements for the STOP analysis model are shown in figures 6.11 and 6.12 respectively. For both the radial and z-displacements, the maximum displacement is decreased by 34% and 35% respectively in the STOP analysis model compared to the reference model. This is in line with the decrease in the temperature. Again in lens 3 most of the radial displacements are observed. The z-displacements occur again mostly in lenses 3 and 5. Therefore, the deformations in lenses 3 and 5 might be significant contributors to the total optical performance degradation after lens heating.

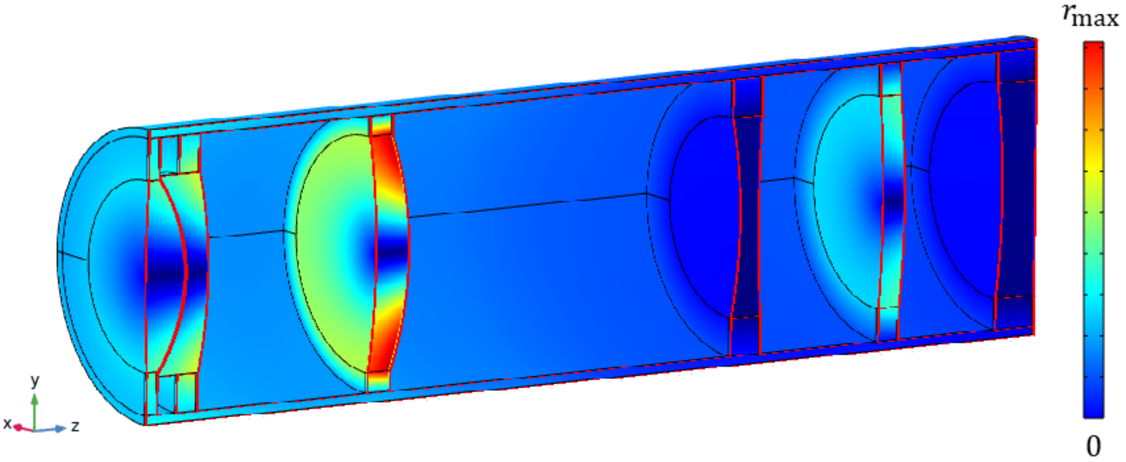

Figure 6.11: Radial displacement mapping of the system at steady state for the STOP analysis model.

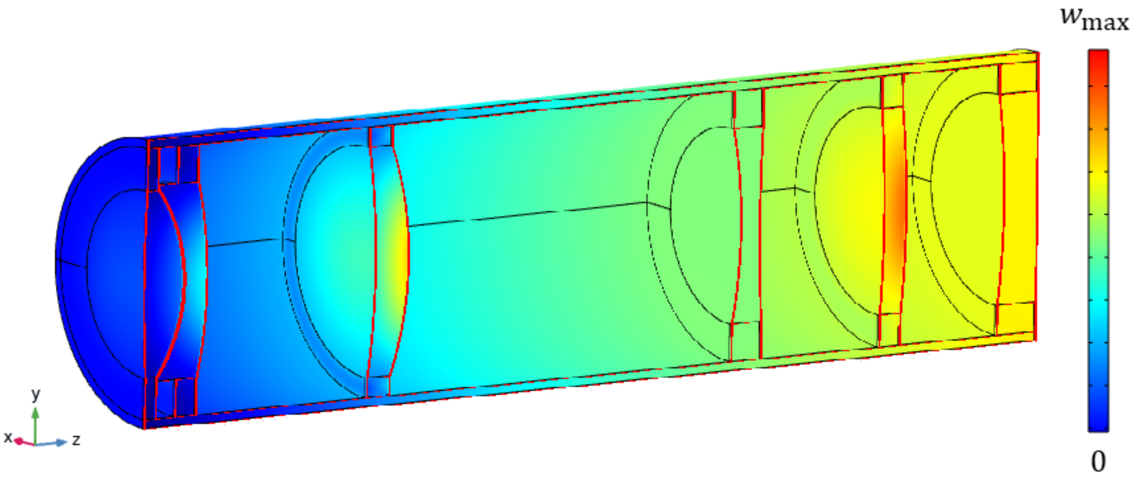

Figure 6.12: Z-displacement mapping of the system at steady state for the STOP analysis model.

6.3.2 Direction dependent radiation

As mentioned before, the STOP analysis model is solved with a reduced hemispherical emissivity to account for the directional dependence of the radiative heat transfer. However, in COMSOL it is possible to include directional dependent emissivities for surface-to-surface radiation. In table 6.9 the heat balances are shown for three different types of radiative heat transfer. The hemispherical column shows the heat balance for the model which uses the reduced hemispherical emissivities ($\epsilon_{\text{FS}} = 0.55$, $\epsilon_{\text{I-line}} = 0.60$). The ideal black bodies column considers ideal hemispherical emissivities of 1 on all interior surfaces. The directional column considers directional dependent emissivities for the lens surfaces. The table shows that in the case with the directional dependent emissivities more heat is transferred by radiation compared to the hemispherical and even the ideal black bodies case. This would imply that the hemispherical equivalent of the directional emissivity would be higher than 1 which is not possible. However, the model considering directional dependent emissivities is computationally expensive to solve. Because of this, the model could not be tested if it truly was converged. Any further p- or h-type refinement, or radiation resolution refinement resulted in running out of memory.

Table 6.9: Heat balance for all lenses combined for different types of radiative heat transfer.

Heat Balance	**Hemispherical**	**Ideal black bodies**	**Directional**
Heat IN lenses	100%	100%	100%
Conduction to Gas	-15%	-15%	-14%
Conduction to Housing	-43%	-38%	-36%
Convection Lens 1	-7%	-7%	-7%
Radiation	-34%	-40%	-43%
Total	0%	-0%	0%

Looking at the temperature profile inside lens 5 for the different types of radiative heat transfer, figure 6.13 shows that with the directional dependent model the temperature is lower in the lens compared to the hemispherical models and the ideal black body models. This is in line with table 6.9, since the directional model predicted more radiative heat transfer. But since it outperforms even the ideal black body model and the model could not be evaluated whether it is converged or not, the model is not trusted and further analysis is continued with the reduced hemispherical emissivities model. However, it is recommended for future analysis of the model to attempt to create a working model which includes directional dependent surface-to-surface radiative heat transfer.

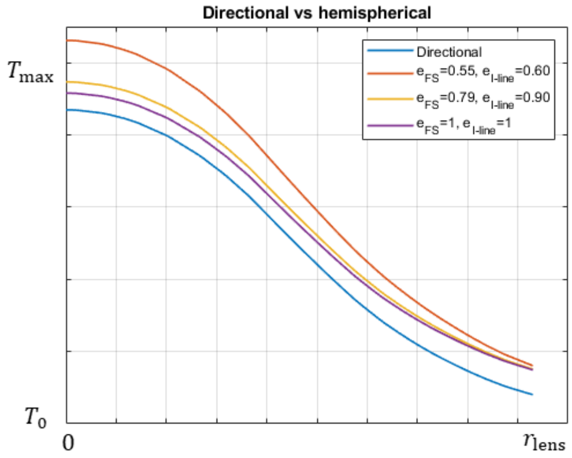

Figure 6.13: Radial temperature plots for lens 5 of the STOP analysis model, modeled with directional dependent emissivity and with different cases of hemispherical emissivities.

6.3.3 Optical performance

In the fourth and final step of the STOP analysis work flow, ray tracing is performed in the thermally and structurally deformed model. To evaluate the optical performance, again spot diagrams are evaluated, as well as Zernike wavefront aberrations and the Maréchal criterion. The temperature mapping and displacements calculated in by COMSOL are also imported in Zemax to compare the optical performance calculated by Zemax and COMSOL.

Spot diagrams

In figure 6.14 the spot diagrams are shown for the 9 field points focused on the minimal radial RMS spot size of field point 5. The overall shape of the spots are changed compared to the nominal case from figure 6.1 for both COMSOL and Zemax. Between the Zemax and COMSOL spot diagrams, similar features are recognizable, especially the shape of the 365 nm wavelength rays in blue, but the general shape of the spots are not as similar as in the nominal case. This is because due to lens heating, a focus shift occurs and between Zemax and COMSOL, there is a 4% difference in the calculated focus shift. Even though in both cases the radial RMS spot size of field point 5 of the 3 wavelengths combined was used as the definition for best focus, still a difference in focus shift between COMSOL and Zemax was obtained.

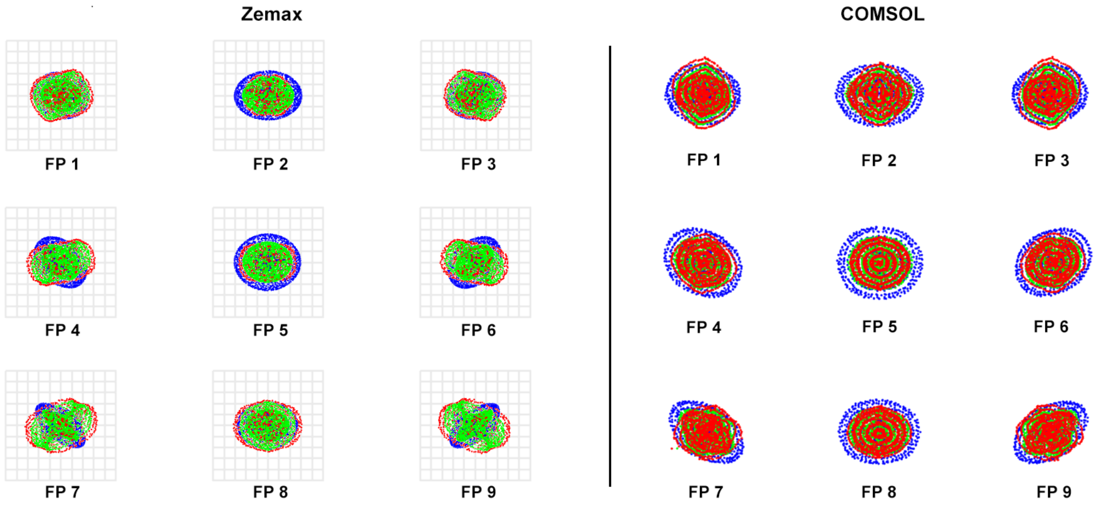

Figure 6.14: Spot diagram of the thermally and structurally deformed Wynne-Dyson projection lens system at steady-state obtained from Zemax in the left image and from COMSOL in the right image. Colors indicate the wavelength (blue = 365 nm, green = 405 nm and red = 436 nm).

In table 6.10, the radial RMS spot sizes as a percentage of the diffraction limit is given, calculated from both Zemax and COMSOL. Comparing the spot sizes with the results from the nominal model from table 6.1 shows that the spot sizes have increased roughly by a factor of 10. However, even with the increase in spot size, according to the spot sizes, the optical system is still below the diffraction limit. Also, again the Zemax model gives smaller spot sizes compared to COMSOL. The difference between COMSOL and Zemax from the nominal model is also scaled with the spot size in the STOP analysis model.

Table 6.10: Percentage of the radial RMS spot sizes per field point w.r.t. the diffraction limit for the STOP analysis model at steady-state.

Field point	Zemax	COMSOL
1	50%	64%
2	53%	66%
3	50%	64%
4	52%	64%
5	54%	65%
6	52%	63%
7	55%	63%
8	52%	63%
9	55%	63%

Zernike wavefront aberrations

To evaluate the wavefront, a Zernike wavefront composition is made from the Zernike coefficients. The composed wavefronts are shown in figure 6.15 for field point 5 at best focus, defined as the minimum radial RMS spot size. The piston ($Z(0,0)$), tip ($Z(1,1)$) and tilt ($Z(1,-1)$) terms are excluded from the wavefront composition, since they do not contribute in the wavefront degradation. The Zernike coefficients are shown in the barplots from figure 6.16. In the barplots also the Zernike coefficients of the nominal model obtained from COMSOL are included. Both the Zernike wavefront composition and the Zernike coefficient barplots are normalized w.r.t. the largest RMS wavefront error σ_W between the Zemax and COMSOL computed wavefronts.

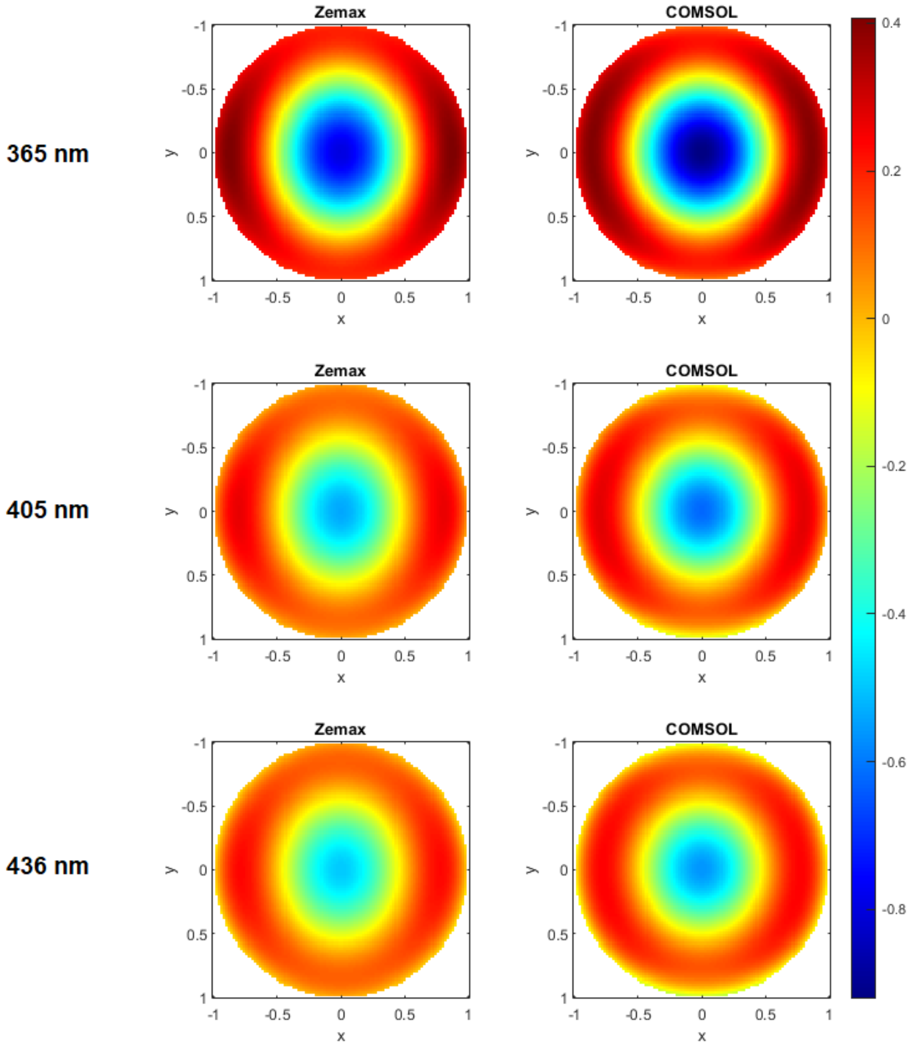

Figure 6.15: Zernike wavefront aberrations composition for field point 5 of the STOP analysis model at steady state, normalized w.r.t. largest σ_W between the Zemax and COMSOL computed wavefronts. The piston ($Z(0,0)$), tip ($Z(1,1)$) and tilt ($Z(1,-1)$) terms are not included.

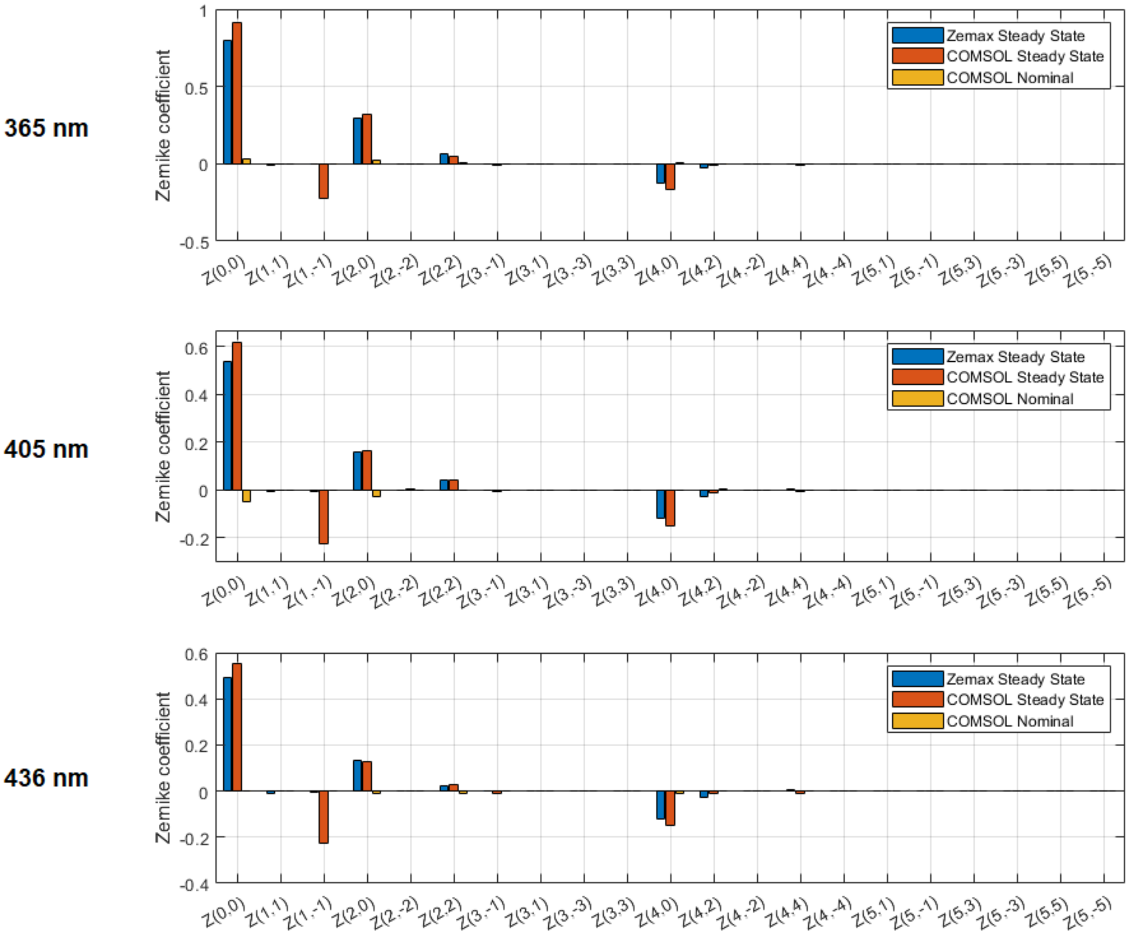

Figure 6.16: Zernike coefficients for field point 5 of the STOP analysis model at steady state for Zemax and COMSOL and of the nominal model from COMSOL, normalized w.r.t. largest σ_W between the Zemax and COMSOL computed wavefronts.

After the system is thermally and structurally deformed, the Zernike wavefront compositions from COMSOL and Zemax look similar for all three wavelengths. This is also seen in the barplots where the same Zernike terms are dominant. Comparing the Zernike coefficients at steady state to the nominal case, it is clear from the barplots that the wavefront error has increased significantly. Similar to the nominal model, again the wavefront errors are composed from a dominant defocus ($Z(2,0)$) and spherical aberration ($Z(4,0)$) terms. From the defocus term it can be noted that after lens heating, a substantial focus shift occurs. The spherical aberration ($Z(4,0)$) are more present in the COMSOL result compared to the Zemax results. Both COMSOL and Zemax also show some vertical astigmatism ($Z(2,2)$) and vertical secondary astigmatism ($Z(4,2)$). The vertical secondary astigmatism ($Z(4,2)$) is however less present in the COMSOL results compared to the Zemax results. For the 405 nm and 436 nm wavelength in the COMSOL wavefront composition, a trace of the vertical astigmatism ($Z(2,2)$) is visible on the top and bottom sides of the wavefront.

Even though the vertical tilt ($Z(1,-1)$) does not contribute to the wavefront degradation, COMSOL shows a strong presence of this term. This is because in COMSOL a reference hemisphere is manually defined. Its axis direction is set to the direction of the chief ray of field point 5 from the nominal model. However, after lens heating, this changes, while the axis direction of the reference hemisphere is not changed and thus more vertical tilt is present. In Zemax, the change in direction of the chief rays are taken into account and therefore the vertical tilt ($Z(1,-1)$) term is not as large as in the COMSOL results.

Maréchal criterion

To evaluate the image quality, the Maréchal criterion is used, which is met for a Strehl ratio larger than 0.8 or equivalently if the RMS wavefront error is smaller than the wavelength divided by 14. The Strehl ratio is calculated for the composed wavefronts from Zemax and COMSOL for field point 5, and the results are shown in table 6.11. For the STOP analysis model, the Strehl ratio is only for the 405 nm and 436 nm wavelengths above 0.8 in both Zemax and COMSOL. These wavelengths still meet the Maréchal criterion and thus the optical system is well corrected and has a good image quality for these wavelengths. The 365 nm wavelength does not meet the Maréchal criterion, as the Strehl ratio is smaller than 0.8. Some design changes are needed to also get a good image quality for the 365 nm wavelength. Between COMSOL and Zemax, again similar results are found.

Table 6.11: Strehl ratio for field point 5 of the STOP analysis model at steady state.

Wavelength	**Zemax**	**COMSOL**
365	0.783	0.741
405	0.927	0.909
436	0.949	0.938

6.3.4 Design analysis

To evaluate the projection lens design, the contribution of different aspects are evaluated that degrade the optical performance. Table 6.12 shows the focus shift and radial RMS spot size for some different load cases. The focus shift is given as a percentage where 100% is equivalent to the focus shift for the STOP analysis case which includes all loads on the system, and 0% to no focus shift. The radial RMS spot size is a percentage w.r.t. the diffraction limit.

As a reference, the first load case shows that even the nominal model has some focus shift according to the COMSOL, but it can be neglected, since it will be within the depth of focus. The radial RMS spot size is well below the diffraction limit.

The second case is again a reference case, which is actually the results from the STOP analysis model which includes all load on the system. In this load case the focus shift is at maximum since all deformations of the system are considered.

The third and fourth load cases only consider temperature and structural changes, respectively, obtained from the STOP analysis model. From both the focus shift and the radial RMS spot size, it shows that the structural deformations are more dominant in deteriorating the optical performance. However, the temperature changes also have a significant contribution in increasing the spot size.

The fifth load case excluded any structural deformations form the housing and the mirror. This shows that the expansion of the housing, which causes drift in the lenses, and the deformations in the mirror, have a negligible effect on the optical performance compared to the structural and thermal deformations of the lenses.

In the sixth load case, the structural deformation on the fifth lens is excluded. The focus shift is decreases by 36.2% and the radial RMS spot size decreases by 46.8% compared to the STOP analysis which includes all loads. This shows that decreasing the structural deformations of lens 5 is a valuable aspect to optimize the design for. The strong influence of the structural deformations of lens 5 were also expected when looking at the temperature gradient from figure 6.10, which showed a strong local temperature gradient for this lens element.

The seventh load case excludes structural deformations on lens 3, since this lens has the most radial and z-displacements as can be seen in figures 6.11 and 6.12. However, optimizing the design to minimize deformations on lens 3 is less effective compared to lens 5.

Load case 8 excludes structural deformations in lenses 1, 2 and 4. The results show that optimizing the design to minimize structural deformations on these lenses will also not be as effective compared to lens 5.

Table 6.12: Focus shift and spot sizes for different load cases for field point 5. The focus shift is given as a percentage where 100% is equivalent to the focus shift for the STOP analysis case and 0% to no focus shift. The radial RMS spot size is a percentage w.r.t. the diffraction limit.

Load case	**Focus shift**	**RMS spot size to diffraction limit**
1) Nominal	-0.1%	5.5%
2) Combined thermal and structural	100%	65.5%
3) Temperature changes only	7.0%	25.3%
4) Structural deformations only	92.7%	49.4%
5) No housing and mirror deformations	98.8%	65.0%
6) No deformation on lens 5	62.8%	37.2%
7) No deformation on lens 3	73.2%	56.9%
8) No deformation on lenses 1, 2 and 4	72.6%	58.3%

In figure 6.17 the Zernike coefficients are plotted for the different load cases. For the 405 nm and 436 nm wavelengths, it shows that the structural deformations in the system are the dominant factor causing defocus ($Z(2,0)$). The structural deformations in lens 5 is a significant contributor to this, since excluding this also decreases the defocus significantly. For the 365 nm wavelength, both the structural and thermal changes contribute to the defocus aberration.

Looking at the vertical astigmatism ($Z(2,2)$) coefficients, the thermal changes partly compensate the vertical astigmatism caused by the structural deformations for all three wavelengths. Optimizing the structural deformations on lens 5 will not reduce this aberration term.

There is also spherical aberrations ($Z(4,0)$), which is caused by both the structural and thermal changes. Optimizing the structural deformations on lens 5 will reduce this aberration term.

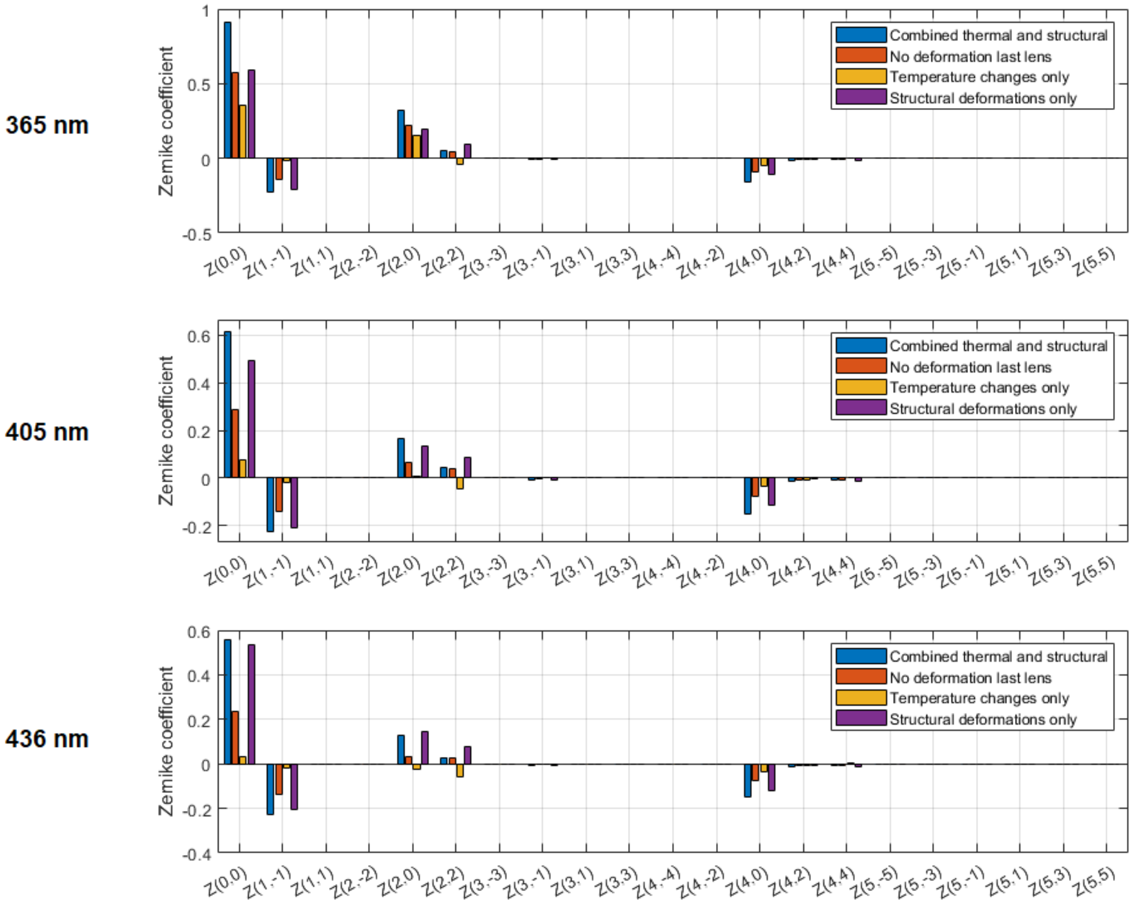

Figure 6.17: Zernike coefficients for field point 5 of the for different load cases, normalized w.r.t. σ_W from STOP analysis model which includes all loads.

In order to get a good image quality, the Maréchal criterion needs to be met, which is met for a Strehl ratio larger than 0.8. For the STOP analysis model which includes all loads, the Maréchal criterion is not met for the 365 nm wavelength. Table 6.13 shows the Strehl ratio's for the different load cases at the three wavelengths. It shows that the structural deformations are a large cause in decreasing the Strehl ratio. It is the combination of the thermal and structural loads that reduces the Strehl ratio until the Maréchal criterion is not met for the 365 nm wavelength. Optimizing for the structural deformation on lens 5 will result in all three wavelengths meeting the Maréchal criterion, and then the lens system can be classified as diffraction limited.

Table 6.13: Strehl ratio for field point 5 for different load cases.

λ [nm]	**Combined Temp. and Struc.**	**Temperature changes only**	**Structural changes only**	**No structural changes L5**
365	0.741	0.941	0.876	0.880
405	0.909	0.994	0.932	0.979
436	0.938	0.992	0.936	0.988

6.3.5 Transient behaviour

To perform a transient STOP analysis, step 2 from the work flow presented in figure 5.10 from chapter 5.3 needs to be solved with a transient solver instead of a steady state solver. Steps 3 and 4 are then repeated for desired time steps to obtain results on how the optical performance change over time. The transient model is solved over a time period until no significant differences with the steady state condition are found.

Heat transfer

To check if the time period for which the transient model is solved can be considered to have reached steady state, the heat balances from tables 6.14 and 6.15 are evaluated. Both tables show that the heat transfer in the transient model is in balance and the same heat transfer distribution between the different paths is found as in the steady state model. Therefore, the time period for which the transient model is solved can be considered to have reached steady state.

Table 6.14: Comparison of the heat transfer distribution between different paths out of the system for the steady state model and the transient model at steady state.

Heat Balance	**Steady State**	**Transient**	**Difference**
Heat IN	100%	100%	0%
Convection housing	-86.0%	-86.0%	0%
Convection lens 1	-7.3%	-7.3%	0%
Radiation lens 1	-6.7%	-6.7%	0%
Total	0%	0%	0%

Table 6.15: Comparison of the heat balance for all the lenses combined for the steady state model and the transient model at steady state.

Heat Balance	**Steady State**	**Transient**	**Difference**
Heat IN lenses	100%	100%	0%
Conduction to Gas	-15%	-15%	0%
Conduction to Housing	-43%	-43%	0%
Convection Lens 1	-7%	-7%	0%
Radiation	-34%	-34%	0%
Total	0%	0%	0%

In figure 6.18 the maximum temperature is plotted against the time for the lenses separately and the entire lens system. Figure 6.19 shows the derivative of the maximum temperature over time for the lenses and the entire lens system. On the left plot the time axis is on a linear scale, while on the right plot a semi-logarithmic scale is used for the time. The plots shows that at first the maximum temperature for lens 5 increases the fastest and is the highest temperature in the system, but over time and getting closer to steady state, lens 3 reaches a higher maximum temperature.

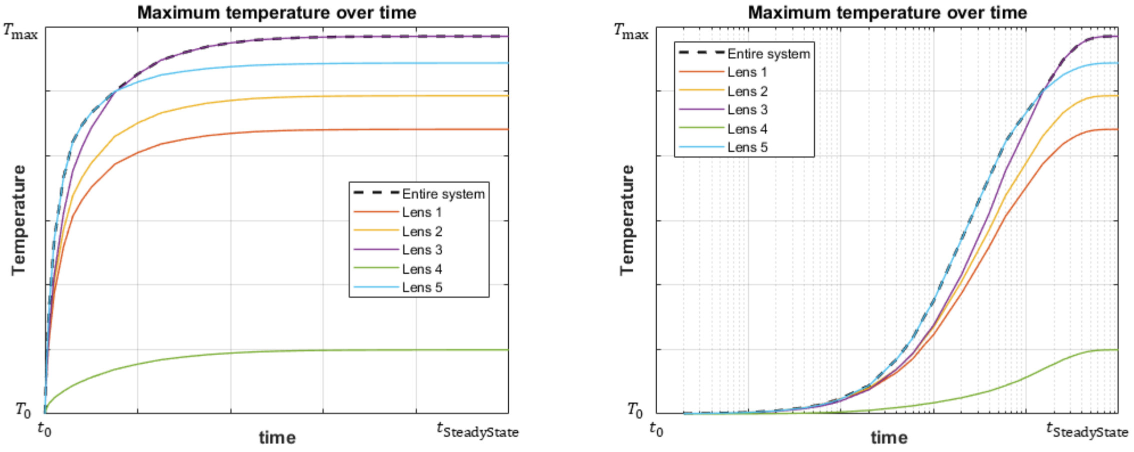

Figure 6.18: Plot of the maximum temperature against time on a linear (left) and semi-logarithmic (right) scale.

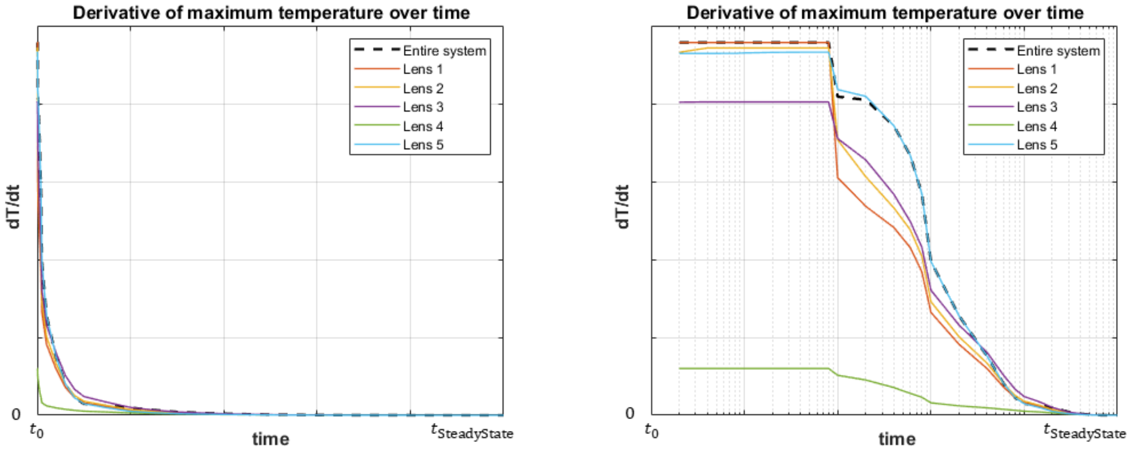

Figure 6.19: Plot of the derivative of the maximum temperature against time on a linear (left) and semi-logarithmic (right) scale.

Optical performance

With the temperature changing over time, also the optical performance change. In figure 6.20 two plots are shown. On the left the focus shift is plotted which is normalized to the focus shift at steady state. On the right, the radial RMS spot size of field point 5 is plotted changing over time, which is shown as a percentage of the diffraction limit. In order to obtain the radial RMS spot sizes as given in the right plot, the focus needs to be shifted according to the left plot over time. The development over time of both plots looks similar to the maximum temperature increase, except that the radial RMS spot size and focus shift reach steady state earlier compared to the maximum temperature in the lenses. While all the lenses are still increasing in temperature, the spot size and focus shift are settling at steady state. However, the derivative of the temperature plots shows that when the change in the temperature is reaching zero, also the optical performance are settling at steady state. This is as expected, since the change in temperature is the driving force that eventually degrades the optical performance.

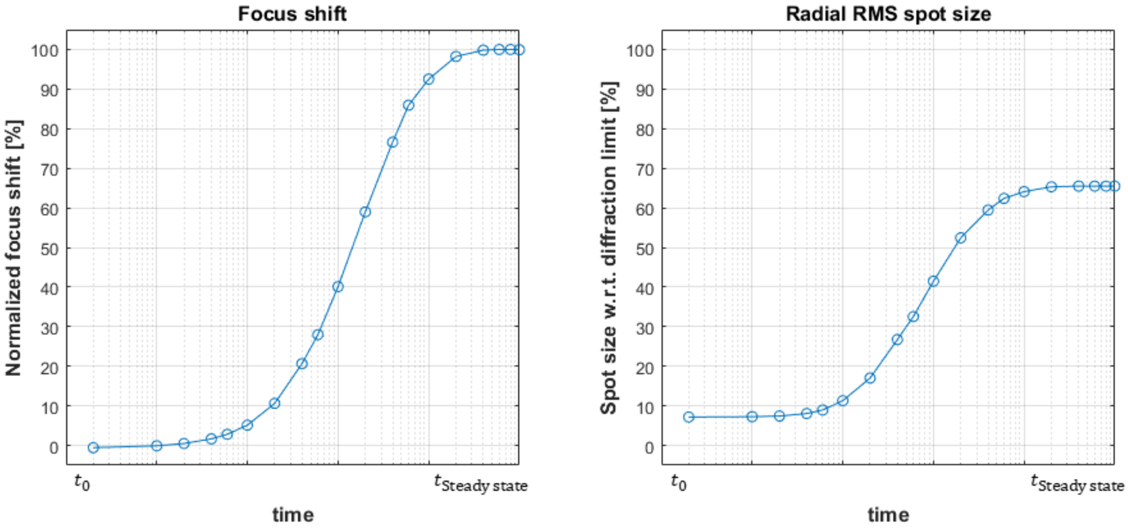

Figure 6.20: Left: focus shift over time. Right: change of radial RMS of field point 5 over time. X-axes in both plots are on a logarithmic scale.

In figure 6.21 the Zernike coefficients are plotted against the time. The coefficients are normalized w.r.t. σ_W from the steady state STOP analysis model and the time axes are on a logarithmic scale.
The plots show again that the defocus ($Z(2,0)$), vertical astigmatism ($Z(2,2)$) and spherical aberrations ($Z(4,0)$) coefficients become the most dominant and significant aberration terms over time. For all three wavelengths, there is some defocus at t_0, however, due to the lens heating effects, over time a shift in the focus occurs. Defocus aberrations are typically considered to be simple to resolve by shifting the focus plane. However, even after shifting the focus plane, some defocus will remain between the three wavelengths. This is because the three wavelengths do not exactly share the same focus planes. Notable is a slight decrease in the vertical astigmatism ($Z(2,2)$) before increasing over time for all three wavelengths. For the 436 nm wavelength, the vertical astigmatism even changes in sign over time. Again, the overall development over time of the aberrations is similar to the change of the temperature, which is again as expected, since the change in temperature is the driving force that eventually degrades the optical performance.

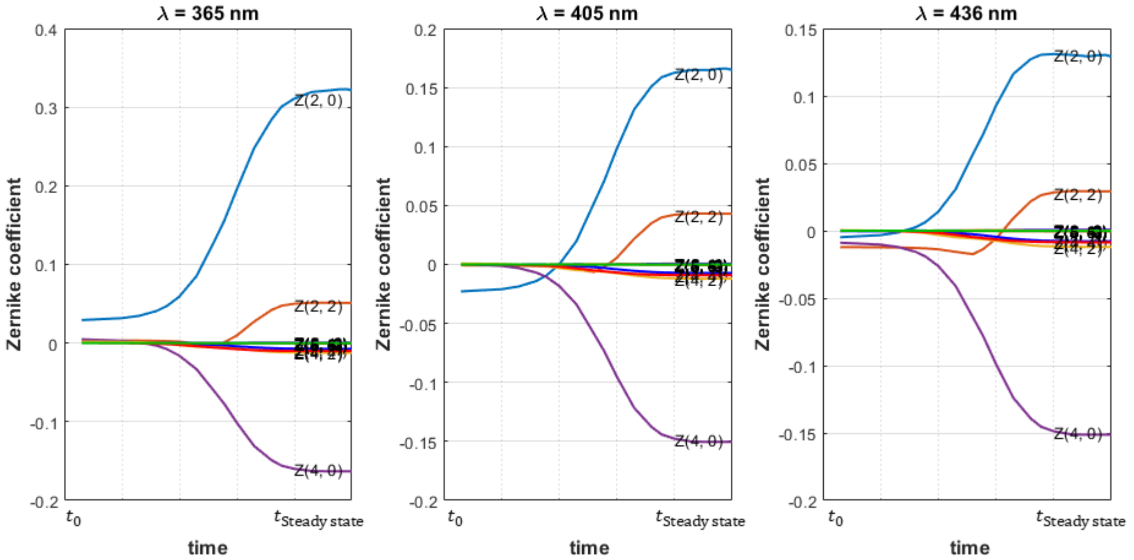

Figure 6.21: Zernike coefficients development over time for the 3 wavelengths separately, normalized w.r.t. σ_W from the steady state STOP analysis model. The time axes are on a logarithmic scale.

Also the Strehl ratio is plotted over time in figure 6.22 for the three wavelengths separately. The time axis in this plot is on a logarithmic scale. The red line marks the boundary above which the Maréchal criterion is met. The plot shows that the lens system takes about 4% of the total time to reach steady state until the 365 nm wavelength rays are not properly imaged and the system is not considered to be diffraction limited for this wavelength anymore.

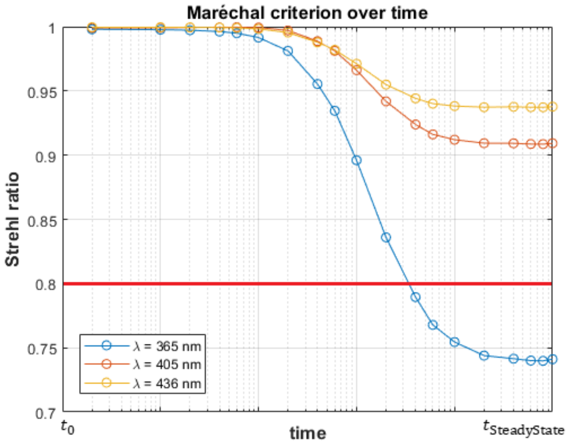

Figure 6.22: Plot of the Strehl ratio over time for 3 wavelengths separately. Strehl ratio's above the red line meet the Maréchal criterion.

Chapter 7

Thermal design changes

Because of the lens heating effects, the optical performance of the projection lens system degrade. The current design does not meet the Maréchal criterion for the 365 nm wavelength. Therefore, to improve the optical performance, design changes are needed to reduce the thermal changes, which are the driving force of the refractive index changes and structural deformations. Here, some design changes are presented, but note that not all changes are applicable for a projection lens system.

7.1 Increase emissivity with baffles

In order for the non-optical interior surfaces to act like a thermal radiative heat sink, its emissivity needs to be as high as possible and ideally equal to 1. An emissivity of around 0.95 is already achievable with various types of coatings. The 3M Scotch Super 33+ used in the experiments described in chapter 4.6.2 has a hemispherical emissivity of 0.95 for a spectral range of 8-14 µm[13] and Acktar Ultra Black coating has an emissivity of >0.93 for a spectral range of 3-30 µm[17].

To make the emissivity approach 1, baffles can be used on the non-optical interior surfaces of the housing as shown in figure 7.1. With baffles, the incoming radiation gets reflected multiple times before it reflects away from the housing surfaces. With every reflection some radiative heat is absorbed by the surface, decreasing the power of the radiation exponentially. After multiple reflections the radiation can be considered to be absorbed by the housing and the baffles. For example, 99.6% of the radiation coming in at an angle for which the emissivity equals 0.5 is absorbed after the fifth reflection.
Also, using baffles allows the radiation to hit the baffles at smaller incident angles, which means that the directional dependence of the emissivity becomes less significant.

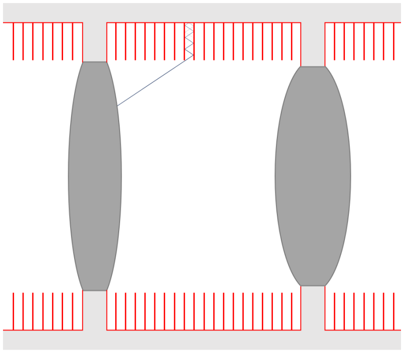

Figure 7.1: Addition of baffles to enhance radiative heat absorption in the non-optical interior boundaries. Surfaces marked red are supposed to be coated with a high emissivity coating.

7.2 Increase external convection

To decrease the temperature in the lenses, forced convection can be applied on the outer surfaces of the housing. Instead of the 6.2 W/(m^{2}K) convective heat boundary, the convective heat transfer coefficient h_c is increased to 25 W/(m^{2}K). Figure 7.2 shows that the overall temperature in lens 5 decreases as a result of the increased h_c. An offset decrease in the temperature w.r.t. the maximum temperature of 7.4% happens when h_c is increased to 25 W/(m^{2}K). However, the radial temperature gradient in the lens does not change.

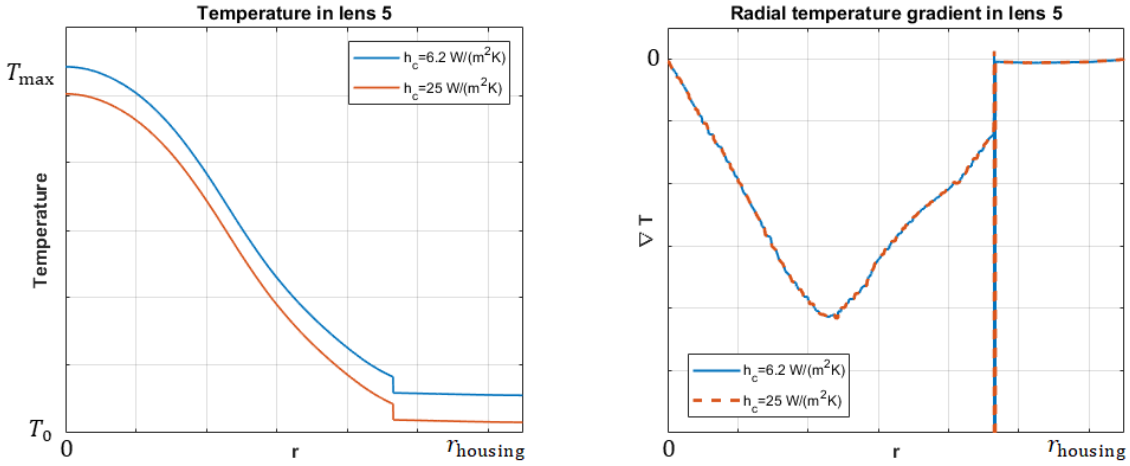

Figure 7.2: Left plot shows radial temperature profile and right shows radial temperature gradient for lens 5 for different external heat transfer coefficients.

The decrease in the temperature also does not significantly change the radial RMS spot sizes, as can be seen in table 7.1. This is because the temperature gradient did not change between the two h_c values.

Table 7.1: Comparison of percentage of the radial RMS spot size per field point for different external convective heat transfer coefficients w.r.t. the diffraction limit for the STOP analysis model at steady-state.

Field point	**6.2 W/(m^{2}K)**	**25 W/(m^{2}K)**
1	64%	64%
2	66%	66%
3	64%	64%
4	64%	63%
5	65%	65%
6	63%	63%
7	63%	63%
8	63%	63%
9	63%	63%

Looking at the Strehl ratio, for all three wavelengths, it is decreased by 0.2-0.4%. The 405 nm and 436 nm wavelengths are still above 0.8 and thus meet the Maréchal criterion, while the 365 nm does not.

Table 7.2: Strehl ratio for field point 5 for different external convective heat transfer coefficients.

Wavelength	**6.2 W/(m^{2}K)**	**25 W/(m^{2}K)**
365	0.741	0.738
405	0.909	0.907
436	0.938	0.936

Because of these results, cooling the external surfaces of the housing has a negligible effect on the optical performance. Therefore, it is not worth to optimize the design on this design aspect.

7.3 Actively heated lens mount

To achieve smaller thermal gradients in the lenses, the lens mounts can be actively heated. This way the lenses heat up in the center by the absorbed rays and at the edge by the lens mount. The lenses will have a more homogeneous temperature distribution, which leads to smaller temperature gradients and thus less structural deformations.

A variation on the steady state STOP analysis model is created, where the lens mount of lens 5 is heated with an internal heat source. Also, the TCC boundary layer is increased to have better conduction between the lens and the lens mount. Table 7.3 shows the heat transfer balance for two cases with the heated mount and the unheated mount of lens 5. The balance shows that when heating the mount with 1 W, 4% more of the heat gets transferred through the optical surface instead of through the edge of the lens. When using 3.5 W it increases to 16% more of the heat transfer through the optical surface.

Table 7.3: Comparison of the heat balance for a heated and unheated lens mount for lens 5.

Heat Balance	**Unheated**	**1 W heated**	**3.5 W heated**
Heat IN lenses	100%	100%	100%
Conduction to Gas	-15%	-15%	-16%
Conduction to Housing	-43%	-39%	-27%
Convection Lens 1	-7%	-9%	-10%
Radiation	-34%	-37%	-47%
Total	0%	0%	0%

In figure 7.3 the temperature profile and gradient in lens 5 is shown for the unheated and the two heated lens mount cases. It shows that by heating the lens mount, the overall temperature in the lenses also increase. For the 1 W heated lens mount, the temperature difference with T_0 at the maximum temperature is increased almost by a factor of 2, while for the 3.5 W heated mount, it is about a factor of 4.3. However, the temperature gradient did decrease, which means that a more homogeneous temperature distribution is obtained, which was the desired effect of heating the lens mount.

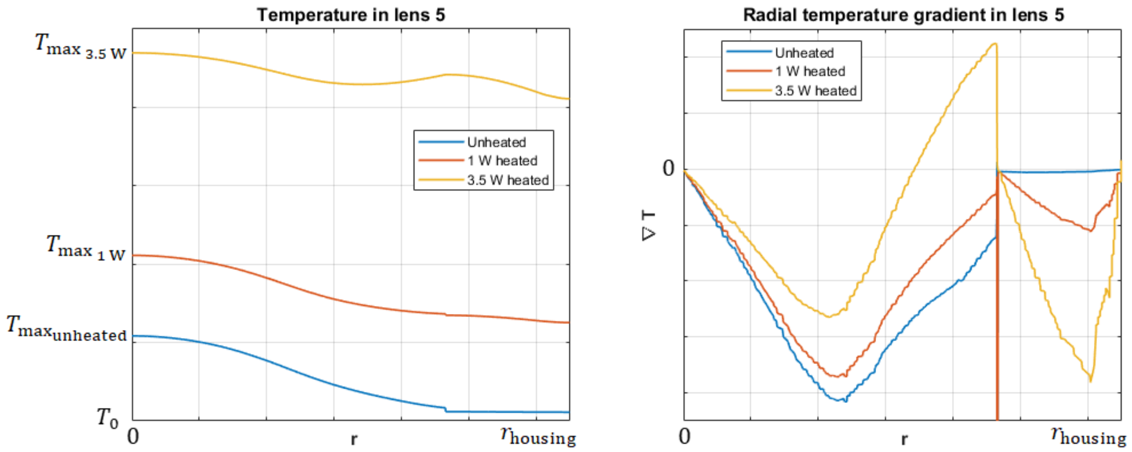

Figure 7.3: Temperature profile and gradient in lens 5 for a heated and unheated lens mount.

Even though a more homogeneous temperature is obtained in lens 5, the increase in the overall temperature in the lens cause optical performance degradation. This can be seen in table 7.4, where the radial RMS spot sizes of each field point is shown to have increased.

Table 7.4: Comparison of the percentage of radial RMS spot size per field point for the heated and unheated lens mount models w.r.t. the diffraction limit for the STOP analysis model at steady-state.

Field point	Unheated	1 W heated	3.5 W heated
1	64%	65%	66%
2	66%	67%	69%
3	64%	65%	66%
4	64%	64%	67%
5	65%	67%	70%
6	63%	64%	66%
7	63%	64%	65%
8	63%	64%	67%
9	63%	63%	65%

Consequently, also the Strehl ratio is decreased when heating the lens mount, as can be seen in table 7.5.

Table 7.5: Strehl ratio per wavelength for the heated and unheated lens mount models.

λ [nm]	Unheated	1 W heated	3.5 W heated
365	0.741	0.732	0.720
405	0.909	0.898	0.874
436	0.938	0.928	0.902

As this is a way to reduce the thermal gradient in lenses, unfortunately the overall temperature increase does reduce the optical performance in the system. Therefore, this is not considered as a viable solution to increase the optical performance.

7.4 Low thermal contact conductance

A passive way to increase the temperature at the edge of the lens is by changing the lens mount design to reduce the conductive heat transfer into the housing. This will lead to a higher temperature but also a more homogeneous temperature distribution, because the heat will spread more inside the lens. Reducing the thermal gradient then also reduces the local structural deformations. In the FEM model, changing the lens mount design is equivalent to a change in the thermal contact conductance (TCC).

The steady state STOP analysis model is solved for 3 different cases where the TCC is multiplied by a factor of 0.1, 1 and 10. In table 7.6 the heat transfer balance is shown for the three different cases. The factor 1 multiplication is added as a reference case, since this is the model with the current TCC values.

Table 7.6: Comparison of the heat balance for all the lenses combined for different values of the TCC.

Heat Balance	**0.1×**	**1×**	**10×**
Heat IN lenses	100%	100%	100%
Conduction to Gas	-22%	-15%	-8%
Conduction to Housing	-35%	-43%	-52%
Convection Lens 1	-9%	-7%	-8%
Radiation	-35%	-34%	-32%
Total	0%	0%	0%

The table shows that by reducing the TCC, more heat is transferred from the optical surfaces in stead of through the edge of the lens. With the reduced TCC 65% of the heat is transferred through the edge, while with the enhanced TCC it is 48%. However, looking at the temperature profile in lens 5, figure 7.4 shows that the temperature profile shifts, but the general shape of the profile stays the same when changing the TCC. Except at the edge of the lens, the temperature deviates more which is also closer to where the TCC boundary condition is located. Figure 7.4 also shows that the temperature gradient mainly changes near the edge of the lens. Reducing the TCC does reduce the thermal gradient near the edge.

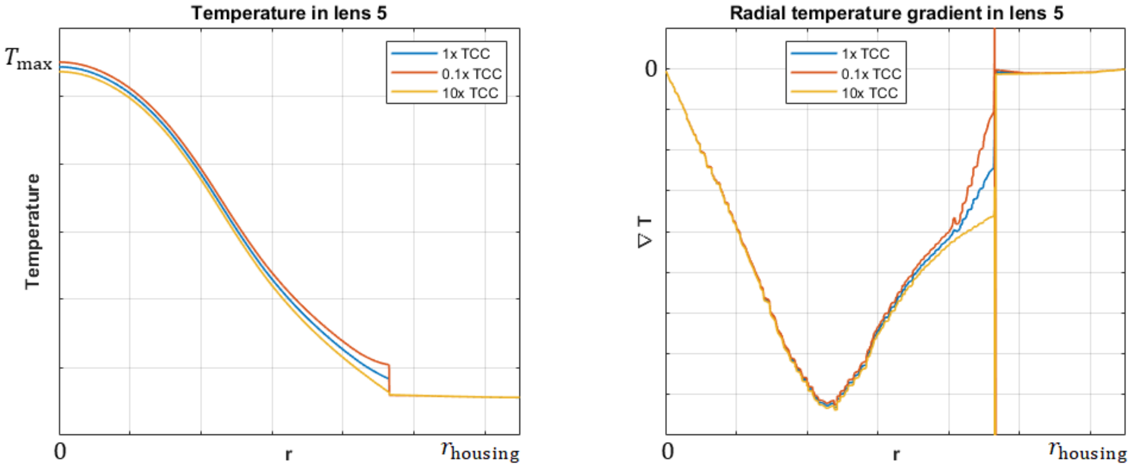

Figure 7.4: Temperature profile and gradient in lens 5 for different TCC cases.

Looking at the optical performance when the TCC is multiplied by 0.1 and 10, table 7.7 shows the percentage of change of the radial RMS spot size per field point in both cases w.r.t. the nominal TCC case. The table shows that a lower TCC results in smaller radial RMS spot sizes, while for larger TCC the spot sizes increase. However, the changes are small and this shows that changing the TCC has an minimal effect on the spot size.

Table 7.7: Change of radial RMS spot size per field point for TCC multiplied by 0.1 and 10 compared to nominal TCC.

Field point	**0.1×**	**10×**
1	-0.1%	0.1%
2	0.1%	0.0%
3	-0.3%	0.1%
4	-0.6%	0.7%
5	-0.3%	0.3%
6	-0.6%	0.7%
7	-1.9%	2.4%
8	-1.1%	1.4%
9	-2.0%	2.2%

Also the Strehl ratio is computed for the two cases where the TCC is multiplied by 0.1 and 10. Table 7.8 shows the Strehl ratio per wavelength for the TCC multiplied by 0.1, 1 and 10. For the reduced TCC the Strehl ratio increase, while for the enhanced TCC it reduced. This shows again that reducing the TCC enhances the optical performance. However, a factor of 0.1 of the TCC is still not enough to meet the Maréchal criterion for the 365 nm wavelength.

Table 7.8: Strehl ratio per wavelength for TCC multiplied by 0.1, 1 and 10.

λ [nm]	**0.1×**	**1×**	**10×**
365	0.743	0.741	0.739
405	0.909	0.909	0.909
436	0.938	0.938	0.938

Reducing the TCC and thus changing the lens mount design helps increasing the heat transfer from the optical surface in stead of the edge of the lens. However, on the optical performance the effects are negligible, since the thermal gradient is not reduced significantly with this design change.

7.5 Thermal conductance layer

Because the thermal conductivity of the lens material is much lower than that of the housing and lens mount, but much higher than that of the gas, heat inside the lens conducts towards the edge. However, the relatively low thermal conductivity of the lens compared to the housing makes it more difficult for the heat to transfer through the lens and eventually reach the edge of the lens. To enhance the heat transfer to the housing and spread the heat more equally inside the lens, an additional thermal conductance layer can be applied on the optical surface of the lens, as shown in figure 7.5. The conductance layer should have a higher thermal conductivity than the lens. As the red arrows show, heat from the center of the lenses will travel into the thermal conductance layer. From the thermal conductance layer some heat will be transferred back into the lens and heat up the colder edge of the lens, leading to a more homogeneous temperature distribution inside the lens. With smaller thermal gradients also less local structural deformations will be created and therefore the optical performance will be less degraded. However, this solution would be useful if a thick layer of several millimeters could be applied on the lens surface, but that would interfere with the light passing through the lens system and even degrade the optical performance. Some coatings, for example anti-reflection coatings, can be applied on lenses, but their layer thickness is typically too thin to effectively work as a thermal conductance layer.

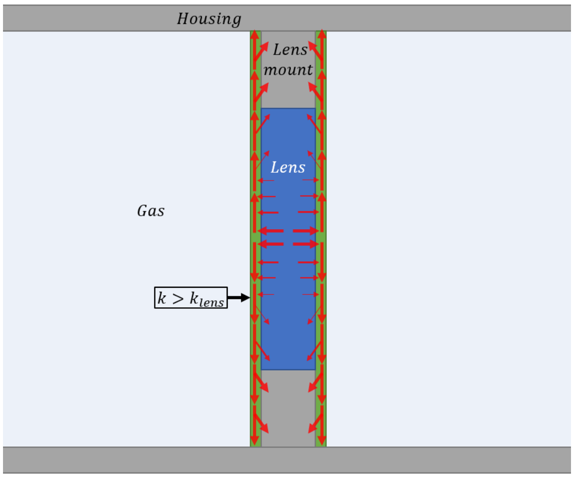

Figure 7.5: Schematic drawing of a thermal conductance layer to enhance conductive heat transfer in the lens and to the lens mount.

7.6 High conductive enclosure medium

The thermal conductance layer principle as explained in the section before could be realised by changing the medium which is used in the enclosures between the lenses and the housing. The design now uses a gas with a low thermal conductivity w.r.t. the conductivity of the lens. By changing the gas with another medium which has a higher thermal conductivity than the lens, the principles of the thermal conductance layer could be used to spread the heat more equally in the lens. Unfortunately, gasses have typically a low thermal conductivity and certainly not higher than that of the material of the lenses. Using a liquid or solid is an undesired option, because it would interfere with the light and the optical design would change.

The current design uses nitrogen gas as the enclosure medium. Replacing the nitrogen with helium gas, which has a higher thermal conductivity compared to nitrogen, increases the heat conduction from the lenses to the gas. This is shown in the heat balance from table 7.9. The table shows that when helium is used a total of 58% of the heat is transferred from the optical surface, since more heat is being transferred by conduction to the gas.

Table 7.9: Comparison of the heat balance with nitrogen and helium as enclosure medium in the lens system.

Heat Balance	**Nitrogen**	**Helium**
Heat IN lenses	100%	100%
Conduction to Gas	-15%	-31%
Conduction to Housing	-43%	-35%
Convection Lens 1	-7%	-8%
Radiation	-34%	-27%
Total	0%	0%

With the helium gas, the maximum temperature T_{max} in the system decreases by 20% and the temperature difference ΔT decreases by 22%. Figure 7.6 shows the temperature profile and gradient in lens 5, where it can be seen that the temperature in the lens is lower with the helium gas. Also, a smaller gradient is accomplished, which is promising for the optical performance.

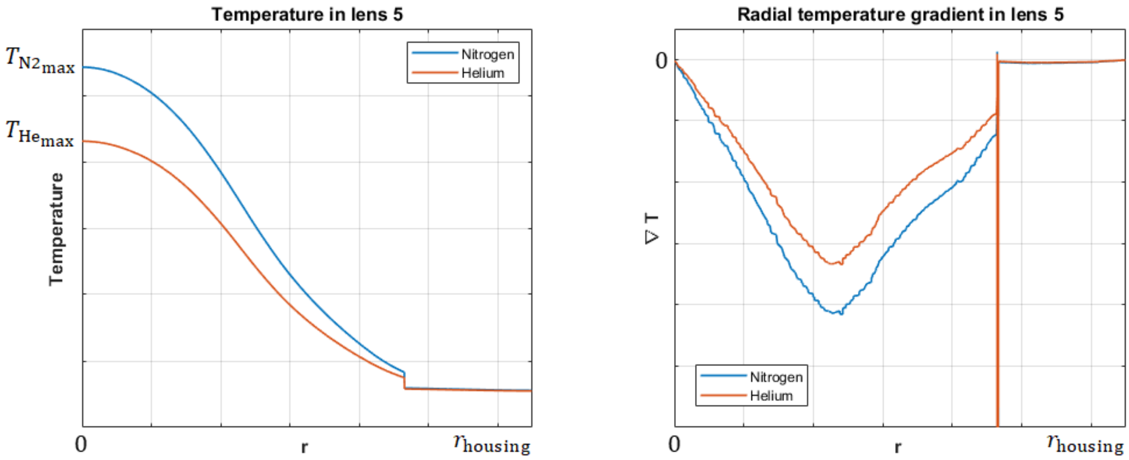

Figure 7.6: Comparison of the temperature profile and gradient in lens 5 between nitrogen and helium as enclosure medium in the lens system.

Looking at the optical performance, the radial RMS spot sizes can be found in table 7.10 for both nitrogen and helium. The radial RMS spot sizes decrease on average 11.4% w.r.t. the diffraction limit when helium is used instead of nitrogen.

Table 7.10: Comparison of the radial RMS spot size per field point between nitrogen and helium as enclosure medium in the lens system.

Field point	**Nitrogen**	**Helium**
1	64%	53%
2	66%	54%
3	64%	53%
4	64%	52%
5	65%	54%
6	63%	52%
7	63%	52%
8	63%	52%
9	63%	52%

Also the Zernike coefficients are decreased when using helium, as can be seen in the barplots in figure 7.7. The same Zernike terms are dominant in both cases, but the coefficients are smaller, which indicates that the wavefront error is smaller when using helium instead of nitrogen.

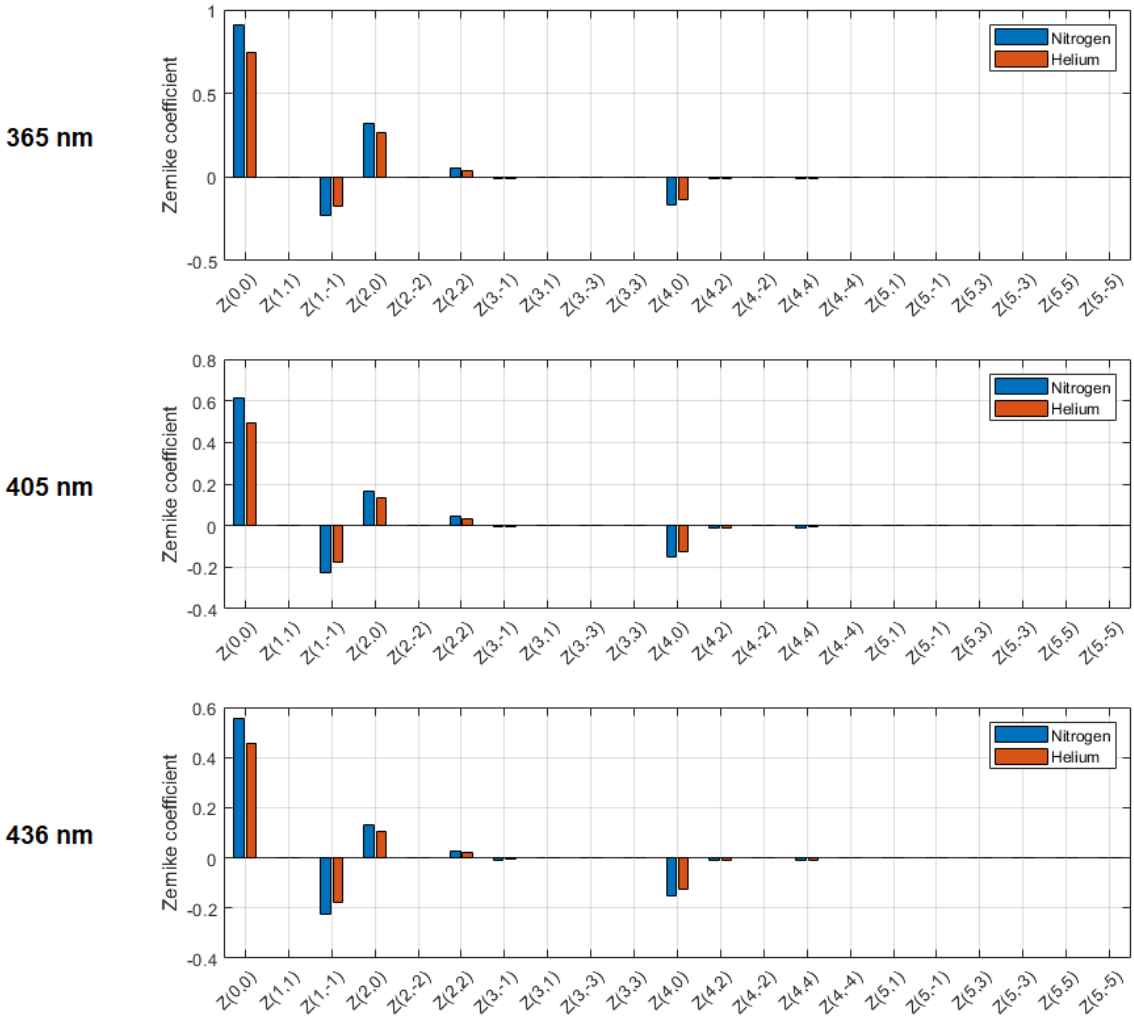

Figure 7.7: Zernike coefficients for field point 5 for nitrogen and helium as enclosure medium in the lens system, normalized w.r.t. σ_W from STOP analysis model.

In table 7.11 the Strehl ratio is again calculated. When using helium, for all three wavelengths the Maréchal criterion is met, since for all three wavelengths the Strehl ratio is larger than 0.8. The system with helium can be considered to be diffraction limited and to have good image quality according to the Maréchal criterion. This was not the case when nitrogen was used for the 365 nm wavelength.

Table 7.11: Strehl ratio for field point 5 for different enclosure media.

Wavelength	**Nitrogen**	**Helium**
365	0.741	0.817
405	0.909	0.941
436	0.938	0.957

From these results, using helium instead of nitrogen looks like a promising option to enhance the optical performance. It is recommended for a future analysis of the lens system to look at the possibility of using helium instead of nitrogen inside the lens system.

Chapter 8

Conclusion and Discussion

Modelling

COMSOL Multiphysics turned out to be a feasible option for building a FEM model to perform a STOP analysis of a projection lens system from a high-end lithography machine. COMSOL is capable of combining the physics of solid mechanics, heat transfer and geometrical optics in a single FEM model. COMSOL also offers a ray tracing, steady state and transient solver to solve the different physics modules.

Building a STOP analysis model in a single multiphysics model requires that the same mesh is used to compute each physics module. This is to prevent introducing additional numerical errors and to be able to evaluate correct optical results. However, this is computationally inefficient, because for the optics to resolve, the mesh needs to be smaller (h-refinement) and of higher mesh element order (p-refinement) than what is needed to converge the computations for the solid mechanics and heat transfer. The fine mesh becomes computationally costly when radiative heat transfer is computed, especially when directional dependent radiative heat transfer is accounted for. Solving each physics module in a separate step but in the same model, makes computing STOP analysis models more feasible to find a solution. To eventually obtain the STOP analysis model of a high-end lithography systems, the help from the COMSOL support team was needed in making models feasible to complete and to fill in the gaps of lack of experience in COMSOL. Because of the involvement of the relatively new optics module, often help of developers of the optics module was needed.

Optical modeling

Comparing the results of the optical performance for a high-end lithography projection lens system obtained from COMSOL and Zemax, it shows that COMSOL is capable of generating similar results as Zemax. However, the Zemax results show slightly better performance. The models were evaluated on spot diagrams, radial RMS spot sizes, Zernike wavefront aberrations and tested for the Maréchal criterion. For each of these optical performance indicators, the same characteristics of the optical system as found by Zemax are identifiable in COMSOL. The optical performance calculated in COMSOL deviate a few percent from the Zemax results. The difference between the COMSOL and Zemax results is partly because COMSOL introduces discretization errors, because the mesh plays a part in determining the surface normals of the optical interfaces, while Zemax uses an analytical expression to evaluate this when performing ray tracing. Also, in COMSOL the location and orientation of imaging planes are assigned manually, which also introduces differences with the Zemax results if a different plane is chosen. Overall, the optical results obtained from COMSOL correspond to the Zemax results well enough to continue and trust the optical performance results obtained from the STOP analysis models.

The results of the optical performance for the nominal model show that the Wynne-Dyson projection lens design is a well corrected and diffraction limited design. According to the COMSOL results, the radial RMS spot sizes are for all field points smaller than 7.4% of the diffraction limit. The main aberrations in the system are defocus, vertical astigmatism and spherical aberrations. However, the Strehl ratio is well over 0.8 which shows that the RMS wavefront error is small and that the Maréchal criterion is met. Therefore, the system is diffraction limited and has a good image quality. The design also leaves room for thermal and structural loads to degrade the optical performance and still maintain the diffraction limit as the fundamental limit for the resolution.

Dominant heat transfer paths

Inside the projection lens system where the lenses heat up due to lens heating, many different heat transfer paths arise. However, the main heat transfer paths that transfer heat away from the lenses are the conduction from the lenses towards the housing and the radiation from the lens surfaces to the housing. Convection from the lens surfaces to the gas is neglected because a relatively small heat transfer coefficient h_c is approximated inside cylindrical enclosures. The gas between the lenses is instead modeled as a stagnant solid body. Therefore, between the lenses and the gas conductive heat transfer is instead considered. In order to model the radiation correctly, the directional dependence of the emissivity needs to be taken into account, since most of the radiation to the housing is from angles that have a reduced emissivity. The conduction from the lens to the housing is also partly restricted, because the lens is mounted to a lens mount which has cut-outs for flexures and these restrict thermal conduction. Also the lenses are fixed to the mounts with an adhesive at a few points around the edge, reducing the contact area, which adds additional thermal resistance.

Directional emissivity experiment

From the experiments to determine the directional dependence of the emissivity, fitted functions are obtained for a fused silica and I-line glass lens, which show a strong directional dependence of the emissivity at large angles. For angles up to around 50° the emissivity can be considered to be constant. For larger angles the emissivity decreases quickly.

Heat transfer and structural mechanics model

The results from the model of chapter 6.2 were mainly to gain confidence in the heat transfer and structural mechanics modeling in COMSOL. The COMSOL results showed similar results as the previously solved model in ANSYS. The main difference was found in the heat transfer distribution when looking at a single lens. In COMSOL more heat was transferred by conduction into the housing. A reason for this could be because a different TCC for this lens was used. Nevertheless, the temperature and the displacements calculated in COMSOL and ANSYS differ at most by 2%. Also, comparing the temperature profile in lens 5 as obtained from the analytic model and COMSOL, similar results are found. Having three separate and independent models and getting similar results from them increases the confidence in the models. Therefore, also confidence is gained in the heat transfer and structural mechanics modelling performed by COMSOL.

Directional dependent radiation modeling

In COMSOL, surface-to-surface radiation can be solved by either considering a hemispherical or directional dependent emissivity for the surfaces. However, when comparing the results of an identical model but solved for a hemispherical ideal black body or a directional dependent emissivity, the directional dependent emissivity out performs the ideal black body case. When using the directional dependent emissivities, the model could not be verified if it had converged yet, since any further refinement resulted in running out of memory. Therefore, the current directional dependent models are not trusted and reduced hemispherical emissivities are used to account for the directional dependence. It is however recommended to further investigate the directional dependent radiative heat transfer in future analysis of the lens system.

Steady state STOP analysis

The STOP analysis model from chapter 6.3 shows that in the heat transfer balance, radiation is an important heat transfer mechanism that cannot be neglected, as was done in the reference model from chapter 6.2. With radiation included, 57% of the heat from the lenses is transferred away from the optical surface of the lenses instead of the edges through conduction to the housing. The overall temperature in the system drops by about 38% and accordingly the displacements reduce by 35%.

Due to the lens heating effect, the radial RMS spot sizes increased roughly by a factor of 10, but the spot sizes are still below the diffraction limit. However, the wavefront error has increased significantly. For the 405 nm and 436 nm wavelengths the Maréchal criterion is still met after the lens heating effect at steady state, but this is not the case for the 365 nm. Because of this, thermal design changes are needed in order to have a good image quality for the 365 nm wavelength and to classify the system as diffraction limited even after the lens heating effects.

The structural deformations in lens 5 cause a large portion of the total optical performance degradation. Excluding these structural deformations from the model reduces the radial RMS spot size by 47%. Also, the defocus and spherical aberrations are reduced significantly, which are the most dominant aberration terms. The Maréchal criterion is also met for the 365 nm wavelength after excluding the structural defromations in lens 5. Therefore, optimizing the thermal design in lens 5 has a lot of potential to improve the optical performance of the system.

Transient STOP analysis

Performing a transient STOP analysis of a projection lens system of a high-end lithography machine turned out to be feasible in COMSOL. It does however take effort to build a computationally efficient model in order not to run out of memory. Using the 4 step workflow described in figure 5.10 helps with this.

The transient STOP analysis model shows how the system changes from the nominal model to the steady state model over time. Looking at the transient behaviour of the maximum temperature of each lens, the optical performance decrease accordingly to the change in temperature since this is the driving force that degrades the optical performance. The transient temperature results show again that lens 5 changes in temperature the fastest, but lens 3 eventually has the highest temperature. The lens system takes about 4% of the time to reach steady state until it does not meet the Maréchal criterion for the 365 nm wavelength.

Thermal design changes

In order to improve the optical performance, some thermal design changes are needed. Making the interior non-optical surfaces to have an emissivity of 1 showed to improve the radiative heat transfer from the lenses. This allows for more heat to leave the lenses from the optical surfaces instead of the edge of the lenses, which decreases the radial thermal gradient. Using baffles and coat them to have a high emissivity is a viable option, which also decreases the incident angles and therefore the emissivity is typically higher.
Increasing the external convection, actively heating the lens mount and changing the TCC between the lens and the lens mount, all three options did not improve the optical performance. Therefore, optimizing the thermal design for these thermal aspects is not effective. Changing the enclosure medium from nitrogen to helium improves the system to a degree where all three wavelengths meet the Maréchal criterion. It allows for more heat to conduct from the lens into the gas and as a result the temperature and the temperature gradient both get reduced. Using helium instead of nitrogen is a recommended option to further look into in future analysis of the lens system.

Recommendations

The projection lens design still needs to be developed and improved further in order to perform within the stringent requirements of a lithography system at high throughput conditions. Some recommendations for future analysis are given below.

- To increase the optical performance even after the lens heating, the temperature gradient in the lenses (especially lens 5) should be decreased. Further analysis in the possibility to change the nitrogen gas with helium gas can be done, as this showed promising improvements in the optical performance.
- Since radiative heat transfer is an important heat transfer path, modeling actual directional dependent radiation in the STOP analysis can be further analyzed than was done in this report.
- Possibilities to change or add lens elements to compensate for the optical performance degradation can be further analyzed.
- In the actual lithography system, lens 1 is adjacent to a reticle which also heats up and thus acts as an additional heat source for L1. This only applies on 1 side (top side) of the lens surface since the other side is adjacent to the relatively cold wafer. This additional heat source should also be taken into account, even though the structural deformations of lens 5 is the most dominant degrading factor of the optical performance.
- Having more insight/knowledge in the reference models, like the Zemax and ANSYS models, allows to be more efficient in comparing results. For example, when making sure that the results obtained from both models are at the same conditions, e.g. for the definition of the best focus plane. This is recommended because it can save a lot of time in bug fixing the models.

Bibliography

[1] "Packaging - semiconductor engineering." [Online]. Available: https://semiengineering.com/knowledge_centers/packaging/

[2] C. A. Mack, Field guide to optical lithography. SPIE Press Bellingham, WA, 2006, vol. 6.

[3] P. Zhao, E. M. True, R. Ellis, and A. M. Hawryluk, "Wynne-dyson projection lens with reduced susceptibility to uv damage," Sep. 6 2016, uS Patent 9,436,103.

[4] C. Mack, Fundamental principles of optical lithography: the science of microfabrication. John Wiley & Sons, 2008.

[5] G. R. Fowles, Introduction to modern optics. Courier Corporation, 1989.

[6] SCHOTT, "Temperature coefficient of refractive index," Technical Documents, vol. TIE-19, 2016. [Online]. Available: https://www.schott.com/d/advanced_optics/3794eded-edd2-461d-aec5-0a1d2dc9c523/1.1/schott_tie-19_temperature_coefficient_of_refractive_index_eng.pdf

[7] G. Vdovin, Elementary technical optics. TU Delft, 2020.

[8] "thermal properties of optical substrates," 2021. [Online]. Available: https://www.edmundoptics.com/knowledge-center/application-notes/lasers/thermal-properties-of-optical-substrates/

[9] A. Faghri, Y. Zhang, and J. R. Howell, Advanced heat and mass transfer. Global Digital Press, 2010.

[10] S. Ostrach, Natural Convection in Enclosures, ser. Advances in Heat Transfer, J. P. Hartnett and T. F. Irvine, Eds. Elsevier, 1972, vol. 8. [Online]. Available: https://www.sciencedirect.com/science/article/pii/S006527170870039X

[11] M. F. Modest, Radiative heat transfer. Academic press, 2013.

[12] A. Mills and C. Coimbra, Basic heat and mass transfer, 3rd ed. Temporal Publishing, LLC, 2015.

[13] FLIR, User manual FLIR TG167. FLIR, 2016.

[14] R. Toogood and P. Eng, "Pro/mechanica tutorial structure," Schroff Development Corporation, 2001.

[15] "Comsol multiphysics reference manual," 2020. [Online]. Available: https://doc.comsol.com/5.6/doc/com.comsol.help.comsol/COMSOL_ReferenceManual.pdf

[16] "Tgrid 5.0 user's guide," 2008. [Online]. Available: https://romeo.univ-reims.fr/documents/fluent/tgrid/ug/tgrid50-ug.pdf

[17] Acktar, "Ultra black coating for mwir and lwir | acktar black coatings," 2021. [Online]. Available: https://www.acktar.com/product/ultra-black/